Photophysical Kinetics in TICT-forming Compounds – Derivatives of DMABN

DISSERTATION

zur Erlangung des akademischen Grades

d o c t o r   r e r u m   n a t u r a l i u m

(Dr. rer. nat.)

im Fach Chemie

eingereicht an der

Mathematisch-Naturwissenschaftlichen Fakultät I

der Humboldt-Universität zu Berlin

von

M. Phil. Murali Sukumaran

geb. am 05.06.1978 in Cheyyar, Indien

Präsident der Humboldt-Universität zu Berlin

Prof. Dr. J. Mlynek

Dekan der Mathematisch-Naturwissenschaftlichen Fakultät I

Prof. T. Buckhout, Ph.D.

Gutachter: 1. Prof. Dr. W. Rettig
2. Prof. Dr. W. Abraham
3. Prof. Dr. H.-G. Löhmannsröben

Tag der mündlichen Prüfung: 10.6.2005

Zusammenfassung

Die photophysikalische Kinetik von TICT-Zustände bildenden Verbindungen –Derivate von DMABN

Das Hauptaugenmerk der vorliegenden Arbeit richtet sich auf die Untersuchung der photophysikalischen Eigenschaften von Derivaten von N,N-Dimethylaminobenzonitril (DMABN) und N-Phenyl-pyrrolobenzonitril (PBN) als Donor-Akzeptor Verbindungen. Die untersuchten Verbindungen zeichnen sich durch Einführung von Fluor-Substituenten durch eine erhöhte Akzeptorstärke aus, wodurch neue Erkenntnisse bzgl. der intramolekularen Charge-Transfer-Zustände (ICT) gewonnen werden konnten. Hierbei wurden die Ergebnisse zum Verhalten der untersuchten Moleküle im angeregten Zustand mit denen der entsprechenden Basisverbindungen verglichen.

Die spektroskopischen und photophysikalischen Eigenschaften wurden sowohl durch die Anwendung der stationären und zeitaufgelösten Fluoreszenzspektroskopie bei Raum- und Tieftemperatur als auch durch Nutzung der transienten Absorptionsspektroskopie in Kombination mit quantenchemischen Berechnungen untersucht.

Im Unterschied zu den Basisverbindungen DMABN und PBN zeigen die Spektren der fluorierten Derivate nur eine einzige stark rotverschobene Fluoreszenzbande, die dem ICT-Zustand zugeordnet werden kann. Die extrem kleinen Quantenausbeuten, die typisch für alle fluorierten Derivate sind, können auf die Existenz eines weiteren strahlungslosen Deaktivierungskanals zurückgeführt werden. Der beobachtete ICT kann mit dem TICT-Modell (Twisted intramolecular Charge Transfer), bei dem von einer gegenseitigen Verdrillung der Donor- und Akzeptoreinheiten ausgegangen wird, erklärt werden. Weiterhin wurden die Variation der Verknüpfungsposition zwischen Donor- und Akzeptoreinheit sowie der Einfluss zusätzlicher Akzeptor-Substituenten auf die Eigenschaften der ICT-Zustände untersucht.

Durch die Ergebnisse dieser Arbeit konnte ein vertieftes Verständnis über die Ladungstrennungsprozesse in Donor-Akzeptor-Systemen, die sich durch eine starke Solvatochromie und die Existenz von strahlungslosen Deaktivierungskanälen auszeichnen, entwickelt werden. Es konnte die Möglichkeit der Besetzung von zwei verschiedenen ICT-Zuständen (TICT – verboten, mesomerer ICT – erlaubt) gezeigt werden.

Schlagwörter:
DMABN, Charge transfer, dual fluorescence, TICT

Abstract

The focus of this work is mainly concerned with the investigation of photophysical properties of electron donor-acceptor compounds, namely, derivatives of N,N-dimethylamino benzonitrile (DMABN) and N-phenyl-pyrrolobenzonitrile (PBN). New insights into the intramolecular charge transfer (ICT) states were obtained while dealing with an acceptor moiety of increased strength in the form of fluorinated analogues of both these compounds. The molecules studied in this work have been compared with their corresponding parent compounds to get more useful information on the excited state behaviour.

The spectroscopic and photophysical properties were studied using steady-state and time-resolved fluorescence at room and low temperature as well as with transient absorption spectroscopy in conjunction with quantum chemical calculations.

Unlike in the parent compounds DMABN and PBN, their fluorinated derivatives show only a single strongly red-shifted fluorescence emitted from the ICT state, and possess low quantum yields. The nearly non-fluorescent behaviour for all of these fluorinated derivatives investigated is due to the presence of a photochemical mechanism additional to that of ICT, which acts as a new non-radiative funnel. The ICT observed in these compounds can be explained by twisting motion taking place between the donor and acceptor moieties. Thus, twisted intramolecular charge transfer (TICT) model supports the observations. Apart from the changes in the strength of the acceptor moieties, the ICT nature has been further explored by changing their linking positions as well as with additional acceptor substituents.

From the findings obtained in this work, a deeper understanding of the charge separation processes occurring in donor-acceptor systems with high solvatochromism and non-radiative decay properties was obtained. The possibility for populating two different ICT states (of forbidden nature – TICT, and allowed nature – mesomeric ICT) has been exemplified.

To
My Parents

Contents

1   Introduction

1.1   Background and Motivation

Electron transfer (ET) processes play a major role in the photophysics of donor-acceptor aromatic systems. They can occur between separate molecules (intermolecular) or among the distinct regions within the same molecule (intramolecular). The resulting product, which occurs in these latter processes, is called intramolecular charge transfer (CT) state. The photoinitiated ET processes and CT states are of paramount importance in elucidating the photosynthesis in plants, and in the application of molecular device technology. Among the intramolecular CT processes, twisted intramolecular charge transfer (TICT) states have been the focus for many years due to the burgeoning area of physical, physical-organic and organic chemistry connected with a rationalization of the excited state behaviour of many dye systems. The innumerable applications are growing in various fields such as tailor-made fluorescent dyes [1, 2], sensing of free volume in polymers [3, 4], fluorescent pH or ion indicators [5, 6], fluorescent solar collectors [2], and electron transfer photochemistry [7]. The aim of this thesis lies in the investigation of the CT characteristics of fluorinated derivatives of N,N-dimethylamino benzonitrile (DMABN) and N-phenyl pyrroles. The central part of this dissertation deals with the nature of the excited states and dipole moment changes of different donor-acceptor systems. Furthermore, the modification of either the donor or acceptor strength in these types of molecules resulted in changes of photophysical properties that have been well studied in this work. Apart from that, also the change of the position of the acceptor or donor part influences the excited state properties of these systems. In order to gain further insight into the excited state of these investigated molecules, quantum chemical calculations were also done to support the experimental findings. The main families of the molecules investigated in this thesis are as follows:

DMABN   DMABN-F4

p-PBN   **m-PBN**
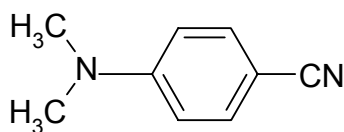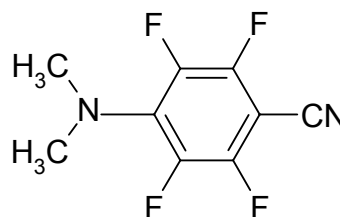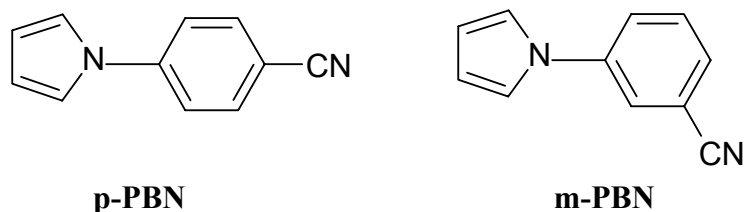
1.2   Outline of other Chapters

This introductory chapter presents the general motivation of this thesis, and serves as a guide to other chapter's work. Each following chapter contains its own introduction to the molecules investigated and its corresponding references.

In Chapter 2, the necessary theoretical background for the understanding of the work is clearly described. It also gives the general introduction of the concepts involved in this work.

Chapter 3 give details about the solvents used and their purification, and about the experimental methods like absorption spectroscopy, transient absorption spectroscopy, steady state and time resolved-fluorescence at different temperature used in this work.

In chapter 4, absorption and emission properties of the tetrafluoro analogue of DMABN, DMABN-F4 have been investigated and compared with the parent compound. The formation of a CT state of DMABN-F4 is a quasi-barrierless process in both polar and non polar solvents when compared to DMABN, and the TICT character has been confirmed by the combination of time resolved absorption and emission spectroscopy. The assumptions of Onsager radii by different methods on the excited state dipole moments values has been discussed. Electronic structure and conformational analysis of the investigated molecules were studied by quantum chemical calculations using semiempirical method.

Chapter 5 discusses mainly steady state absorption and emission characteristics of fluorinated derivatives of anilines and p-PBN such as such as ABN-F4, A-F5 and PBN-F4. Their non-fluorescent properties have been compared with DMABN-F4. The main reason for their non-fluorescent behaviour has been rationalized in terms of 'F' atom substitution, which acts as a new non-radiative funnel in all these type of compounds.

In Chapter 6, the photophysical properties of meta- and para-cyano N-phenyl pyrrole (m- and p-PBN) are compared. It has been found that both compounds show highly red shifted and strongly forbidden emission in polar solvents, assigned to a twisted intramolecular charge transfer state (TICT). Comparison to quantum chemical calculations

indicates that the twisted structure possesses an antiquinoid distortion of the benzonitrile group. It has been concluded that m-PBN differs from p-PBN by a less exergonic formation of the TICT state from the LE/ICT quinoid state, and it therefore shows only single LE/ICT fluorescence in nonpolar alkane solvents, whereas p-PBN shows dual fluorescence (LE/ICT and TICT).

Chapter 7 covers the photophysical studies on the meta-positioning effect on the dimethyl derivative of N-phenylpyrrole such as p-DPBN and m-DPBN. The results indicate that the CT state arises due to the twisting of the acceptor group. The twisting was enhanced by the positioning of the cyano group in the acceptor moiety that would lead to the higher rate of non-radiative decay in m-DPBN. The conclusion was drawn from the fact that irrespective of the meta positioning effect, these molecules possess similar excited state properties.

Chapter 8 presents photophysical studies on donor-acceptor compounds with a different linkage position on the donor such as MP2BN and additionally by changing the orientation of the acceptor part by increasing its strength such as MP2-B25CN. The mesomeric interaction between donor and the different acceptor units has been investigated, and it was found that the behaviour could switch between ICT states with large mesomeric interaction (MICT -Mesomeric Intramolecular Charge Transfer) such as in MP2BN, and with the minimum mesomeric interaction (TICT – Twisted Intramolecular Charge Transfer) states such as in p-PBN and MP2-B25CN. The factors are i) the relative energies of LE/ICT (MICT) and TICT state ii) the strength of the mesomeric interaction in the MICT state.

2   Theoretical Background

2.1   Mechanism of Dual Fluorescence

In general, fluorescent compounds possess a single fluorescence band, there are however, where two fluorescence bands are observed in compounds even in the case of a simple donor-acceptor benzene called 4,N,N-dimethylaminobenzonitrile (DMABN). This phenomenon was first discovered by Lippert et al. [8] The first band around 350 nm corresponds to the "normal" band for closely related benzene derivatives, the other one, at considerably longer wavelengths was assigned to an anomalous band. Lippert proposed a solvent-induced reversal of excited states. The anomalous band was assigned to fluorescence from the more polar ^1L_a-type state, which is preferentially stabilized by solvation. This has led to the nomenclature in photophysics: 'A' band for the "anomalous" emission from the ^1L_a-type state or charge transfer (CT) state and 'B' band for the normal short wavelength emission from the ^1L_b-type state or locally excited (LE) state. These emitting states are also called B* and A* states, and can be in thermal equilibrium. Lippert et al. [8] observed that the dual fluorescence strongly depends on the solvent polarity and on the temperature. In polar solvents, the long wavelength fluorescence band grows in relative intensity, while the intensity of the first band decreases with increasing polarity of the medium. The kinetic scheme for this process is shown below in Fig. 2.1

$$B^* \underset{k_{AB}}{\overset{k_{BA}}{\rightleftharpoons}} A^*$$

$$k_{Bf} \quad k_B^o \qquad k_{Af} \quad k_A^o$$
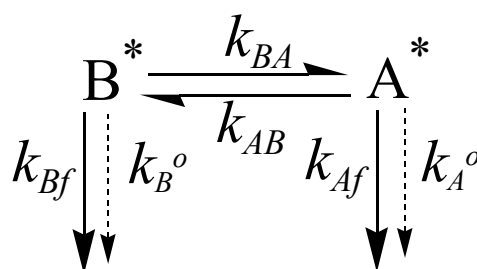
Figure 2.1: Kinetic scheme for the dual fluorescence of DMABN. Straight arrows represent radiative channels and dotted arrows represent non-radiative channels from the respective states.

The above scheme in Fig. 2.1 contains the reaction rate constants k_{BA} (forward reaction) and k_{BA} (backward reaction) as well as the radiative decay constants (k_{Bf} and k_{Af}) and the non-radiative decay constants k_B^0 and k_A^0 to the ground state. The origin of the dual fluorescence can be well-described in terms of photoinduced charge separation via

twisted intramolecular charge transfer (TICT) [9]. It occurs by an adiabatic photoreaction [10] taking place on the excited state potential energy hypersurface. The following sections will give a short description on the principles of photoinduced electron transfer.

2.2   Photoinduced Charge Transfer

In order to describe an electron transfer process, it is useful to draw potential energy surfaces, a graphical representation that allows one to visualize the details of the complex mechanism. A potential energy surface is a topological representation of the approximated coordinate dependence of the total energy parabolic curve, which can give an overview of a chemical reaction. Intersections of parabolic curves were used to represent the course of electron transfer from reactant to product. According to Marcus electron transfer theory [11, 12, 13, 14], there are two types of electron transfer reactions [15] taking place in donor-acceptor systems:
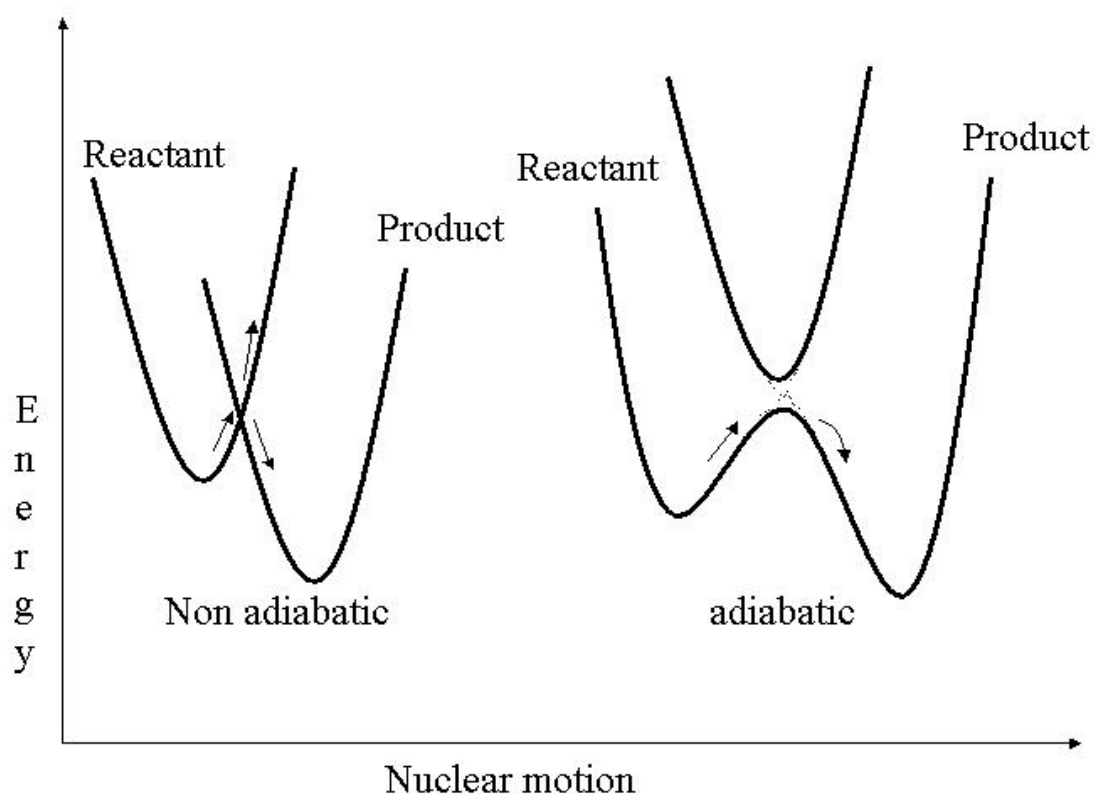
Figure 2.2: Potential energy diagrams of adiabatic and non adiabatic intersecting curves during electron transfer.

11

(i) Adiabatic: Electron transfer reactions that take place on a single potential energy surface with out intersecting one another.

(ii) Non adiabatic or diabatic: Process in which the potential energy surfaces that do not interact but intersect since the interaction between diabatic curves is weak as compared with the strong mixing in the adiabatic case.

There are different classes of adiabatic and non adiabatic photoreactions taking place in donor-acceptor systems. Here only the intramolecular and intermolecular electron transfer processes are considered in the following sections.

2.2.1 Intramolecular Electron Transfer

Intramolecular electron transfer is one of the main types of an adiabatic photoreaction, which forms the basis for dual fluorescence. The direct contact of the donor and acceptor molecules seems to be necessary for efficient electron transfer, particularly in the photoinduced electron transfer reactions. To be precise, after electronic excitation, electron transfer takes place from initial molecular orbital (MO) of the donor (D) state, to a MO of the final of the acceptor (A) state. When the donor and acceptor molecules are linked together by covalent bonds so that they are part of a single molecule, and the resulting electron transfer is called intramolecular. If an electron transfer from D to A is energetically feasible in the excited state, the product of such an intramolecular ET reaction is a charge-separated species, D^+.... A^-. Its electronic structure corresponds to the ground state of the free radical ion pair of opposite charges, consisting of a radical cation D^+ and radical anion A^-. This results in changes in the dipole moment values between ground and excited state that led to the charge transfer (CT) state. Relaxation processes e.g pyramidalization or planarization, linearization, bending or twisting etc. accompanied by during or after electron transfer reactions will cause various modifications in their electronic structure of the excited molecules. It is interesting to know which of the reaction coordinate determines the feasibility of electron transfer in this kind of donor-acceptor systems. There have been various mechanisms proposed to explain the phenomena of dual fluorescence, and these are as follows:

(i)   TICT- mechanism (Twisted Intramolecular Charge Transfer)

The TICT model was first put forward by Grabowski and coworkers [16, 17, 18] to account for the observation that the dual fluorescence of DMABN with its "normal" band (B- band) and its "anomalous" one depends on the conformational freedom of the dimethylamino (DMA) group, coupled with an electron transfer in the orthogonal conformation. In the case of DMABN, there exists a reaction path in the excited state leading from the near planar conformation (emitter of the B-band) to an excited photochemical product with an energetic minimum at the perpendicular conformation (emitter of the A-band). These two emitting states possess a mother-daughter relationship, which has been revealed by direct kinetic measurements [19]. In many cases, the back reaction A* → B* also occurs leading to an excited state equilibrium. The ground state of DMABN is known to possess an energy barrier for the perpendicular conformation (the rotational barrier), therefore the emission from the perpendicular excited-state minimum occurs to a repulsive potential and is expected to lead to structureless spectra. The key point here is that the reaction coordinate is not only the intramolecular twisting motion but involves other coordinates, too, such as electron transfer, solvent dipolar relaxation and, most probably, some rehybridization at the amino nitrogen. For the perpendicular TICT conformation, donor (dialkylamino group) and acceptor (benzonitrile) π-orbitals are orthogonal (zero overlap) and thus decoupled leading to a maximum for the dipole moment in the excited state (and a minimum in the ground state). This maximum of the dipole moment (near full electron transfer from donor to acceptor) connected with the energetic minimum for the perpendicular conformation are essential ingredients of the so-called "minimum overlap rule" [16]. For the near planar conformation (B* state), mesomeric interaction between the donor and acceptor π-systems exists and diminishes the dipole moment of B* state, and as schematically shown below:
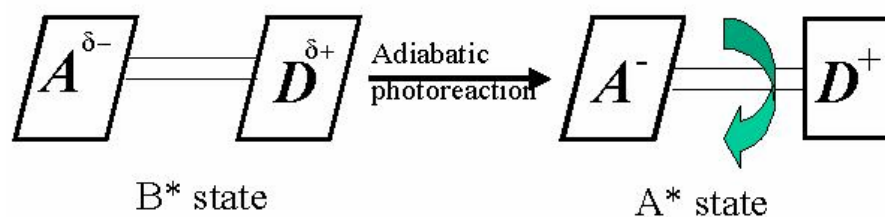
B* state   A* state

Figure 2.3: The TICT model involves a twisted product species with charge transfer or charge shift properties (A* state) formed through an adiabatic photoreaction from the precursor (B* state) with a nearly coplanar conformation.

$$E_{B^*} - E_{TICT} > 0 \qquad (2.1)$$

$$E_{TICT} = IP(D) - EA(A) + C + E_{sol} \qquad (2.2)$$

The above equations 2.1 and 2.2 can be used to predict possible new TICT systems. Whether or not the energetic minimum of the A*/TICT state is lower than that of the precursor B* state (inequality Eq. 2.1 fulfilled) sensitively depends on the electron donor-acceptor properties of the sub systems which can be quantified by ionization (or oxidation) potential and electron affinity EA (or reduction potential) of donor D and acceptor A.

The B* state responds much less to changes in donor and acceptor properties than the TICT state, and Eq. 2.1 can often easily be fulfilled by increasing donor and /or acceptor strength. In addition to these two factors which deliver the decisive part of the reaction driving force, polar solvent stabilization E_{sol} and the mutual Coulombic attraction C of the linked donor and acceptor radical anion/cation pair also help to preferentially stabilize the TICT state with respect to the precursor B* state.

(ii)   Pseudo – Jahn-Teller Mechanism:

Zachariasse et al. found a new explanation for the occurrence of dual fluorescence in DMABN based on a Pseudo – Jahn-Teller (PJT) distortion of the molecular structure. It correlates between the efficiency of the CT state formation and the $^1L_a-\,^1L_b$ energy gap in the absorption spectrum. They postulated that the proximity of these two electronic states favors the CT state. The PJT coupling of ^1L_a and ^1L_b states via the inversion mode (rehybridization) of the amino group is assumed to lead to a pyramidal geometry in the ICT state [20, 21, 22].

(iii)   Rehybridization of the acceptor (RICT model):

Apart from the amino group (donor) involvement in the CT state, there can also be another site of structural changes in the cyano substituent (acceptor), that is, a bending of the cyano group (rehybridization) taking place in the excited state. It was suggested that the latter could be responsible for the anomalous emission from the A* state [23, 24].

2.3   Intermolecular Electron Transfer

Intermolecular electron transfer is defined as the transfer of an electron density from one molecule to another molecule in the excited state. As a result, it forms a complex. It can be either excimer (excited dimer) or exciplex (excited complex). Collision between an excited and an identical unexcited molecule forms excimer whereas exciplexes are formed by collision of an excited molecule (electron donor or acceptor) with an unlike unexcited molecule (electron acceptor or donor). Excimer and exciplex formation processes are diffusion-controlled. The photophysical effects can thus be detected at relatively high concentrations of the species so that a sufficient number of collisions can occur during the excited-state lifetime. Temperature and viscosity are major governing parameters.

2.4   TICT Model Compounds

The TICT phenomenon is observed not only in DMABN, but also in its numerous derivatives and analogous compounds, with modified donor or acceptor groups in the benzene ring. When methyl groups were introduced in ortho or meta position to the N-Me$_2$ group of DMABN, different effects were observed. To analyse the possible role of the steric effect, a series of model compounds was synthesized [16, 17, 25, 26, 27], with the dialkylamino group structurally fixed nearly coplanar to the ring (MIN), or strongly sterically hindered (TMABN), or rigidly fixed in a position perpendicular to the aromatic ring (CBQ).

MIN   TMABN   CBQ   m-DMABN
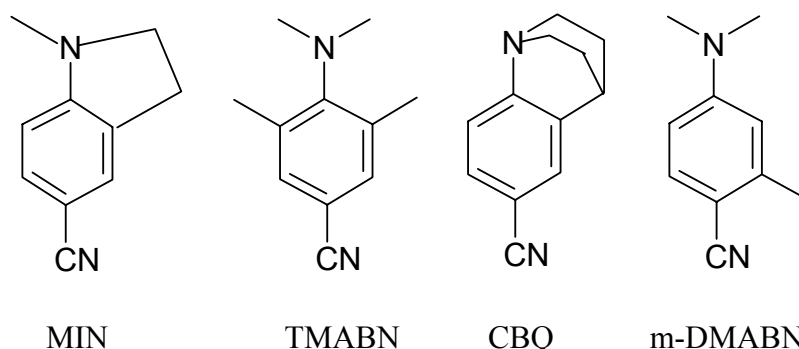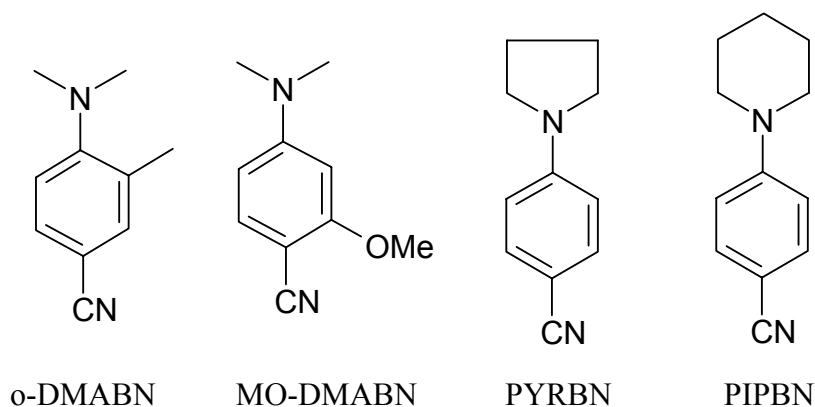
Figure 2.4: Scheme of model compounds

Compounds with a possible rotational degree of freedom around the benzene – amine bond such as DMABN, m-DMABN, MO-DMABN [17], PYRBN and PIPBN [28] exhibit a dual fluorescence, whereas for compounds MIN and CBQ with fixed rigid structure, only one band was observed: the 'B' band in MIN and the 'A' band in CBQ similar to DMABN. In the case of o-DMABN, only 'A' band has been observed. This was interpreted in terms of a steric effect: the methyl substituent in the position ortho to the $-NMe_2$ group sterically hinders the coplanar (quinoid) structure. Similarly, for pretwisted compounds such as TMABN and CBQ, where the nitrogen lone pair is nearly in-plane with the benzonitrile skeleton and perpendicular to the π–orbital system, only the A-band was observed. Thus the emission spectra of the model compounds exemplify the effect of the substituents sterically hindering the coplanarity of the $-NR_2$ group with the ring.

3   Experimental Section

3.1   Synthesis of the Investigated Compounds

DMABN

DMABN-F4

ABN-F4

A-F5

PBN-F4

p-PBN

m-PBN

p-DPBN

m-DPBN

MP2BN

MP2-B25CN
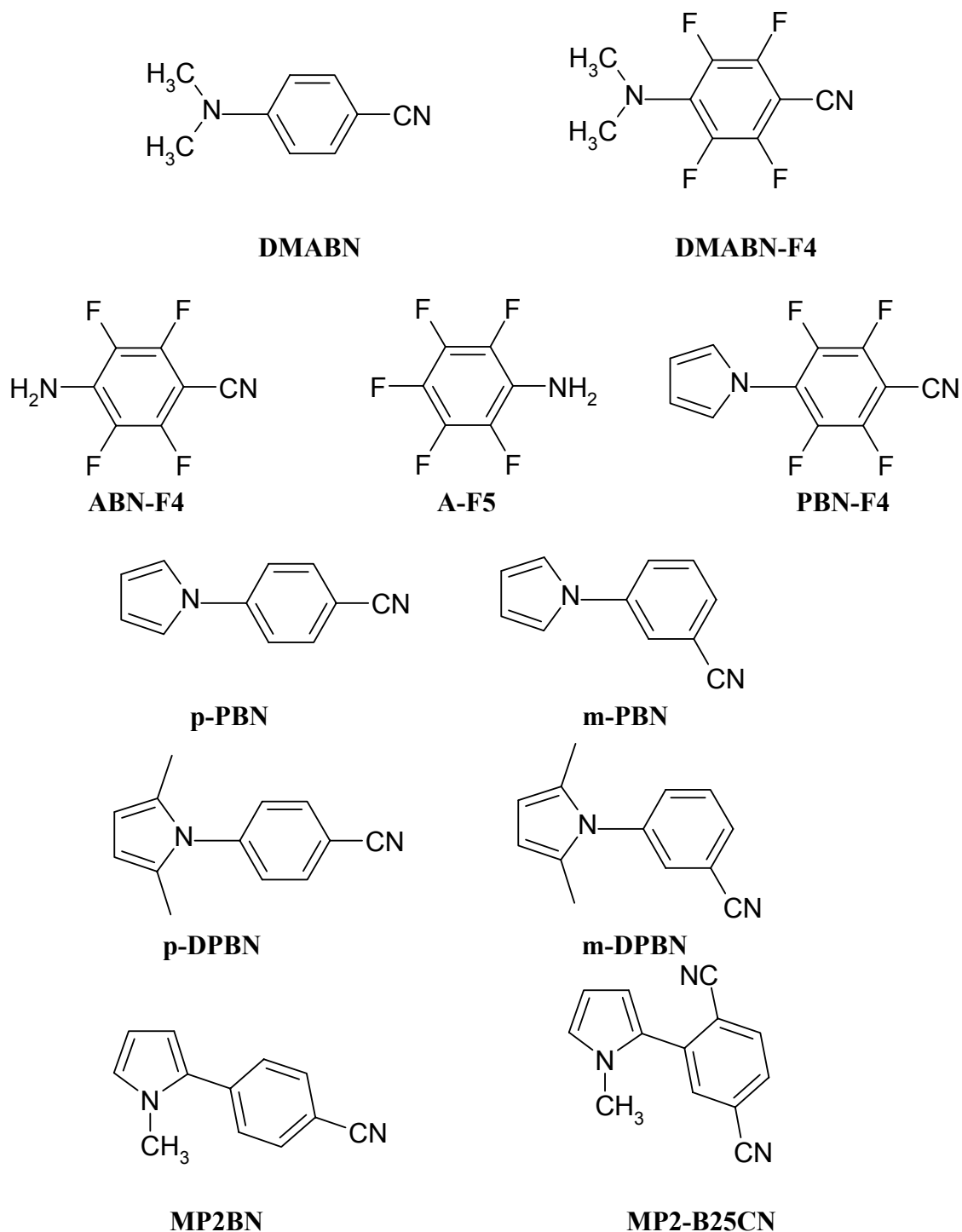
(i)   *DMABN – 4-(N,N-dimethylamino)benzonitrile:* It was obtained from Aldrich. Compounds p-PBN and m-PBN were synthesized in our group according to the

procedure [29, 30]. The absence of possible traces of impurities was checked by thin layer chromatography (TLC).

(ii) *DMABN-F4 – 2,3,5,6-tetrafluoro-4-(N,N-dimethylamino)benzonitrile:* It was synthesized by the reaction of pentafluorobenzonitrile with dimethylformamide using the procedure as described in ref. [31] The compounds was a gift of Prof. Alexei I. Tolmachev, Institute for organic chemistry of the national academy of sciences of Ukraine, Kiew, Ukaraine. The other fluorinated analogues ABN-F4, A-F5 and PBN-F4 were also a gift of the latter group.

(iii) p-DPBN - and m-DPBN: p-DPBN was synthesized by the condensation of 2,5-hexanedione with 4-aminobenzonitrile and taken from a previous publication [32]. m-DPBN was synthesized by the cyclocondensation of 2,5-hexanedione with 3-aminobenzonitrile [33]. The latter synthesis was kindly done by Mr. Sascha Jautze. The absence of impurities has been confirmed by NMR method and elemental analysis.

(iv) The other pyrrole derivatives such as MP2BN and MP2-B25CN were a gift of Prof. René Lapouyade, Ecole nationale supérieure de chimie et de physique de Bordeaux, Bordeaux, France.

3.2   Solvents Used

The solvents used in this work range from non-polar (alkane) to polar solvents (acetonitrile) and are of spectroscopic grade Merck (Uvasol) except n-butlychloride (Lichrosolv) and butyronitrile. The absorption and fluorescence spectra of all solvents were checked to make sure that they are devoid of impurities. The following table gives a list of the solvents and their parameters used in this work.

Table 3.1: Solvents used in this work and their parameters

Solvents	Abbreviations	ε^{20}	n_d^{20}	Δf [b)]	$\Delta f'$ [c)]
n-Hexane	HEX	1.89	1.375	0.000	0.0919
dibutylether	BOB	3.08	1.399	0.096	0.1931
diethylether	EOE	4.34	1.352	0.167	0.2558
n-butyl chloride	BCl	7.40	1.402	0.209	0.3071
Tetrahydrofuran	THF	7.58	1.407	0.210	0.3182

Acetonitrile	ACN	35.94	1.344	0.305	0.3928
Butyronitrile	BCN	20.30	1.384	0.275	0.3756
Methyl cyclohexane and isopentane (1:4)	MCH:IP	0.64	1.384	0.0	0.0000

b) $\dfrac{\varepsilon-1}{2\varepsilon+1}-\dfrac{n^2-1}{2n^2+1}$

c) $\dfrac{\varepsilon-1}{2\varepsilon+1}-0.5\dfrac{n^2-1}{2n^2+1}$

Where $\varepsilon-$ Relative dielectric constant of the solvent

               $n-$ Refractive index of the solvent.

3.2.1   Purification of Butyronitrile

To 500 ml of butyronitrile were added 2.5 spoons of charcoal and left to stand for one day. After filtration 2.5 g of potassium carbonate (K_2CO_3) were added. The mixture was allowed to stand for another day and then filtered. 20 g of phosphorus pentoxide were added to the filtrate and after allowing to stand for one day, a distillation was carried out. The purity of butyronitrile was tested by both absorption and fluorescence measurements.

3.3   Absorption and Fluorescence Measurements

Absorption spectra were measured on ATI UNICAM UV Series Spectrometer UV4-21113. Before measuring the absorption spectrum of the sample, the base line correction was done by placing solvent in both sample and reference Quartz cuvettes of 1 cm. The true absorption spectrum was measured by maintaining optical density of a solution between 0.1 and 0.2.

Fluorescence spectra were measured by using an AMINCO-Bowmann series 2 Luminescence spectrometer in which the excitation source is a 150 W Xenon lamp. The emission parameters in the set up are adjusted by keeping the optimum voltage of the photomultiplier between 600 and 800 V, slit widths of both excitation and emission monochromators at 4 nm and setting a scan rate of 2 or 3 nm per second.

3.3.1 Correction of the Emission Spectra

The emission spectrum recorded directly from a fluorescence spectrometer, when the emission monochromator is scanned at constant slit width and constant photomultiplier sensitivity, is an uncorrected spectrum. To determine the true spectrum, the observed spectrum has to be corrected with the wavelength dependent factors, namely the quantum efficiency of the photomultiplier, the band width of the monochromator and the transmission factor of the monochromator. These factors were determined by the manufacturer using a calibrated tungsten lamp. A reflector made of freshly prepared magnesium oxide is introduced into the sample holder and set at 45°, and is illuminated by the lamp externally positioned at right angles. The spectral response of the detection system is recorded and the correction factors are obtained by dividing this spectral response by the spectral output data provided with the lamp. For wavelengths shorter than about 320 nm, where the intensity of tungsten lamps is too low to get reliable correction factors, a hydrogen or deuterium lamp can be used. Here in this work, all the uncorrected fluorescence and excitation spectra have been corrected with the help of a correction file, determined in this way.

3.3.2 Low Temperature Measurements

Temperature dependent fluorescence spectra were measured with a homemade cooling apparatus that allows to simultaneously freeze and control the temperature of four samples in quartz cuvettes by pumping cold nitrogen gas through the cryostat. The temperature in the cuvettes was monitored using PT 100 resistor. The lowest temperature achieved with this set-up was 100 K.

For the 77 K measurements, a dewar flask with an optical access was filled with liquid nitrogen in which a quartz tube was filled with the sample solution was inserted. The solvents that form a glassy matrix are used for this kind of low temperature measurement. e.g. the MCH:IP alkane mixture, EOE and BCl.

3.3.3 Determination of Fluorescence Quantum Yields

For the determination of the fluorescence quantum yields of the probe ϕ_f^p, the optical densities of the solutions were determined at the excitation wavelengths in a 1cm absorption quartz cell and were adjusted to a value in the range 0.1-0.2 with a precision of 0.001. Fluorescence quantum yields of any substance can be determined by comparing with a

fluorescence standard whose quantum yield value is already known. For that purpose, the fluorescence standard, quinine bisulfate was used. The latter can be prepared as a solution in 0.05M in H_2SO_4, and the reference value is $\phi_f^s = 0.515$ [34]. While calculating the quantum yield of a sample, the value has to be corrected for the refractive index of the solvents using [35] equation (3.1).

$$\phi_f^p = \phi_f^s \frac{n_p^2 \, OD_s \, A_p}{n_s^2 \, OD_p \, A_s} \qquad \textbf{(3.1)}$$

where n_p and n_s are refractive indices of the solvents , OD_p and OD_s are the optical densities, ϕ_f^p and ϕ_f^s are the quantum yields, and A_p and A_s denote the computed area of the corrected fluorescence bands, each parameter for the sample solution and standard (reference), respectively.

The temperature dependent relative fluorescent intensities $I_f(T)$ are corrected for the linear increase of the refractive index n(T) [36] and density [36] of the solvent relative to room temperature conditions using equation (3.2).

$$\phi_f^{LT} = \phi_f^{RT} \frac{n_{LT}^2 \, \rho_{RT} \, A_{LT}}{n_{RT}^2 \, \rho_{LT} \, A_{RT}} \qquad \textbf{(3.2)}$$

where the terms in the above equation have their usual meanings. The error of the low temperature fluorescence quantum yields ϕ_f^p determined from the integrated intensity area relative to the values at room temperature is estimated to be 10%.

3.4 Time Resolved Fluorescence

The fluorescence decay measurements were performed by using time correlated single photon counting (TCSPC) [37]. They have been done either with Synchrotron radiation from the Berlin Storage Ring for Synchrotron radiation (BESSY) or with a ps-laser source. Both the methods are explained in the following sub sections.

3.4.1 BESSY II

Synchrotron radiation from the Berlin Synchrotron facility BESSY II was used as light source in conjunction with an excitation monochromator (Jobin Yvon, II, 10 UV). It delivers a 1.25 MHz pulse train with characteristic pulse widths of 30-50 ps. The fluorescence decays were detected by a microchannel plate photomultiplier (MCP, Hamamatsu R 1564-U-01) cooled to $-30\ ^{o}$C, coupled to an emission monochromator (Jobin Yvon II, 10 VIR) by means of quartz fiber optics. The signal from a constant fraction discriminator (CFD, Tennelec 454) was used as the start pulse for the time-to-amplitude converter (TAC, Tennelec TC864) operating in the reverse mode. The BESSY II synchronisation pulse was used as the stop pulse. The MCP pulses were amplified by an amplifier (INA 10386) and coupled into the CFD. A multichannel analyser (Fast Comtec MCDLAP) was used for data accumulation. The decays were analysed by the "least squares" iterative reconvolution method on the basis of the Marquardt-Levenberg algorithm, which is implemented in the commercial global analysis program [38]. The instrument response function was obtained by the detection of Rayleigh scattered light in a scattering solution and had a width of 120 ps. The quality of the exponential fits was evaluated on the basis of the reduced χ^2 values.
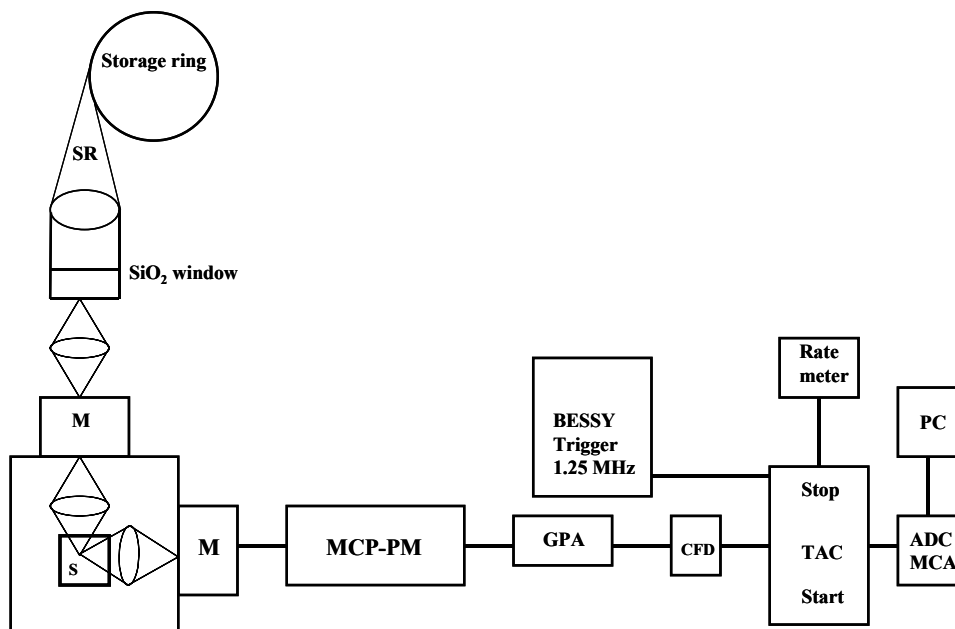
Figure 3.1: Construction of the Single Photon Counting (SPC) set up

M   :   Monochromators
S   :   Sample holder

MCP-PM	*:*	*Microchannel plate photomultiplier (Hamamatsu R 1564-U-01)*
GPA	*:*	*Gigahertz pre amplifier (INA 10386)*
CFD	*:*	*Constant fraction discriminator*
TAC	*:*	*Time to amplitude converter*
ADC	*:*	*Analog to Digital converter*
MCA	*:*	*Multi channel analyser*
PC	*:*	*personal computer*
SR	*:*	*Synchrotron radiation*

3.4.2 ps-Laser

The measurement has been done with a conventional setup using an argon ion laser-pumped, passively mode locked Ti:sapphire laser as the excitation source. The pulse duration is about 80 fs, and the repetition rate is 82 MHz. The excitation wavelength was obtained by frequency doubling or tripling of the fundamental wavelength of about 800 nm. The fluorescence and scatter light were detected as described in the method above. The instrument response function was obtained by detection of Rayleigh scattered light in pure solvents and had a width of 50-60 ps at the excitation wavelength and is dominated by the optical path difference in the monochromator. Detection without the monochromator yielded a pulse width of 28 ps. The entire operation of the equipment is also described in detail elsewhere [39, 40].
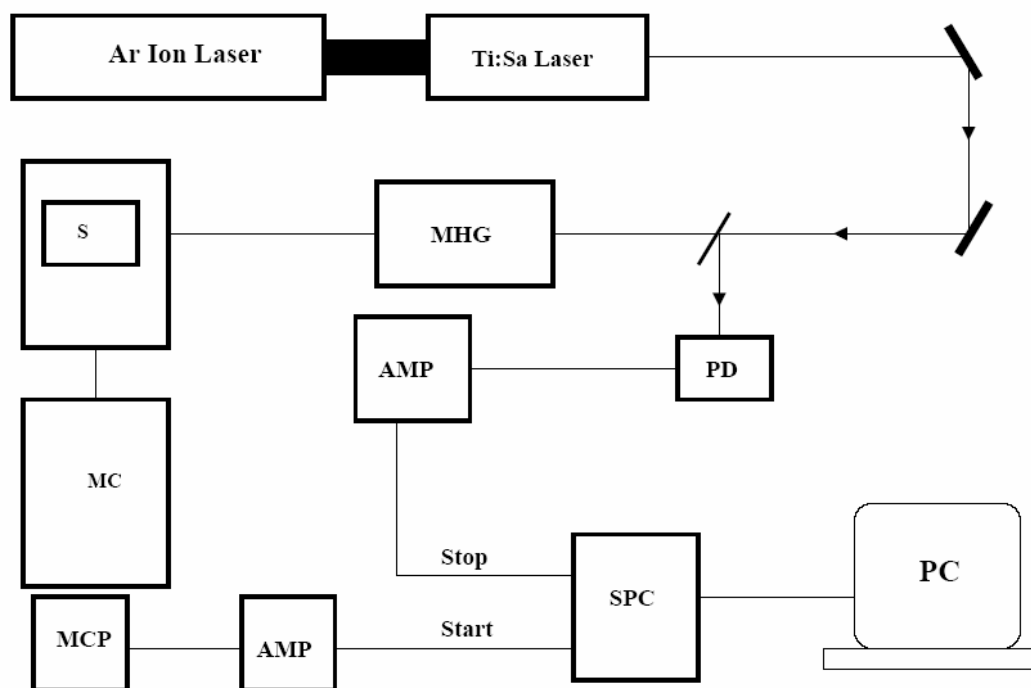
Figure 3. 2: Block diagram for the time resolved fluorescence measurements with the ps laser

MHG	*:*	*Multi harmonic generation*

S	:	Sample
MC	:	Monochromator
MCP	:	Micro channel plate photomultiplier
AMP	:	Amplifier
PD	:	Photodiode
SPC	:	Single photon counting setup
PC	:	Personal computer

3.5   Transient Absorption Spectroscopy

Time-resolved transient absorption and gain experiments were performed at the *Ecole Normale Supérieure, Paris* in collaboration with Dr. Monique Martin with the pump-probe technique using a home-made dye laser described in details elsewhere [41]. Subpicosecond pulses were generated at 610 nm and frequency doubled in order to obtain excitation pulses at 305 nm. The probe was a white-light continuum produced by focusing the residual 610-nm into a 1-cm water cell. The differential absorbance spectra were recorded in the 340-700 nm range through a polychromator by a CCD camera.
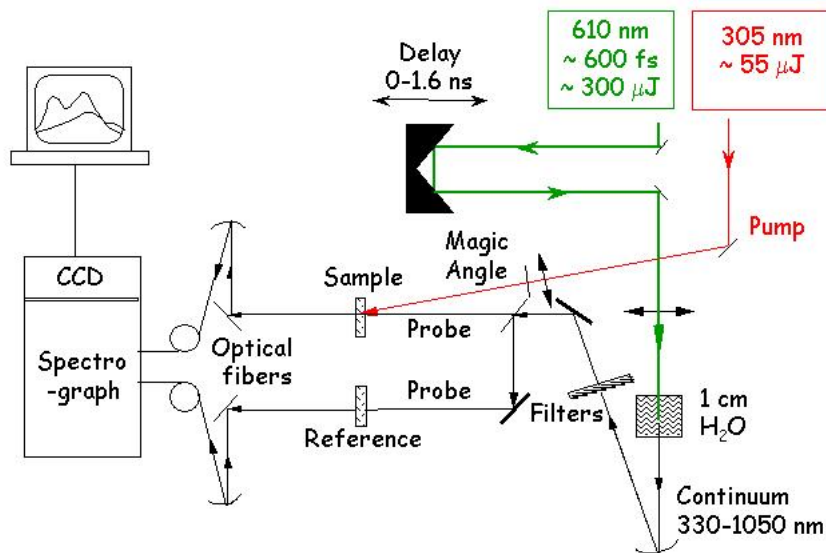
Figure 3.3: Pump-Probe set-up of Trasient Absorption Spectroscopy.

24

The energy of the pump beam was determined found to be 55 micro joule. The spectra were averaged over 500 laser shots and corrected for the group velocity dispersion in the probe beam. The experimental time resolution was estimated to be about 1.5 ps.

3.6 Quantum chemical Calculations

The electronic properties of a molecule can be calculated by solving the Schrödinger equation,

$$H\Psi = E\Psi \tag{3.2}$$

There are various methods available to calculate the structural and electronic properties of a molecule, such as *ab initio*, semiempirical and density functional theory (DFT) methods. The latter method has been gaining popularity over the recent years because of the intermediacy between *ab initio* and semiempirical methods. The Hartree-Fock procedure or self-consistent field (SCF) model plays a crucial role in electronic structure calculations. The SCF model uses the idea of particles moving in an average electrostatic field and therefore cannot accurately treat the instantaneous interaction between electrons (electron correlation). The SCF model for the calculation of orbitals makes use of the variational principle to minimize the energy of the system iteratively until it is self-consistent. *Ab initio* methods are characterized by the introduction of chosen basis set for expanding the molecular orbitals and then the explicit calculation of all required integrals involving this basis set. The same is valid for Density Functional Theory (DFT) calculations. DFT calculations have a different effective Hamiltonian than Hartree-Fock calculations but the SCF procedure used to solve for the molecular orbitals (Kohn-Sham orbitals in one case and Hartree-Fock orbitals in the other case) is very similar.

Ab initio calculations can be extremely demanding in terms of the computational resources. But nevertheless, improvements in the computer hardware have made it possible that *ab initio* methods are a widely used computational tool nowadays. The approximate quantum chemical methods require significantly less computational resources. Especially, semi-empirical methods, which satisfy the latter criteria by incorporating the parameter, derived from the experimental data can calculate some electronic properties more accurately than even very high levels of *ab initio* calculations. There are number of ways in which

correlation effects can be incorporated into the molecular orbital (MO) calculation. One popular approach is configuration interaction, in which various excited configurations are included in the description of an electronic state. The electron correlation problem is meticulously handled on the basis of configuration interaction by both *ab initio* and semi-empirical method. In this work, mainly the semiempirical method AM1 (Austin model 1) [42, 43], which has an increased improvement over the other semiempirical method like MNDO, was used together with multiexcited configuration interaction.

The treatment of the compounds studied in this work included full geometry optimization in the ground state without configuration interaction using the AM1 method [42] contained in the AMPAC program package [44] running under the Linux operating system. Single point calculations (1SCF) for the Franck-Condon excited states were performed by taking the fixed optimized ground state geometry and using configuration interaction including 300-400 singly and multiply excited configurations constructed on the basis of the central sixteen molecular orbitals.

4 The Tetrafluoro Analogue of DMABN: Anomalous Fluorescence and Mechanistic Considerations

Abstract

Absorption and emission properties of DMABN-F4, the tetrafluoro analogue of DMABN, have been investigated and compared with the parent compound. Unlike in DMABN, this new compound exhibits only a highly solvatochromic and strongly redshifted fluorescence CT and is characterized by the absence of an LE band even in nonpolar solvents. This evidences the faster formation of CT in the excited state as compared to DMABN. The low quantum yield values of DMABN-F4 suggest that the high rate of non-radiative decay takes place via internal conversion (*IC*) rather than intersystem crossing (*ISC*) as no phosphorescence is observed in rigid glass solvents at 77 K in contrast to DMABN. The emission transition moment and radiative rate constant values of DMABN-F4 in medium and highly polar solvents point to a forbidden emission in the excited state similar to DMABN. Electronic structure and twist potentials were also studied by quantum chemical calculations using ab initio and semiempirical methods. In contrast to DMABN, DMABN-F4 is found to be twisted by around 30-50°, but the photophysics are concluded to be analogous to DMABN with the addition of a very fast IC channel.

4.1 Introduction

Donor-Acceptor substituted benzenes have been the focus for many years regarding the nature of dual fluorescence or of emissions with very large Stokes shifts. *Lippert* et al. [8] showed that DMABN emits a dual fluorescence consisting of two bands assigned to two different excited states: The A band for the "anomalous" emission from the ^1L_a-type state, B band for the normal short wavelength arises from the ^1L_b-type/CT state. The emitting species, also called A* and B* states, can be in thermal equilibrium.

The photophysics of electron donor-acceptor aromatic systems has been well explained with the help of the TICT model ("Twisted Intramolecular Charge Transfer"). According to this model, [1, 9, 16, 19] the untwisted dimethylamino group (electron donor) rotates after photoexcitation towards an orthogonal orientation of the donor group relative to the aromatic ring system. In nonpolar solvents and under jet-cooled conditions, DMABN

emits only from the near planar LE excited state, [22] whereas a second minimum at a twisted conformation is populated on the excited state energy surface in more polar solvents.

Recently, the effect of F-substitution in DMABN-derivatives has been investigated for 4-(azetidinyl)benzonitrile by Druzhinin et al [45] who stated that there is no indication of dual fluorescence, and that internal conversion is enhanced by the fluoro substituent.

DMABN-F4 which differs more from DMABN by the further increased strength of the acceptor unit leads to the expectation of an increased CT nature of the excited state. In the present chapter, DMABN-F4 is characterised spectroscopically and compared with DMABN. The investigation of the spectroscopic behaviour includes both polarity and temperature effects. The red shift of both absorption and more strongly fluorescence spectra can be ascribed to this increase of the acceptor nature quantifiable by an enhancement of the electron affinity (EA) by 0.78eV.

In order to compare and interpret the spectroscopic properties, quantum chemical calculations were performed using ab initio and semiempirical methods.
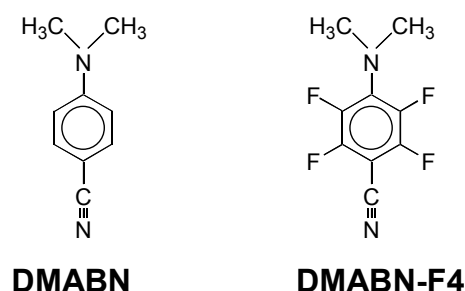
DMABN   **DMABN-F4**

Figure 4.1: Structure of the molecules investigated

4.2 Experimental Section

4.2.1 Materials

The compounds with their structures and abbreviations are shown in Fig. 4.1 DMABN-F4 was synthesized by the reaction of pentafluorobenzonitrile with dimethylformamide using the procedure described in ref. [46] DMABN was a sample previously used. The absence of possible traces of impurities was confirmed by thin layer chromatography (TLC).

4.2.2 Apparatus and Methods

The experimental details about the absorption, fluorescence, lifetime and quantum yield measurements are described in chapter 3.

4.2.3 Calculational Details

Semiempirical calculations for the compounds **DMABN** and **DMABN-F4** were carried out with full geometry optimization and with a vibrational analysis of the optimized structures by the Newton algorithm using the AM1 program contained in the AMPAC 6.0 package [42, 44].

The study of equilibrium and transition structures for the compounds by ab initio calculations at Hartree-Fock theory HF and Density Functional Theory DFT levels were realized with different basis sets (6-31G(d), 6-311++(d,p), cc-pVDZ, and D95(d,p)) using Gaussian 98 [47]. Full optimization of the ground state including vibrational analysis was performed to detect stable minima and transition geometries. The twist angle between the compound fragments was determined as the torsional angle between the lone pair on the nitrogen atom and the benzene plane from the bisector between the optimized torsional angles of the carbon atoms of the dimethylamino group (see Scheme 2). The study of the fragment rotation in the S_0-state was carried out by fixing the torsional angle of one carbon atom of the dimethylamino-group optimizing all other geometrical parameters.

The calculations of the transition energies and oscillator strengths for the ground state optimized geometries were carried out using configuration interaction (CI) for the optimized structures with inclusion of 10 unoccupied and 10 occupied orbitals (C.I. = 10) by ZINDO/s (CIS) included in Gaussian 98.

4.3 Results and Discussion

4.3.1 Absorption Spectra

The absorption spectra of DMABN-F4 in various solvents of different polarity are depicted in Fig.1a. The corresponding spectra of DMABN are also presented for comparison (Fig. 4.2b). All spectra of DMABN-F4 as compared with the spectra of DMABN are shifted to the red (Table 4.1a). But in contrast to DMABN, in the spectrum of DMABN-F4 in hexane the weak shoulder is not visible, which is found at the red side of the main absorption maximum of DMABN and ascribed to absorption to the ^1L_b-S_1 state. It can be concluded that

29

the weak ^1L_b absorption band of DMABN-F4 is hidden by the stronger ^1L_a type band. It is even possible that the ^1L_a state is S_1 in this compound.
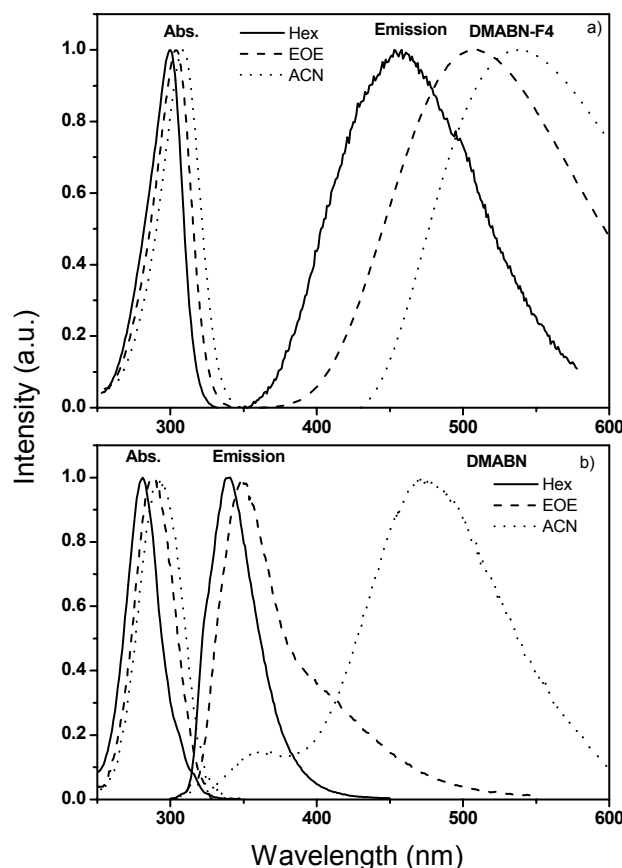
Figure 4.2: Absorption and normalised fluorescence spectra at room temperature of DMABN-F4 (a) and DMABN (b) in various solvents of different polarity. Hex = n-hexane; BCl = n-butyl chloride ; EOE =diethyl ether; ACN = acetonitrile.

The molar extinction coefficient values for both compounds determined in n-hexane are approximately equal [ε (λ_{282}^{max}) = 28,911 and ε (λ_{300}^{max}) = 34,436 respectively for DMABN and DMABN-F4]. In view of the twisted ground state structure of DMABN-F4, this might indicate a different vibronic mixing of the two lowest singlet states, ^1L_a and ^1L_b.

Analogous to DMABN, the long wavelength absorption band of DMABN-F4 is shifted to the red by increasing the solvent polarity (Fig. 4.2a and Tables 4.1a and 4.1b).

4.3.2   Fluorescence at Room Temperature

TABLE 4.1a: Photophysical parameters of DMABN-F4 in Various Solvents at Room Temperature

Solvent[a]	λ_{abs} (nm)	λ_{flu} (nm)	$\Delta\nu_{st}$ (10^3 cm^{-1})	ϕ_f	k_r (10^6 s^{-1})	k_{nr} (10^8 s^{-1})	M_f (D)
Hex	300	456	11.40	0.0006	2.22	37	0.53
BOB	302	490	12.70	0.0018	1.74	9.6	0.50
BCl	306	496	12.52	0.0016	1.34	8.4	0.45
ACN	308	537	20.86	0.0001	0.47	47	0.33

TABLE 4.1b: Photophysical parameters of DMABN in Various Solvents at Room Temperature

Solvent[a]	λ_{abs} (nm)	λ_{flu} (nm)	$\Delta\nu_{st}$ (10^3 cm^{-1})	ϕ_f	ϕ_{tot}	ϕ_a/ϕ_b	ϕ_{tot}	ϕ_a/ϕ_b
Hex	282	341	6.14	0.1642	0.16	-	0.11[b]	-
BCl	288	349 (B)	6.06 (B)	0.065 (B)	0.12	0.82	0.09[c]	0.8[d]
		390 (A)	9.08 (A)	0.053 (A)				
ACN	292	365 (B)	6.85 (B)	0.0016 (B)	0.02	10.12	0.02[b]	-
		476 (A)	13.24 (A)	0.0162 (A)				

[a] Solvent abbreviations: Hex – n-hexane; BOB – di-n-butyl ether; BCl – n-butyl chloride; ACN – acetonitrile. [b] Rettig, W.; Bliss, B.; Dirnberger, K. *Chemical Physics Letters* **1999**, *305*, 8. [c] Rettig, W.; Wermuth, G.; Lippert, E.; *Ber. Bunsenges. Phys. Chem.* **1979,** 83, 692. [d] Rotkiewicz, K.; Köhler, G.; *J. Lumin.,* **1987,** 37, 219.

In all solvents studied, DMABN-F4 possesses very weak fluorescence (quantum yield $\phi_f \leq 0.002$) with a broad emission band ($\Delta\nu_{1/2} > 6000$ cm^{-1}) shifted unusually far from the long wavelength absorption band (Stokes shift $\Delta\nu_{st} \geq 11000$ cm^{-1}) even in hexane (Table 4.1a and Fig. 4.2a) In contrast, in the latter solvent the emission of DMABN is relatively strong ($\phi_f = 0.17$) and narrow (Fig. 4.2b and Table 4.1b). The absence of dual fluorescence and the indicated fluorescence properties (strong red shift) suggest a very fast formation of an emitting *CT* species in the excited singlet state of DMABN-F4 in contrast to DMABN. As one can see from Table 4.1a, quantum yield values decrease from low-polarity to high-polarity solvents with the exception of hexane, where an anomalously high k_{nr} is found.

The fluorescence decay curves measured for DMABN-F4 in different solvents are monoexponential and similar for different wavelengths of the emission spectra with the fluorescence lifetime ranging between 0.21 and 1.19 ns (Table 4.1a). These measurements support the formation of only one emitting state in all solvents.

If we assume the direct formation of the emitting species without losses (i.e. validity of the Kasha rule), then the radiative k_r and nonradiative k_{nr} rate constants can be calculated according to equations 4.1 and 4.2,

$$k_r = \phi_f / \tau_f \qquad (4.1)$$

$$k_{nr.}^{tot} = k_r (\phi_f^{-1} - 1) \qquad (4.2)$$

where k_{nr}^{tot} corresponds to the sum of all nonradiative processes including triplet formation, internal conversion and the possible formation of nonemissive photochemical products. The k_r values are extremely small and decrease from about 2×10^6 s^{-1} (the corresponding the radiative life time τ_r is 450 ns) in hexane to 0.5×10^6 s^{-1} (τ_r is 2100 ns) (Table 4.1c) in acetonitrile. Similarly low k_r values were observed for a sterically hindered DMABN analogue, TMABN [48, 49] in which two methyl groups are present in ortho positions of the DMABN, in the highly polar solvent propanol (5.1×10^6 s^{-1}). This gives supporting evidence for the forbidden radiative transition from the excited state, which is typical for TICT states.

The formation of full charge transfer (i.e. a TICT state) in DMABN-F4 has been recently confirmed by time resolved absorption spectroscopy [50]. The transient absorption spectrum in acetonitrile at 1 ps delay showed a band around 360 nm. It was attributed to the CT state by its similarity with that reported for DMABN at 100 ps. The much faster appearance time of the CT state of DMABN-F4 suggests that the CT formation is a quasi-barrierless process in both polar and non polar solvents in this molecule and that TICT state formation is strongly favored with respect to DMABN.

TABLE 4.1c: Photophysical Parameters (radiative life time τ_f, radiative k_r and non-radiative k_{nr} rate constants, the CT Transition Dipole Moment, M_f) of DMABN-F4 and DMABN in Various Solvents at Room Temperature

Solvent	DMABN-F4				DMABN			
	τ_f (ns)	k_r (10^6 s^{-1})	M_f (D)	k_{nr} (10^8 s^{-1})	τ_f (ns)[a]	k_r (10^6 s^{-1})	M_f (D)	k_{nr} (10^8 s^{-1})
Hex	0.27	2.22	0.53	37	2.3	48[a]	1.53[d]	3.9[a]
BOB	1.03	1.74	0.50	9.6		-	-	-
BCl	1.19	1.34	0.45	8.4		13.6[b, c]	0.96	-
ACN	0.21	0.47	0.33	47	3.0	7[a]	1.12[e]	3.3[a]

[a] Rettig, W.; Bliss, B.; Dirnberger, K. *Chem Phys Lett* **1999**, *305*, 8-14. [b] Rettig, W.; *J. Lumin.*, **1980,** 26, 21. [c] Van der Auweraer, M.; Grabowski, Z. R.; Rettig, W. *J. Phys. Chem.* **1991**, *95*, 2083. [d] corresponds to the LE state. [e] Okada, T.; Uesugi, M.; Kohler, G.; Rechthaler, K.; Rotkiewicz, K.; Rettig, W.; Grabner, G. *Chem. Phys.* **1999**, *241*, 327.

The radiative transition moment values M_f in Table 4.1c as calculated from eq. 4.3 decrease from hexane to acetonitrile in the case of DMABN-F4 in contrast to DMABN and TMABN, where the M_f values are independent of polarity [49, 51]. The small magnitude of M_f in DMABN-F4 is typical for the twisted structure of a TICT-state. In the case of TMABN, the smaller values of M_f can be interpreted by sterical hindrance, which leads to a narrowing of the angular distribution around 90° as compared to the unhindered compound DMABN and therefore to more strongly forbidden emission. It is remarkable that M_f of DMABN-F4 in acetonitrile is the smallest value ever reported for the TICT fluorescence of an aniline derivative, lower even than for TMABN or other twisted model compounds of DMABN.

$$M_f = \sqrt{3hk_r / 64\pi^4 n^3 \nu_f^3} \qquad (4.3)$$
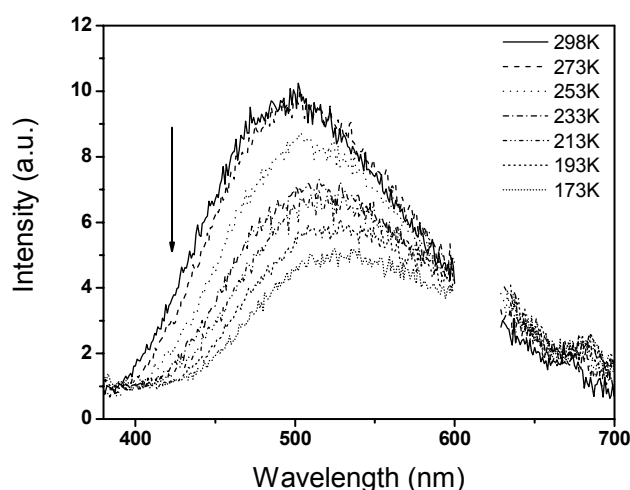
Figure 4.3: Low temperature effects on the fluorescence spectra of DMABN-F4 in n-butyl chloride. Down head arrow indicates the decreasing of temperature. The data points in the range 600-630 were omitted (second order of excitation wavelength).

TABLE 4. 2: Temperature Dependence of the Photophysical Data of DMABN-F4 in BCl

T (K)	λ_{max}^{flu} (nm)	ν_{flu} (cm^{-1})	$\Delta\nu_{1/2}$ (cm^{-1})	ϕ_f	τ_f (ns)	k_r (10^6 s^{-1})	k_{nr} (10^8 s^{-1})
298	501	19960	6320	0.0016	1.19	1.34	8.40
273	505	19802	6910	0.0014	1.20	1.25	8.32
253	510	19608	5730	0.0013	1.19	1.09	8.37
233	516	19380	5910	0.0011	1.15	0.96	8.71
213	521	19194	5850	0.0009	1.09	0.92	9.19
193	530	18868	6300	0.0007	0.99	0.81	10.1
173	535	18692	7100	0.0006	-	-	-
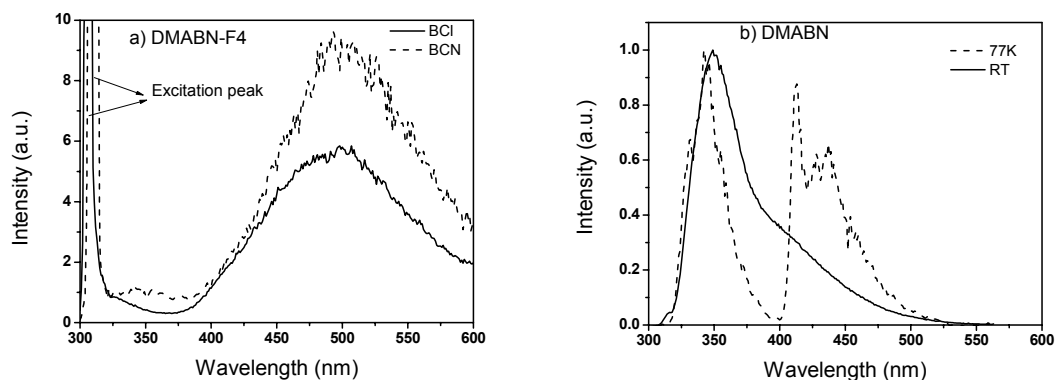
Figure 4.4: Fluorescence spectra of a) DMABN-F4 in BCl and BCN at 77 K and b) DMABN in BCl at room temperature and at 77 K.

4.3.3 Fluorescence at Low Temperatures

The fluorescence study of DMABN-F4 at lower temperatures was done in n-butylchloride in order to study the relaxation processes in a glassy matrix. These measurements detected a weak red shift of the emission maximum from 501 to 535 nm and a decrease of the fluorescence quantum yield by more than a factor of 2 when the solvent is cooled from room temperature to 173 K (Figs. 4.3 and 4.4, Table 4.2). Further cooling until 77 K did not allow quantum yield measurements, but the fluorescence band is found to be weak and shifted somewhat to the blue. However, even with the rigid glass matrix at 77 K the LE emission and phosphorescence are absent. In contrast to this, DMABN at 77 K possesses only the LE emission at 342 nm and phosphorescence is observed at 411 nm with a highly structured band (Fig. 4.4b). The small fluorescence intensity and the redshifted spectrum of DMABN-F4 at 77 K gives evidence that the emission is forbidden and that there is some relaxation even in a highly polar glassy matrix.

4.3.4 Geometry of the Ground State

The calculations indicate that in contrast to planar DMABN, the derivative with fluorine atoms DMABN-F4 possesses a somewhat twisted equilibrium geometry in the ground state (torsional angle between the fragments is 35 – 50 degrees, depending on the calculation method, see Fig. 4.5 and Table 4.3). The reason is a stronger sterical interaction between the two methyl groups of $N(CH3)_2$ and the fluorine atoms in the benzene ring. The

interaction is caused by the longer C-F bond (close to 1.3 Å for all calculation methods) in DMABN-F4 as compared to the C-H bond length close to 1.08 Å in DMABN. The pyramidalization of the dimethylamino group of DMABN-F4 is predicted very differently depending on basis set and method used. For the conditions of Fig. 4.5, it is practically nonpyramidal in the equilibrium structure (near sp^2 hybridization). Similar strong variations of the pyramidalization depending on the method can be observed for DMABN (Table 4.3).
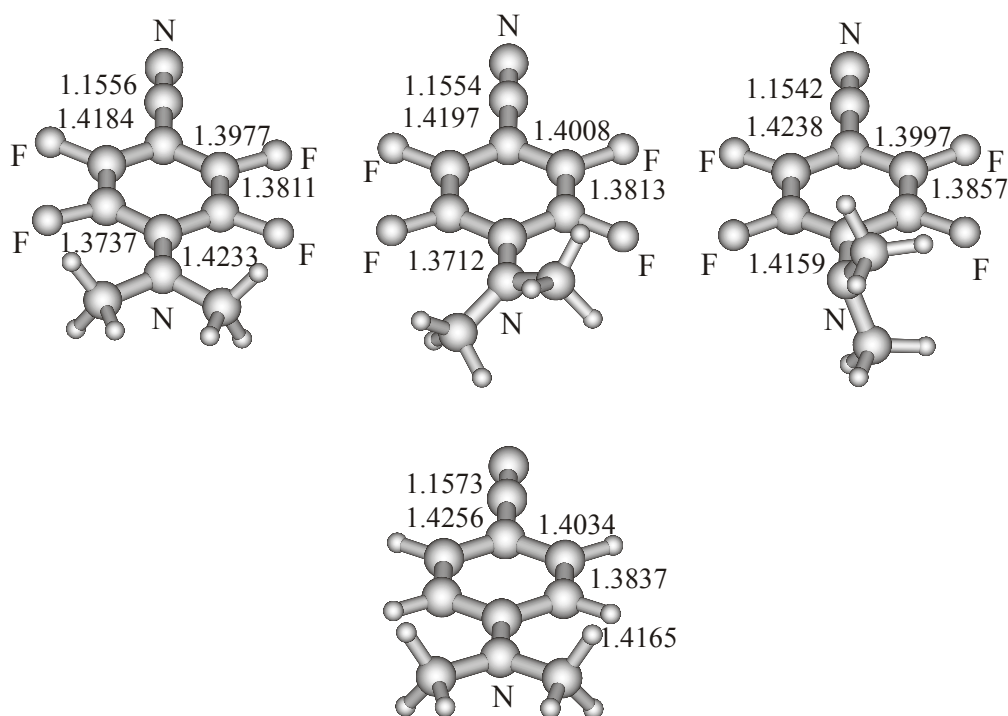
Figure 4.5: The planar transition, twisted equilibrium and perpendicular transition structures of DMABN-F4 and the planar equilibrium geometry of DMABN with some geometrical characteristics calculated by DFT (B3LYP/6-311++G(d)).

For comparable methods, both semiempirical and ab initio calculations demonstrate a smaller sp^3 hybridization of the dimethylamino group for the relaxed

geometries of DMABN-F4 than for DMABN (from AM1, equilibrium pyramidalization angles are around 13° and 29° deg respectively, Table 4.3).

TABLE 4.3: Ground State Characteristics of the molecules studied: Dipole Moment μ_{eq}, Equilibrium Twist Angle α_{eq}, Equilibrium Pyramidalization Angle β_{eq}, Activation Barrier of the Intramolecular Fragment Rotation to the Planar ($\Delta H(00)$) and the Perpendicular ($\Delta H(90)$) Geometry for DMABN-F4 and DMABN as Calculated by Different ab initio and Semiempirical Methods and different basis sets.

Compound	Method	μ_{eq} (D)	α_{eq} (deg)	β_{eq} (deg)	$\Delta H(00)$ (kcal/mol)	$\Delta H(90)$ (kcal/mol)
DMABN-F4	AM1	4.62	29.34	10.84	1.35	2.52
	HF	6.64[a]	33.35	0.07	4.58	0.38[b]
		6.19[c]	51.99	29.56	5.36	0.50[b]
		5.97[d]	51.27	29.86	4.76	0.47[b]
		6.10[e]	53.29	31.98	5.41	0.30[b]
	DFT (Becke3LYP)	7.09[a]	33.70	0.87	3.09	3.32
		7.48[c]	35.09	0.01	3.76	3.23
		6.56[d]	38.18	11.55	2.87	3.05
		7.10[e]	40.09	20.78	3.15	3.08
	MP2	6.58[a]	40.86	0.00	4.27	-
DMABN	AM1	5.35	0.00	25.15	0.00	2.45
	HF	7.29[a]	0.00	14.85	0.00	2.09
	DFT (Becke3LYP)	7.63[a]	0.00	0.95	0.00	5.98
		7.87[f]	0.00	6.50	0.00	11.27
	MP2[g]	-	0.00[a]	28.8	-	-

[a] 6-31G(d) basis set. [b] local minimum. [c] 6-311++G(d) basis set; [d] cc-pVDZ basis set. [e] D95(d,p) basis set. [f] TVZP basis set [Parusel, A. B. J. *Physical Chemistry Chemical Physics* **2000**, *2*, 5545.]. [g] [Sobolewski, A.L.; Sudholt, W.; Domcke, W.; *J. Phys. Chem. A*, **1998**, 102, 2716]
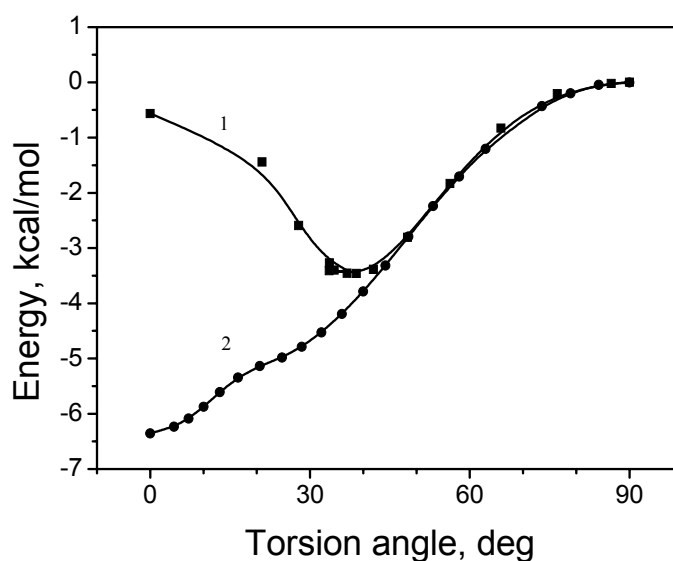
Figure 4.6: The ground state potentials of DMABN-F4 (1) and of DMABN (2) calculated by DFT (B3LYP/6-31G(d)) method. The torsion angle is determined according to figure 4.7. The inflection in the potential for DMABN at around 15° is due to different methyl group conformations being the most stable ones (see Scheme 4.8).

The intramolecular fragment rotation away from the equilibrium geometry to the planar and perpendicular geometry of DMABN-F4 (Table 4.3, Fig. 4.6) increases the potential energy. Both planar and perpendicular geometries possess a C_s symmetry and correspond to a saddle point (Fig. 4.7) (one negative Eigenvalue in the Hessian matrix).

TABLE 4.4: Relative Energy[a] (from DFT-B3LYP/6-31G(d) calculations) in kcal/mol, (number of negative Eigenvalues χ of the Hessian matrix) and the Symmetry Point Group for Planar Arrangements of the Dimethylamino Group (figure 4.8) of the Compounds DMABN and DMABN-F4

Compound	syn1	syn2	syn3
DMABN	0.00 (χ=0)	2.39 (χ=2)	1.39 (χ=2)
	C_s	C_{2v}	C_s
DMABN-F4	0.00 (χ=1)	1.54 (χ=2)	0.62 (χ=2)
	C_s	C_{2v}	C_s

[a] relative to the energies calculated for the nontwisted equilibrium (DMABN) and nontwisted transition geometries (syn1) (DMABN-F4) both slightly pyramidal .
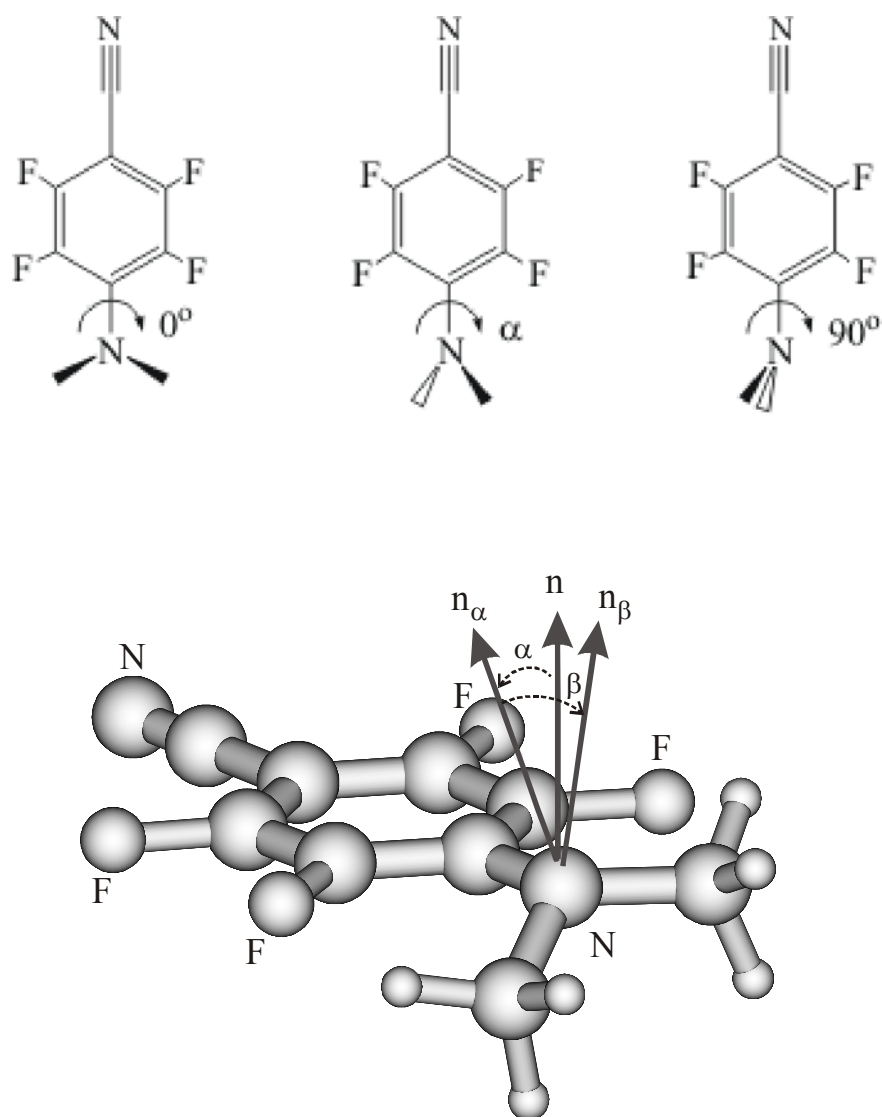
Figure 4.7: Planar, equilibrium and perpendicular structures of the dimethylamino group for **DMABN-F4** in the ground state (top). Determination of the dimethylamino-group twist angle α and the dimethylamino group pyramidalization angle β (bottom): n is a vector perpendicular to the plane of the aromatic ring, n_α is the bisector vector of the two N-methyl bonds of the dimethylamino-group, n_β is a vector perpendicular to the CNC plane of the dimethylamino group.

syn1	**syn2**	**syn3**
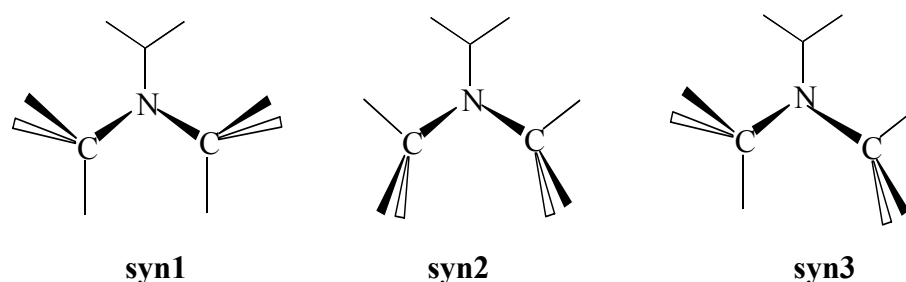
Figure 4.8: conformation of methyl-group of dimethylamino-group for **DMABN-F4** and **DMABN** in the ground state.

A study of the possible conformations of the two methyl group of the dimethylamino $N(CH3)_2$ fragment shows that several conformers are important (Fig. 4.8) that only conformer *syn1* with C_s symmetry for the planar and twisted geometries has the lowest energy, and the Hessian matrix indicates a saddle point of first order. The other conformers *syn2* and *syn3* of the symmetries C_{2v} and C_s possess saddle points of second order (Table 4.4). Depending on the twist angle, the relative energy of the conformers can change. This is the reason for the inflection in the potential for DMABN at around 15° (Fig. 4.6).

4.3.5 Dipole moments at Room Temperature

The excited-state dipole moments μ_e of DMABN-F4 and DMABN were determined from the solvatochromic slopes by applying the Mataga equation (4.4) [52, 53, 54]. The slopes from the corresponding solvatochromic plots of the emission maxima against the solvent polarity parameter, $\Delta f'$ can be used to calculate the excited state dipole moment. Different values result from different assumptions regarding the Onsager radius a. These are compiled in Table 4.5a for the cases where 'a' was calculated from (1) the mass-density formula (eq. 4.5) [55] (2) the molecular volume as calculated using the HF method and (3) using the Lippert approach [52]. In order to gain a more reliable basis, the Onsager radii for different fluorosubstituted benzenes and dimethylaminobenzenes were determined from the experimental densities and the molecular weight (eq. 4.5). As one can see from Table 4.5b, addition of one or more fluorine atoms to benzene do not induce any drastic changes in the value of the Onsager radius. Thus, it is not surprising that both DMABN and DMABN-F4 are predicted to have similar Onsager radii. Hence, all the above mentioned three methods resulted in approximately of the same excited state dipole moment values for the CT state, around 13 D for DMABN-F4 and 18 D for DMABN. For the usual point dipole Onsager model, because of similar Onsager radii, the resulting significantly different CT dipole

moment values are entirely a consequence of the difference of the experimental solvatochromic slopes.

TABLE 4. 5a: Onsagar radius, Solvatochromic Slope of the Mataga plot, Calculated Ground and Derived Excited State Dipole Moments of DMABN and DMABN-F4

Compound	a $(Å)^a$	a $(Å)^b$	a $(Å)^c$	Slope $(10^3 cm^{-1})^f$	$\mu_g(D)$	$\mu_e(D)^a$	$\mu_e(D)^b$	$\mu_e(D)^c$
DMABN	3.7	4.3	4.5^d	6.3(B), 24.2(A)	6.7^d	9.9(B), 14.8(A)	11.1(B), 17.6(A)	11.6(B), 18.5(A)
DMABN-F4	3.8	4.5	4.5	8.4	6.2^e	10.5	12.4	12.4

[a] from the mass-densitiy formula, eq (4.5). [b] from the molecular volume as calculated using the HF method. [c] based on Lippert approach of the long molecular axis in ref. Lippert, E.; Z. Naturforsch., **1955,** 10a, 541. [d] Baumann, W.; Bischof, H.; Froehling, J. C.; Brittinger, C.; Rettig, W.; Rotkiewicz, K. *Journal of Photochemistry and Photobiology, A: Chemistry* **1992**, *64*, 49. [e] approximated from μ_g(DMABN) + $\Delta\mu_{cal.}$(DMABN-F4 - DMABN). [f] Error estimated at less than 10%.

TABLE 4.5b: Densities and Onsager radius, compared for benzene, fluorinated benzenes, DMABN and DMABN-F4.

Molecules	ρ^a, g/cm^3	a^b, Å	a^c, Å
Benzene	0.877	3.28	4.00
F-Benzene	1.022	3.34	3.92
1,2,-F-Benzene	1.157	3.39	4.02
1,2,4,5-F-Benzene	1.319	3.56	3.90
Hexa fluorobenzene	1.6184	3.57	3.71
Dimethylamino benzene	0.956	3.82	4.23
DMABN	1.129^d	3.72	4.28
DMABN-F4	1.561^e	3.81	4.45

[a] CRC Handbook of Chemistry and Physics, 73rd Edition, CRC press, **1992-1993.** [b] from eq. 4.5.
[c] the Onsager radii were determined by Gaussian 98 for the optimised equilibrium geometries using the HF/6-311G(d) method. [d] Heine, A.; Herbstirmer, R.; Stalke, D.; Kuhnle, W.; Zachariasse, KA.; *Acta Crystallogr.* **1994,** *B50,* 363. [e] estimation using DMABN and the difference between 1,2,4,5-F-benzene and benzene

$$v_f = -\frac{2\Delta f'}{4\pi \in_0 hca^3} \mu_e\ (\mu_e\ -\ \mu_g) + \text{const} \qquad\qquad (4.4)$$

where $\Delta f' = (\varepsilon\text{-}1)/(2\varepsilon+1) - 1/2(n^2\text{-}1)/(2n^2+1)$

$$a = \sqrt[3]{3M/4\pi N_A \rho} \qquad\qquad (4.5)$$

In the above equations, μ_e and μ_g are the excited and ground state dipole moments respectively, h is Planck's constant, c is the velocity of light, M is the molecular mass, N_A is Avagadro's number and n and ε are the refractive index and dielectric constant, respectively.

4.4   Theoretical Results

4.4.1   Electronic Property of the Acceptor Fragments

For the discussion of the CT structure and dipole moment, it became important to know more about the properties and relative energies of the acceptor orbitals involved. Although fluorine substitution is expected to lead to an overall lowering of the energy of the acceptor orbitals, a closer look into the reported literature shows that this lowering very strongly depends on the substitution pattern, and that orbitals of different symmetry can exchange their energetic position. We therefore undertook to calculate the orbital energies of both the highest two occupied orbitals and the lowest two unoccupied orbitals by different methods and to compare them to the available experiments (Table 4.6). Especially useful is a look at their energetic difference (Table 4.7), which changes from negative to positive values if the orbitals exchange their energetic position. Both the theoretical and the experimental results (Table 4.6) show that insertion of the fluorine atoms into the benzene ring increases the acceptor property of this fragment. The HF ab initio calculations (Table 4.6) for a series of compounds containing fluorine are in rather good agreement with the experimental ionization energies, but the electron affinities are poorly represented. On the other hand, DFT (B3LYP/6-31G(d)) shows a much better correspondence to the LUMO energies than HF. Fig 4.9 shows that depending on the substitution pattern and the number of fluorine atoms, the

orbitals of different symmetry (labeled with respect to the C2 symmetry point group) exchange their energetic position. Fig. 4.10 depicts the HOMO and LUMO energies calculated with HF and DFT: HF fits much better to the experimental ionization energy, whereas the correspondence of DFT LUMO energies and the experimental electron affinities is much better. But both methods agree in the prediction of the relative changes of orbital energies with the fluorine substitution pattern.

TABLE 4.6: The energies ε of the four frontier orbitals (the orbital symmetries within point group C_2), calculated for optimised geometries of benzene with different substituents (fluorine atom F and CN group) and comparison to the negative experimental values of ionisation potential I_e and the electron affinity EA. (F0 – Benzene, F1 – Fluorobenzene, CN - Cyanobenzene, F 1,4 - 1,4-difluorobenzene, F 1,3,5- 1,3,5-trifluorobenzene, F 1,2,4,5 - 1,2,4,5-tetrafluorobenzene, F 1,2,3,4,5 - 1,2,3,4,5-pentafluorobenzene, F 1,2,4,5,CN - 1,2,4,5-tetrafluorobenzonitrile). The symmetry designations A and B mean that orbitals with A symmetry have a zero orbital coefficient for the atoms lying on the C_2 twist axis, those with B symmetry have a nonzero coefficient for these orbitals and are symmetric with respect to a plane perpendicular to the molecular plane and containing the C_2 axis.

'F' and other Substituents	HF/6-31G(d) ε (MO), eV calc.	$-I_e$, eV[a] Exp.	DFT(B3L/6-31G(d)) ε (MO), eV cal.	$-EA$, eV[b] exp.	ΔEA (exp-calc.)
0	4.07 (B)		0.10 (A)		
(F 0)	4.07 (A)		0.10 (B)	+1.15 [1,2]	1.0
	-9.00 (B)	-9.24	-6.70 (B)		
	-9.00 (A)	-9.24	-6.70 (A)		
1	4.12 (B)		0.10 (B)		
(F 1)	3.65 (A)		-0.24 (A)	+0.89 [1,2]	1.1
	-9.08 (B)	-9.19	-6.62 (B)		
	-9.45 (A)	-9.63	-7.04 (A)		
CN	3.29 (A)		-0.67 (A)		
(CN)	2.45 (B)		-1.41 (B)	+0.23 [3]	1.6
	-9.66 (B)	-	-7.26 (B)		
	-9.84 (A)		-7.52 (A)		
1,4	4.18 (B)		0.10 (B)		
(F 1,4)	3.21 (A)		-0.57 (A)	-	
	-9.16 (B)	-9.32	-6.56 (B)		
	-9.88 (A)	-9.68	-7.37 (A)		
1,3,5	3.59 (B)		-0.36 (B)		
(F 1,3,5)	3.59 (A)		-0.36 (A)	-	

	-9.79 (A)	-9.62	-7.09 (A)		
	-9.79 (B)	-9.62	-7.09 (B)		
1,2,4,5	3.81 (A)		-0.24 (A)		
(F 1,2,4,5)	2.90 (B)		-0.82 (B)	-	
	-9.60 (A)	-9.36	-6.78 (A)		
	-10.34 (B)	-10.04	-7.56 (B)		
1,2,3,4,5	3.42 (A)		-0.52 (A)		
(F 1,2,3,4,5)	2.95 (B)		-0.82 (B)	-0.64 [3];	0.2
	-9.99 (A)	-9.64	-7.06 (A)	-0.86 [4]	
	-10.35 (B)	-	-7.43 (B)		
1,2,3,4,5,6	3.02 (B)		-0.81 (A)		
(F 1,2,3,4,5,6)	3.02 (A)		-0.81 (B)	-0.52 [3];	0.3
	-10.36 (B)	-9.90	-7.33 (A)	-0.73 [4]	
	-10.36 (A)	-9.90	-7.33 (B)		
1,2,4,5,CN	3.13 (A)		-0.89 (A)		
(F1,2,4,5,CN)	1.41 (B)	-	-2.19 (B)	-	
	-10.28 (A)		-7.44 (A)		
	-10.80 (B)		-7.96 (B)		
1,2,3,4,5,CN	2.76 (A)		-1.17 (A)		
	1.45 (B)	-	-2.20 (B)	-1.08 [3]	1.1
	-10.68 (A)		-7.72 (A)		
	-10.79 (B)		-7.86 (B)		
DMABN-F4	3.40 (A)		-0.54 (A)c		
	1.98 (B)	-	-1.54 (B)c	-	
	-9.06 (B)		-6.16 (B)c		
	-10.10 (A)		-7.12 (A)c		

[a] from [D.G. Streets, G.P. Caesar, *Mol. Phys*., **1973,** 26, 1037; C.B. Duce, K.L. Yip, G.P. Caesar, A.W. Potts, D.G. Streets, *J.Chem. Phys*., **1977,** 66, 256] [b] by electron transmission spectroscopy in the gas phase:[1]. K. D. Jordan, J.A. Michejda, P.D. Burrow, *J. Am. Chem. Soc*., **1976,** 98, 7189.[2]. K. D. Jordan, P.D. Burrow, *Acc. Chem. Res*. II, **1978,** 11, 341.[3]. S. Chowdhury, E.P. Grimsrad, T. Heinis, P. Kebarle, *J. Am. Chem. Soc*., **1986,** 108, 3630.[4]. W.E. Wentworthm, T. Limero, C.M. Chen, *J. Phys. Chem.*, **1987,** 91, 241. [c] local symmetry on the acceptor group

Table 4.7: The energy difference $\Delta\varepsilon$ (eV) $= \varepsilon(B) - \varepsilon(A)$, of the molecular orbitals of benzene with different substituents and with different symmetry as calculated by the following methods: HF/6-31G(d), AM1, DFT (B3LYP/6-31G(d)) and compared to experimental values as far as available. Upper rows: difference of the first two LUMOs, lower rows: difference of the two highest occupied orbitals.

Position of F-substituents and other substituents	HF	AM1	DFT (B3LYP/6-31G(d)	exp[a]
0	0.00	0.00	0.00	
	0.00	0.00	0.00	
1	0.47	-0.06	0.34	-
	0.37	0.49	0.42	0.44
CN	-0.84	-0.46	-0.74	-
	0.18	0.15	0.26	-
1,4	0.97	-	0.67	-
	0.72	-	0.81	0.83
1,3,5	0.00	0.00	0.00	-
	0.00	0.00	0.00	0.00
1,2,4,5	-0.91	0.10	-0.58	-
	-0.74	-0.83	-0.78	-0.68
1,2,3,4,5	-0.47	-	-0.30	-
	-0.36	-	-0.37	-
1,2,3,4,5,6	0.00	0.00	0.00	-
	0.00	0.00	0.00	0.00
1,2,4,5,CN	-1.72	-0.26	-1.30	-
	-0.52	-0.68	-0.52	-
1,2,3,4,5,CN	-1.31	-	-1.03	-
	-0.11	-	-0.06	-

[a] Calculated from the negative experimental IP values in ref. D.G. Streets, G.P. Caesar, *Mol. Phys.*, **1973,** 26, 1037

Figure 4.9 and Tables 4.6 and 4.7 show that in some compounds (1 fluoro and 1,4 difluorobenzene), the orbitals of B symmetry are higher lying than the orbitals of A symmetry. In the twisted geometry, the electron transfer from dimethylamino group (the

donor orbital transforming as B) can be to either of the two lowest LUMO orbitals of the acceptor. This could have the consequence that also the energetic position of the two possible TICT states interchanges, and the lowest TICT state could become of B symmetry instead of A symmetry as in DMABN.
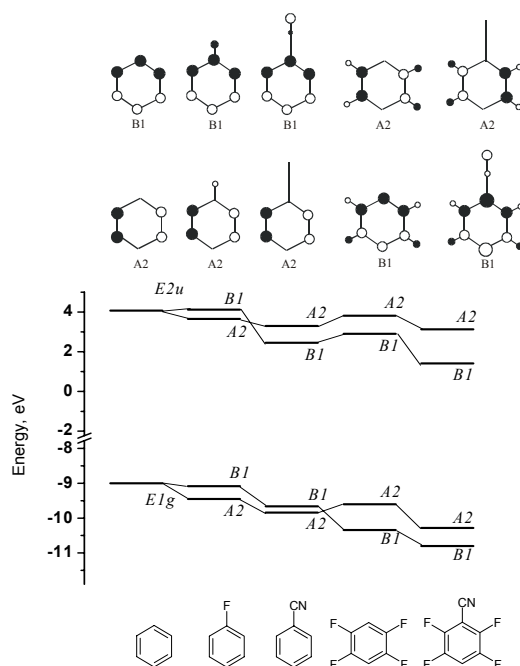
Figure 4.9: Correlation diagram of the energies of the occupied and unoccupied orbitals of fluorinated benzenes and benzonitrile as calculated by HF (values see table 6)
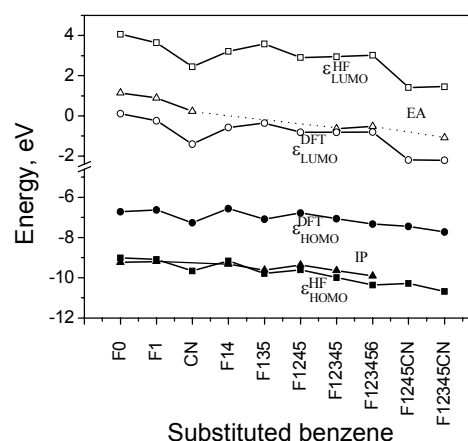
Figure 4.10: The comparison of the orbital energy for HOMO (ε_{homo}) and LUMO [(ε_{lumo}) calculated by different methods (HF/6-31G(d) and DFT (B3LYP/6-31G(d))] with the negative experimental values of electron affinity EA and ionisation potential IP for different compounds. The compounds are defined in table 6.

The results for 1,2,4,5 tetrafluorobenzene, however, clearly show that the B orbital is lower than the A orbital for both the HOMO and the LUMO manifold, and this effect is enhanced for the LUMO by introducing a further cyano group (but weakened for the occupied orbitals of the acceptor). From the DFT-LUMO energies for 1,2,4,5-tetrafluorbenzene and its cyano derivative, we can conclude that the four fluorine atoms lower the LUMO energy by 0.78 eV.

Thus we can conclude that the properties of the lowest TICT state should be the same for DMABN and DMABN-F4 regarding symmetry, and hence also the charge distribution should be similar.

Figure 4.11: Schematic diagram showing the state energies of DMABN and DMABN-F4 in the gas phase, as calculated by ZINDO/s.

This lowering of the TICT energy has also consequences for the reaction enthalpy of the B* → A* reaction. In the gas phase, it is calculated as being uphill (endothermic) for both compounds, but significantly less for so for DMABN-F4. Thus, for a given solvent polarity, where the reaction is exothermic in DMABN, the exothermicity is therefore much larger for DMABN-F4 (Figure 4.11)

4.4.2 Electronic Transitions

The semiempirical ZINDO/s calculations show that the long wavelength absorption region of DMABN and DMABN-F4 consists of two transitions (Table 4.8). The position and intensity of these transitions are characterized by an allowed S_2 transition (4.22 eV, f = 0.49 and 4.59 eV, f = 0.64 for DMABN-F4 and DMABN, respectively) with charge transfer (CT) nature (dipole moment 12.4 D similar to DMABN) and a polarization along the long molecular axis (^1L_a-type according to Platt nomenclature). Thus, there is a clear redshift of the ^1L_a-type state as expected from the increased acceptor strength also shown by the experimental spectra (Fig. 4.2). The forbidden S_1 transition (f = 0.01) with a somewhat lower energy (3.93 eV in DMABN-F4) is of ^1L_b nature and does not lead to a structure in the absorption spectrum (Fig. 4.2a) in contrast to the similar S_1 transition (4.27 eV, f= 0.02) of DMABN which leads to a weak shoulder on red side of the absorption spectrum. The absence of structure in the absorption spectrum of DMABN-F4 in hexane is in contrast to the calculated S_1-S_2 energy difference (Table 4.8), which is even larger for DMABN-F4 (0.52 eV) than for DMABN (0.32 eV). We consider that the energy lowering of the ^1L_b-type state in DMABN-F4 is probably smaller than predicted by the calculations in Table 4.8.

Table 4.8: Comparison of the transition energy ΔE, oscillator strength f, dipole moments and configuration interaction analysis for the long wavelength absorption transitions for DMABN and DMABN-F4 as calculated by ZINDO/s for the optimized ground state equilibrium geometry and two further twist angles. (full optimization at the different fixed twist angles using DFT (B3LYP/6-311++G(d)).

Parameter	DMABN twist angle and symmetry			DMABN-F4 twist angle and symmetry		
	00_cs^{eq}	35_c1 [a]	90_cs	00_cs	35_c1^{eq}	90_cs
$\Delta E(S_0 \to S_1)$, eV (f)	**4.27** (0.02)	**4.27** (0.02)	**4.49** (0.00)	**3.94** (0.01)	**3.93** (0.01)	**4.16** (0.00)
$\mu(S_1)$ $(\mu(S_0)$, D)	8.36 (7.34)	8.33 (7.04)	5.84 (5.94)	8.81 (7.48)	8.87 (7.10)	5.90 (5.85)
$\Delta\mu$, D	1.02	1.29	0.10	1.33	1.77	0.05
CI-coefficient: HOMO+0→LUMO+1	0.58	0.58	0.46	0.56	0.57	0.47
HOMO-1→LUMO+0	0.38	0.39	0.52	-0.42	-0.40	-0.52
nature	^1L_b	^1L_b	$LE(BN)$ [b]	^1L_b	^1L_b	$LE(BN)$ [b]
$\Delta E(S_0 \to S_2)$, eV (f)	**4.59** (0.64)	**4.53** (0.56)	**5.36** (0.00)	**4.46** (0.57)	**4.22** (0.49)	**4.60** (0.00)
$\mu(S_2)$ $(\mu(S_0)$, D)	12.51(7.34)	13.26(7.04)	16.66(5.94)	12.35(7.48)	13.27(7.10)	16.81(5.85)
$\Delta\mu$, D	5.17	8.22	10.72	4.87	6.17	10.96
CI-coefficient: HOMO+0→LUMO+0	0.68	0.68	0.64	0.68	0.68	0.65
nature	L_a/CT	L_a/CT	TICT [c]	L_a/CT	L_a/CT	TICT [c]

[a] fixed torsional angles of the carbon atoms of the dimethylamino group which are equal to the equilibrium orientation of the group for **DMABN-F4**; [b] LE state localised on the benzonitrile moiety; [c] S_4 for DMABN, S_2 for DMABN-F4

The stronger acceptor in DMABN-F4 is also reflected in the energy of the calculated (and observed) TICT state: In DMABN, it is calculated at 5.36 eV, in DMABN at 4.60 eV, i.e. 0.76 eV lower, very close to the value predicted by the lowering of the acceptor orbital energy (0.78 eV, Table 6). As a consequence, in contrast to DMABN, the lowest TICT state of DMABN-F4 calculated for 90° corresponds to S_2, whereas it is S_4 in DMABN in the gas phase according to the ZINDO/s calculations.

4.4.3 The Discrepancy of Experimental and Calculated CT Dipole moments

On the basis of the solvatochromic measurements, the resulting CT dipole moments of DMABN (18 D) and DMABN-F4 (13 D) were found to be strongly different, with that of DMABN-F4 being anomalously low. On the other hand, the calculations indicate that the dipole moments should be similar (16.7 and 16.8 D, respectively, Table 8), and the transient absorption experiments [50] also indicate that the electronic structure is similar and full charge separation has occurred.

This discrepancy is solved if the assumption of equal Onsager radii a is dropped, because the solvatochromic slope is proportional to the ratio μ_e/a^3. An increased a for DMABN-F4 will lead to a correspondingly increased μ_e. In fact, we can estimate that an increase from $a = 3.7$ to $a = 3.8$ is sufficient to result in similar dipole moments for the TICT states of both DMABN and DMABN-F4. On the other hand, using the molecular volumes estimated by quantum chemical calculations and from the densities and molecular weights (Table 4.5b), we concluded that the solvent cavity volume excluded by the solvent should be very similar for the two compounds. Using Onsager's point dipole approximation, which is at the basis of the solvatochromic treatment according to Mataga, we are therefore forced to conclude for different CT dipole moments from the different experimental solvatochromic slopes.

A possibility for justifying differently sized a-factors for the two compounds would be by assuming different solute-solvent interactions for the same value of the a-factor. If the solute-solvent response would be weaker in DMABN-F4 than in DMABN, this would correspond to an increased a-factor in the usual solvatochromic equation. This is equivalent to say that the Onsager point dipole approximation is not valid for this comparison.

We can justify such a point of view by considering the different charge distribution in the two compounds: The pi and pi* orbitals are very similar, hence the CT charge distribution due to the pi-electronic transitions should be similar (see the calculations, Tab. 4.8). But the fluorine atoms on the acceptor are negatively charged (in both ground and excited state) whereas the H-atoms in DMABN are positively charged. The negative charge on the fluorine atoms will prepolarize the solvent dipoles already in the ground state such that upon excitation to the charge transfer state, their relaxation possibility is reduced which is equivalent to say that the solute-solvent interaction is effectively weakened.

This explanation of the dipole moment discrepancy by a break-down of the Onsager point dipole theory is a first attempt to explain the unusual solvatochromic behaviour

of highly fluorinated charge transfer compounds. Further experiments are needed to verify this explanation.

4.4.4 Competing Photochemical Reaction paths

The value of k_{nr} is considerably larger for DMABN-F4 than for DMABN, especially in n-hexane (Table 4.1c). We can conclude that we have an additional nonradiative decay channel: Its nature could be either population of a triplet state (intersystem crossing *ISC*) or population of a transient nonemissive singlet species and/or nonradiative photochemistry through a conical intersection (internal conversion *IC*). As there is no permanent photochemical product these reaction paths have to lead back to the ground state of the starting material. As we do not observe phosphorescence, the triplet path is not probable. The number of fluorine substituents seems to be an important factor in the enhancement of this *IC* path as already stated by Druzhinin et al. [45]. In the tetrafluorinated DMABN, this *IC* path is further enhanced as compared with the monofluorinated derivatives.

A possible reaction path that can be discussed is the folding (relaxation to nonplanarity) of the benzene ring in the excited state. Recent calculations of DMABN indicate that even in this nonfluorinated compound, the TICT state possesses a nonplanar benzene ring [56]. The case of 1,2,4,5 tetrafluorobenzene further exemplifies the effect of the fluorine atoms which enhance the tendency for nonplanar folding: Whereas benzene shows no sign of a deviation from planarity in the emissive excited state, the emissive state of tetrafluorobenzene shows a folding (butterfly motion) resulting in a double minimum potential, as deduced from laser-induced fluorescence spectra [57]. If there is a similar folding in DMABN-F4 (and to some extend even in DMABN which also has a nonnegligible contribution of *IC*), it could lead to a conical intersection along the reaction coordinate leading either to the Dewar isomer (folding of two four-membered rings) or to the benzvalene isomer (folding of two three-membered rings). Such conical intersections are known to play an important role in the nonradiative photochemistry of benzene and its derivatives [58, 59, 60].

4.5   Conclusion

DMABN-F4 is spectroscopically closely related to DMABN but characterized by a higher acceptor strength. The strongly redshifted emission and absence of the short wavelength B-band in the fluorescence spectrum of DMABN-F4 at 77 K indicates the ultrafast formation of a CT structure in the excited state, probably linked to the pretwisted ground state geometry and the increased acceptor strength. The low fluorescence quantum yield values and absence of phosphorescence of DMABN-F4 suggest that the high rate of non-radiative decay takes place through internal conversion rather than intersystem crossing. A possible intersystem crossing reaction path could be the folding (butterfly motion) of the benzene ring either towards a Dewar or a prefulvene deformation. Results from time-resolved measurements indicate that the emission of DMABN-F4 is strongly forbidden consistent with the formation of a twisted intramolecular charge transfer state (TICT) with high dipole moment. The relatively small solvatochromic slope for this CT emission, as compared to expectations from quantum chemical calculations, indicates the possibility for a breakdown of the Onsager point dipole approximation for highly fluorinated CT compounds.

5   Excited State Properties of Fluorinated Analogues of DMABN and PBN

Abstract
        The excited state characteristics of fluorinated derivatives of N,N-dimethylaminobenzonitrile and N-pyrrolobenzonitrile have been characterized by both absorption and emission spectroscopy and the fluorinated have been compared with the corresponding nonfluorinated compounds.   The low fluorescence quantum yield values observed in these compounds are not due to intersystem crossing (no phosphorescence observable) and have been rationalized in terms of the fluoro atom substitution which can enhance the benzene channel III nonradiative pathways. It is tentatively proposed that the non-radiative pathway in the excited state of these compounds can be either bending (Dewar path) or folding (prefulvene path) of the benzene ring.

5.1   Introduction

        Electronically excited molecules are known to undergo a variety of decay processes. In addition to the radiative decay (fluorescence or phosphorescence), the non-radiative decay takes place either by internal conversion *(IC)* or by intersystem crossing *(ISC)*. An *ISC* mechanism from S_1 to T_1 can be evidenced through phosphorescence. For the other non-radiative channel (*IC* to the ground state), formation of dark transient structures such as conical intersections and excited state chemical reactions such as fragmentation and isomerisation have been discussed in this type of molecules. In a simple molecule like benzene, very low fluorescent quantum yields have been observed and interpreted by the existence of a very efficient photochemical pathway (channel III photochemistry) [57, 58, 59, 60, 61, 62] to the electronic ground state.
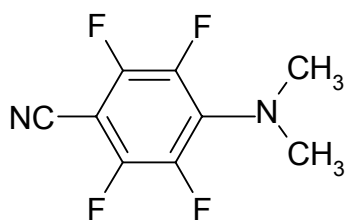
DMABN-F4   P4CF2   P4CF3

51
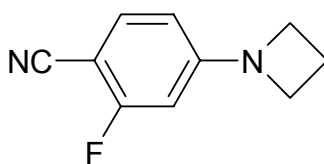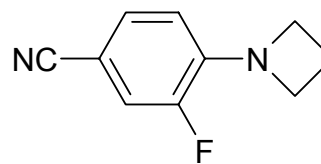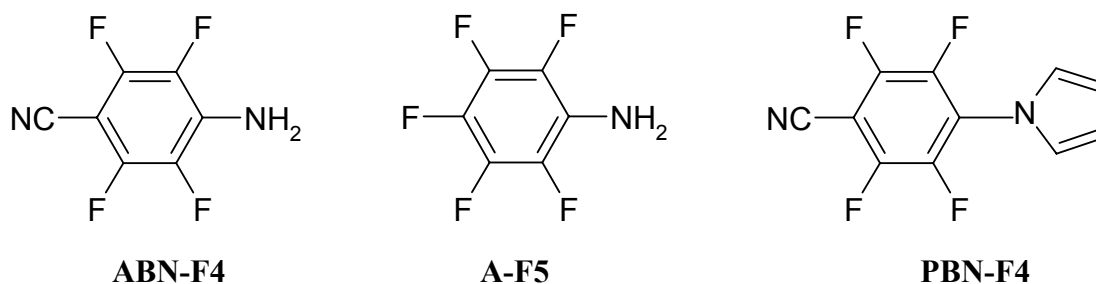
Figure 5.1: Structures of the molecules

The motivation of this chapter arises from the fact that the fluoro analogues of DMABN, namely DMABN-F4 possess a benzonitrile group with strongly increased acceptor properties as compared to DMABN. By increasing the acceptor strength by introducing F-atoms into the donor-acceptor systems, the energy of the intramolecular charge transfer (ICT) state will be preferentially stabilized. This should therefore lead to enhanced charge transfer (CT) formation. But on the other hand, the literature indicates that this substitution will lead to an increased efficient non-radiative decay. Druzhinin [45] reported that F-substitution into the corresponding azetidinyl benzonitriles creates an efficient internal conversion channel. It is possible that the *IC* channels will be further increased by higher fluoro-substitution. In order to investigate this behaviour of fluorinated compounds, further aniline derivatives such as ABN-F4, A-F5 and PBN-F4 are spectroscopically investigated here by means of both absorption and fluorescence spectroscopy.

5.2 Experimental

Technical details about the measurement of absorption and fluorescence spectra and quantum yields are reported in section 3.3

5.2.1 Synthesis of the Compounds used in this Study

The compounds were a gift of Prof. A.I. Tolmachev, Institute for Organic Chemistry of the National Academy of Sciences of Ukraine, Kiew, Ukraine.

5.3 Results and Discussion

5.3.1 Absorption and Emission Spectroscopy

Fig. 5.2 shows the absorption and emission spectra of all the compounds investigated, and the photophysical data are compiled in Table 5.1. The absorption spectrum of ABN-F4 in polar solvents is slightly red shifted when compared to that in non-polar solvent. The absorption spectra of all the compounds in solvents of various polarity are independent of concentration effects. There is no emission observable for ABN-F4 in any of the solvents. Even though, the acceptor strength in ABN-F4 is considerably stronger than in the parent compound ABN, the absorption spectrum in hexane is slightly shifted to the blue as compared to ABN in hexane [63]. The latter phenomenon was also taking place in the case of PBN-F4 with respect to p-PBN. The absorption spectra of DMABN-F4 in all solvents are slightly red shifted with respect to DMABN. The difference between the behaviour of p-PBN and DMABN-F4 with respect to their tetrafluorinated derivative can be linked to the different influence of solvent polarity on the absorption spectra (large for DMABN-F4, negligible for p-PBN), which is a sign of the smaller contribution of the quinoidal resonance structure in p-PBN.
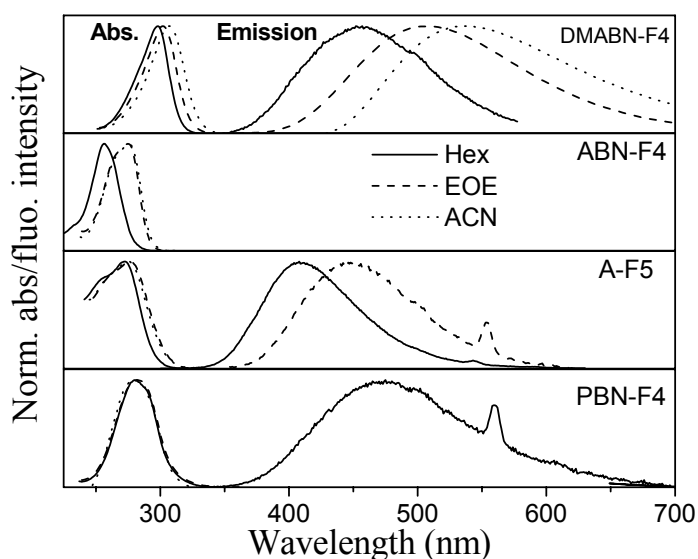

Figure 5.2: Normalised Absorption and fluorescence spectra of ABN-F4, A-F5 and PBN-F4 in various solvents of different polarity (Hex – n-hexane, EOE – diethylether, ACN - acetonitrile). Abs. spectra are superimposed in the case of PBN-F4.

TABLE 5.1: Photophysical parameters of fluorinated analogues of DMABN and aniline in various solvents at room temperature and comparison to nonfluorinated derivatives

Compounds	Solvent	λ_{abs} (nm)	λ_{flu} (nm)	ϕ_f
DMABN-F4	Hex	300	456	0.0006
	EOE	304	501	0.0010
	ACN	308	537	0.0001
DMABN	Hex	282	341	
	ACN	292	365(B), 476(A)	0.0016(B), 0.0162(A)
ABN-F4	Hex	256		$<10^{-4}$
	EOE	275		,,
	Hex:EOE (4:1)	267		,,
	ACN	276		,,
ABN	Hex	261	-	-
A-F5	Hex	272	409	0.0149
	EOE	277	447	0.0056
	Hex:EOE (4:1)	274	440	
	ACN	275		- $<10^{-4}$
PBN-F4	Hex	280	477	0.0016
	EOE	282		$<10^{-4}$
	ACN	280		,,
p-PBN	Hex	287	332	0.077
	ACN	287	460	0.024

For A-F5, the absorption spectra do not show much variation in their maximum in the solvents studied. In contrast to ABN-F4, this compound shows emission in n-hexane and diethyl ether, and the spectra are very broad and show a strong solvatochromic redshift indicating an emissive CT state. Moreover, they are blue shifted when compared to DMABN-F4, which indicates that the donor is probably the amino and dimethylamino group. The emission spectra of A-F5 in hexane and diethyl ether also show broad spectra and significant solvatochromic shifts indicating CT emission. The quantum yield values of A-F5 are drastically decreasing from n-hexane, and the compound eventually is non-fluorescent in acetonitrile. This could be a polarity effect energetically favouring a polarity-sensitive non-radiative channel. Apart from the investigations of fluorinated anilines, the fluorinated analogue of PBN, namely PBN-F4 is also investigated. The absorption spectra do not change

with the polarity of the solvent. Emission is only observable in n-hexane. The compound is non-emissive in medium and highly polar solvents. The fluorescence behaviour of ABN-F4, A-F5 and PBN-F4 has also been studied at 77 K in EOE. Neither fluorescence nor phosphorescence was observed in such conditions.

Regarding the nature of the CT state, it is well-known, that DMABN populates a Twisted Intramolecular Charge Transfer TICT state [9], and this has also been verified for DMABN-F4 [64] The strongly increased TICT formation tendency for DMABN-F4 as compared to DMABN can be explained on the basis of two facts: a) the increased acceptor strength b) a change of equilibrium conformation in the ground state. In the ground state, DMABN assumes a planar equilibrium conformation. The addition of fluorine atoms into the ring considerably increases the twisting of the acceptor moiety as evidenced by quantum chemical calculations [64]. Due to the fluoro substituents on the benzene moiety, PBN-F4 is also expected to be more strongly twisted in the ground state than the parent compound PBN.
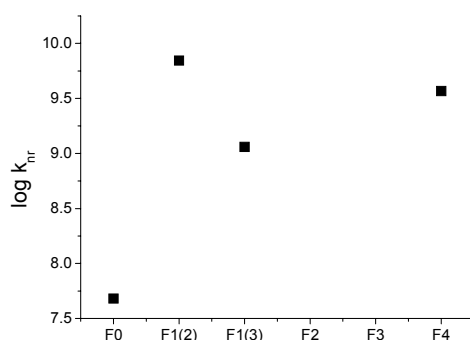
Figure 5.3: Plot of log k_{nr} of DMABN against the number of fluorine atoms. The numbers in the brackets represent the position of the fluorine atoms with respect to the cyano group. The k_{nr} values for the monofluorinated DMABN-derivatives have been extrapolated for labels F1(2) and F1(3) from the compounds (ref.7) P4CF2 and P4CF3 in Fig. 5.1.

The low fluorescence quantum yield values can be explained in terms of the fluorine substitution operating as an additional photochemical pathway such as butterfly folding of the benzene ring. The non–fluorescent behaviour of ABN-F4 can be compared to 1,2,4,5-tetrafluorobenzene where laser-induced fluorescence spectra have evidenced a folding (butterfly motion) resulting in a double minimum excited-state potential [57]. An additional question one can ask is whether the increase of the non-radiative rate constant of DMABN shows a linear dependence on the number of fluorine atoms. This is conceptually represented in Fig. 5.3 by plotting log k_{nr} DMABN versus the number of fluorine atoms. It can be seen

that already one fluoro atom can be as efficient as four fluorine atoms in enhancing k_{nr}. The detailed nature of this fluoro effect necessitates further experimental and theoretical studies.

5.4   Conclusion

The excited state characteristics of fluorinated aniline and phenylpyrrole derivatives have been analysed by absorption and emission spectroscopy at room temperature. The high solvatochromic effect of the emission spectra of DMABN-F4 and A-F5 points to the formation of a CT state. The increase in non-radiative rate constant by the addition of fluorine atoms can be tentatively rationalised on the basis of the benzene channel III pathways [57, 58, 60]. The reaction pathway for non-radiative decay in the excited state of these compounds might be either bending (Dewar path) or folding (prefulvene path) of the benzene ring. Introduction of fluorine atoms into the acceptor part strongly lowers the energy of the CT state and enhances and enhances its population efficiency. But it also lowers the energy of possible conical intersections related with the channel III pathways and therefore induces a k_{nr} pathway efficiently competing with CT formation.

6 TICT Formation and Antiquinoid Distortion in para- and meta-Derivatives of N-Phenyl Pyrrole

Abstract

The photophysical properties of meta- and para-cyano N-phenyl pyrrole (m- and p-PBN) are compared. Both compounds show highly red-shifted and strongly forbidden emission in polar solvents, assigned to a charge transfer state. The forbidden nature is indicative of very weak coupling between the two π-systems, and a twisted emissive structure is suggested (TICT state). Comparison to quantum chemical calculations indicates that the twisted structure possesses an antiquinoid distortion of the benzonitrile group, i.e. the bonds in the ring are lengthened instead of shortened, as in the quinoid state, which is reached in nonpolar solvents. m-PBN is the first meta compound which shows TICT emission. It differs from p-PBN by a less exergonic formation of the TICT state from the LE/ICT quinoid state. It therefore shows only single LE/ICT fluorescence in nonpolar alkane solvents, whereas p-PBN shows dual fluorescence in this solvent (LE/ICT and TICT).

6.1 Introduction

Since the ''Twisted intramolecular charge transfer'' (TICT) concept has been developed some two decades ago, the investigation of charge transfer (CT) in donor-acceptor systems, especially substituted benzenes, unraveled many processes occurring in their excited states. Particularly, this has led to the understanding of the dual fluorescence of 4-cyano-N,N-dimethylaniline (DMABN) which was discovered by Lippert in 1959 [52]. In many compounds, TICT states are formed via an adiabatic photoreaction: If a TICT forming molecule possessing a planar ground state is electronically excited, it relaxes spontaneously in the excited state towards a twisted conformation from where it decays by emission or nonradiatively. The rate of reaching the TICT state with its twisted conformation is determined, at least for compounds similar to DMABN and apart from other factors, by the initial (Franck-Condon) twist angle which is reached directly after light absorption from the ground state. The closer this initial twist angle is to the final one (about 90º), the faster is the TICT population kinetics. In that respect, CT can be explored by variation of the donor and acceptor groups on either side of the benzene moiety stabilizing the CT transfer state. Surprisingly, the dual fluorescence has not been observed in the case of meta derivatives of

DMABN [65]. This is in part due to the larger energy gap between the first two excited states (^1L_a, ^1L_b) for the meta as compared to the para derivatives, and therefore the driving force for the adiabatic photoreaction is strongly reduced for m-DMABN as compared to p-DMABN [9].
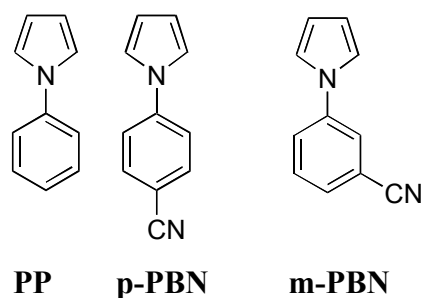
Figure 6.1: Structures of the molecules

Pyrrolobenzonitriles constitute a group of donor-acceptor systems in which the dimethlyamino group is replaced by a better donor moiety, namely pyrrole. The absorption and fluorescence properties of N-pyrrolylbenzonitrile (p-PBN), its ester derivative PBAEE, and a more twisted model compound DPBN with stronger donor-acceptor propeties have been compared by Gude *et al.* [66]. Recently, Yoshihara *et al* [67] reported on the determination of excited state dipole moments of N-phenylpyrroles and DMABN from solvatochromic and thermochromic measurements. Both the para and meta PBN derivatives were shown to populate a CT excited state but the conformational nature remained unclear as transition moments were not determined. This is to be contrasted with the recent investigation of a planar model compound (FPP) of phenyl pyrrole [68] as compared to phenyl pyrrole (PP) itself. In both cases, a red-shifted CT fluorescence band could be shown to be present. This leaves two possibilities: (i) either both FPP and PP possess a planar structure for the relaxed CT state corresponding to a " Planar Intramolecular Charge Transfer " PICT state [69, 70, 71, 72] or (ii) FPP has a planar structure and PP a twisted one. In this case, different emissive properties are expected. Unfortunately, the experimental investigation of transition moments in PP and FPP has not been reported [68].

Zilberg *et al.* [73] performed theoretical calculations on N-phenyl pyrroles. The calculations support the possible existence of two distinct structures for the CT state. One of

them has a quinoid structure with characteristically shortened bonds in the benzene ring, and the two rings are coplanar at the energy minimum. The other one is of anti-quinoid structure (where the quinoid bonds in between are lengthened instead of shortened), has a larger dipole moment than the quinoid one, and has an energy minimum with the pyrrolo group twisted by 90° with respect to the benzene ring.

Only the antiquinoid state is expected to possess forbidden emissive properties. Our results reveal that the CT emission is strongly forbidden in both compounds investigated. The combination of experiment and theory therefore leads to the conclusion of antiquinoid properties and twisted structure of the emitting CT state in both compounds.

The meta isomer of p-PBN, m-PBN is the first compound where a m-substituted cyano derivative shows TICT formation. Like m-DMABN, m-PBN also shows a red-shift in the absorption maximum of S_1. This reduces the exothermicity of CT formation for meta-compounds in general. On the other hand, when comparing p-PBN with DMABN, there is a large exothermicity from LE to TICT formation due to the better donor. As a matter of fact, already nonpolar solvents like n-hexane induce the appearance of dual fluorescence for p-PBN. The combined effect of both factors can achieve that both para isomers DMABN and p-PBN show CT formation whereas only m-PBN populates a CT state, but m-DMABN emits from an LE state.

6.2   Experimental

6.2.1   Materials

The compounds were synthesized according to the procedures described in refs. [29, 30] and sublimed. The experimental details about the absorption, fluorescence, lifetime and quantum yield measurements are described in chapter 3.

6.2.2   Quantum Chemical Calculations

The ab initio calculations were performed with GAMESS [74] using the cc-pVDZ basis set [75] in collaboration with Dr. Shmuel Zilberg at Department of Physical Chemistry and the Farkas Center for Light Induced Processes, The Hebrew University of Jerusalem, Jerusalem, Israel. Full geometry optimization was performed for the doublet ground state of benzonitrile radical anion by using CASSCF calculations (CAS(11/10)/cc-pVDZ (11electrons on 10 orbitals)).

6.3   Results

6.3.1   Room Temperature Spectroscopy

The absorption and emission spectra of p-PBN and m-PBN in various solvents of different polarity are compared in Fig. 6.2. The main absorption band of m-PBN is shifted to the blue region compared to p-PBN in n-hexane. There is also a weak shoulder in the red edge of the absorption spectrum of m-PBN, which can be interpreted as a weak transition, which is red-shifted when compared to the corresponding one in p-PBN. All the emission spectra exhibit a strong red-shift of their maxima increasing from weakly polar to strongly polar solvents. The emission of p-PBN in n-hexane is broad as compared to the narrower band in m-PBN. Yoshihara *et al.* [67] reported dual fluorescence for m-PBN dissolved in the medium polar solvent diethyl ether (EOE). This is has been verified here by comparing an aerated and a deaerated solution, and the shoulder in the fluorescence spectrum is not present for both freshly prepared solutions but rises for the aerated solution only for a prolonged stay of the sample in the dark. The shoulder reported in ref. [67] is therefore assigned to the appearance of a thermal oxidation product. No shoulder appeared on photolysis of the deaerated solution. Emission maxima observed in this work differ somewhat from the previous work of Gude *et al.* [66] and Yoshihara *et al.* [67] due to the use of different fluorescence spectrometers and correction curves. The quality of the emission correction curve is especially important for broad and structureless CT spectra as observed for m-PBN and p-PBN in polar solvents. We have verified the quality of the correction curve used here by comparing to spectra measured on a freshly calibrated fluorimeter.
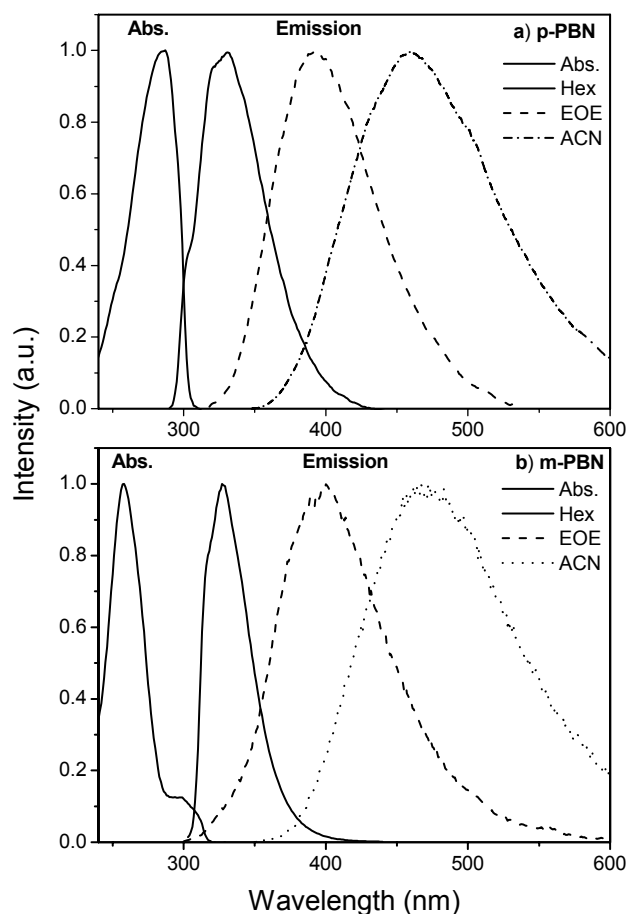
Figure 6.2: Normalised Absorption and fluorescence spectra of p-PBN and m-PBN in various solvents of different polarity (HEX- n-hexane, EOE – diethylether, ACN - Acetonitrile).

Comparison of the spectra of m-PBN with p-PBN exhibits rather similar features except in nonpolar solvents such as n-hexane where the emission spectrum is narrower for m-PBN than for p-PBN in n-hexane. The solvatochromic red-shift in going from low to high polar solvents is a substantial indication of the charge transfer (CT) nature of the emitting state in both compounds. (see section 6.3.2)

The molar extinction coefficient values determined for p-PBN and m-PBN in n-hexane are ε (λ_{287}^{max}) = 25747 and ε (λ_{258}^{max}) = 25400 respectively. In the case of p-PBN, the bands due to the S_1 and S_2 states are strongly overlapping (see below), whereas the redshift of the S_1 absorption in m-PBN leads to the appearance of the shoulder with small extinction coefficient in the absorption spectrum (Fig. 6.2). The blue shift of the main absorption band (see Fig. 6.2) and the small absorption shoulder at ca. 300nm for m-PBN is a consequence of

the meta-effect [76]. As the calculations described below show, the single main absorption band of p-PBN hides a weak band which can be assigned to the ^1L_b state in Platt's nomenclature. Due to the meta-effect, the S_1 state of m-PBN is therefore at lower energy than for p-PBN.

TABLE 6.1: Photophysical Characteristics of m-PBN and p-PBN in Solvents of Different Polarity at Room Temperature

	Sol	λ_{flu} (nm)	Δv_{st}^b ($10^3 cm^{-1}$)	ϕ_f	τ_f^c (ns)	k_f ($10^7 s^{-1}$)	k_{nr} ($10^8 s^{-1}$)	M_f (D)
p-PBN[a]								
	Hex	332	4.722	0.077	2.42	3.18	3.8	3.77
	EOE	393	9.397	0.023	3.80	0.61	2.6	2.18
	THF	422	11.146	0.024				--
	DCM	412	10.571	0.022	3.10	0.71	3.2	2.35
	ACN	460	13.104	0.024	8.20	0.29	1.2	1.93
m-PBN[d,e]	Hex	327	2.752	0.155	3.31	4.68	2.5	4.47
	BOB	369	6.233	0.023	-	-	-	
	EOE	397	8.144	0.019	3.76	0.47	2.6	1.94
	THF	429	10.023	0.016	5.01	0.32	1.9	1.70
	DCM	415	9.236	0.013		--	-	
	ACN	476	12.324	0.013	5.35	0.24	1.8	1.85

[a] λ_{max}^{abs} = 287nm used as the excitation wavelength for all solvents (absorption maximum is independent of polarity). [b] The Stokes shift is measured from the weak absorption shoulder at 300nm. [c] from ref. 4. . [d] λ_{max}^{abs} = 258nm used as the excitation wavelength for all solvents (absorption maximum is independent of polarity). [e] S_1 corresponds to the shoulder at 300nm in the absorption spectrum .

Stokes shift values with reference to the first absorption band have been calculated and tabulated for both m-PBN and p-PBN in Table 6.1. It is found that they are slightly smaller for m-PBN due to the red-shift of S_1. But, in the case of highly polar solvents, the Stokes shift values are large in number for both compounds indicating emission from a CT state. The fluorescence decay curves are monoexponential, allowing the evaluation of radiative and nonradiative rate constants according to equations 6.2 and 6.3. In eq. 6.3, $k_{nr.}^{tot}$ corresponds to the sum of all nonradiative processes including triplet formation. The emission transition dipole moments were calculated using (eq. 6.4) [77] and are the characteristics of the excited states. The measured data and calculated photophysical values are collected in Table 6.1.

$$k_f = \phi_f / \tau_f \qquad (6.2)$$

$$k_{nr.}^{tot} = k_f(\phi_f^{-1}-1) \qquad (6.3)$$
$$M_f^2 = (3hk_f/64\pi^4n^3 v_f^3) \qquad (6.4)$$

The k_f values decrease when going from hexane to polar solvents in parallel to the quantum yield values for both p-PBN and m-PBN. In the case of m-PBN, the k_f values in the more polar solvents are even smaller than in p-PBN, indicating the enhancement of forbidden character present in the emitting state.

6.3.2 Solvatochromic Measurements

The solvatochromic slopes were analysed to get quantitative information on the dipole moments for both compounds, by applying the Mataga equation (eq. 6.5) [52, 53, 54] and the resulting values are collected in Table 6.2. The plot of the emission maximum versus the polarity parameter, $\Delta f'$ is shown in Fig. 6.3. Similarly, a new type of Mataga plot has also been made by using low temperature fluorescence spectra: In this case, the emission maxima at different temperatures in diethylether were plotted versus the temperature dependent $\Delta f'$ values (fig. 6.4) In this case, $\Delta f'$ was calculated by taking dielectric constant, ε and refractive index, n as a function of temperature [36]. The plots show a linear relationship in both cases. It is found that the solvatochromic slope values (Table 6.2), which are determined from the second type of Mataga plot at different temperatures, are somewhat larger than from the room-temperature Mataga plot, but in both types of Mataga plots, the slope values are slightly higher for m-PBN than for p-PBN. The Onsager radius, a= 4.1 Å for p-PBN [66] and m-PBN was calculated by the mass-density formula (eq. 6.5) [55] by taking an average density ρ = 0.95g/cm [66]. This approach neglects the different molecular shapes of p-PBN and m-PBN.

TABLE 6.2: Results of the Solvatochromic Measurements at Room Temperature and Low Temperature (Solvatochromic slopes, assumed Onsager factor a, μ_g(D) and derived μ_e(D) for the 2 methods)

	a (Å)	Slope $(10^3 cm^{-1})$[a]	Slope $(10^3 cm^{-1})$[b]	μ_g(D)[c]	μ_e(D)
p-PBN	4.1	-27.501[d]	-27.500	2.09	14.8
	4.1	-35.489[e]		2.09	16.6
m-PBN	4.1	-30.306[d]	-28.000	2.78	15.8
	4.1	-40.067[e]		2.78	18.0

[a] Error less than 10%. [b]Based on crystal density; ref. 5 [c]Calculated by AM1. [d] from the Mataga plot at room temperature. [e] from the Mataga plot in diethyl ether at low temperatures.
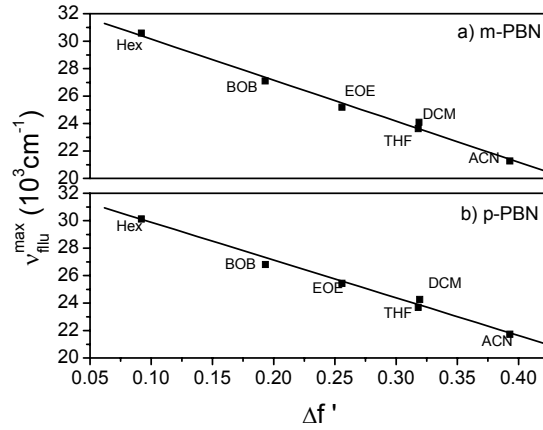
Figure 6.3: Solvatochromic fluorescence plot of a) m-PBN and b) p-PBN derived from differently polar solvents at room temperature. (HEX- n-hexane, BOB- dibutyl ether, EOE – diethyl ether, THF- tetrahydrofuran, DCM- dichloromethane, ACN - acetonitrile).
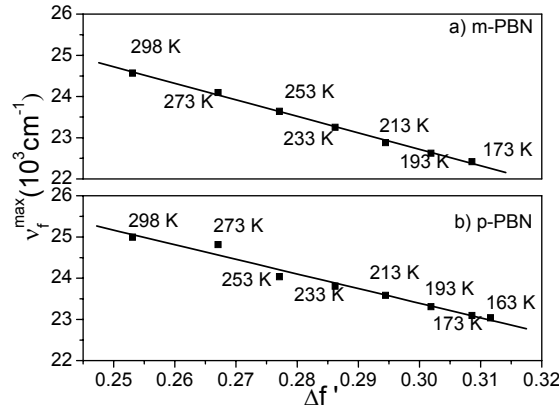
Figure 6.4: Solvatochromic fluorescence plot of a) m-PBN and b) p-PBN derived from measurements in diethyl ether at variable temperature

$$\nu_f = -\frac{2\Delta f'}{4\pi \in_0 hca^3} \mu_e \, (\mu_e - \mu_g) + \text{const} \qquad (6.5)$$

where $\Delta f' = (\varepsilon\text{-}1)/(2\varepsilon+1) - 1/2(n^2\text{-}1)/(2n^2+1)$

$$a = \sqrt[3]{3M/4\pi N_A \rho} \qquad (6.6)$$

In the above equations, μ_e and μ_g are the excited and ground state dipole moments respectively, h is Planck's constant, c is the velocity of light, and n and ε are the refractive index and dielectric constant, respectively. The resulting excited state dipole moments are determined using the calculated ground state dipole moments are very close for both

64

solvatochromic methods and are even slightly larger for m-PBN as compared to p-PBN (Table 6.2). These large μ_e values suggest that the emissive state is of CT nature and is similar in both compounds regardless of the position of the cyano substituent.

6.3.3 Spectroscopic Measurements at Low Temperatures

Fluorescence measurements at low temperatures were done in the nonpolar solvent mixture methylcyclohexane – isopentane (1:4), and in the medium polar solvent diethyl ether. For m-PBN in EOE, with the lowering of temperature, a red-shift of the emission maxima is observed (Fig. 6.5) and analyzed using the Mataga equation. A red-shift of the emission has also been observed for p-PBN in EOE. This thermochromic red-shift is mainly due to the enhancement of the dielectric constant and the refractive index with the lowering of temperature and can be ascribed to the stabilization of the CT state.
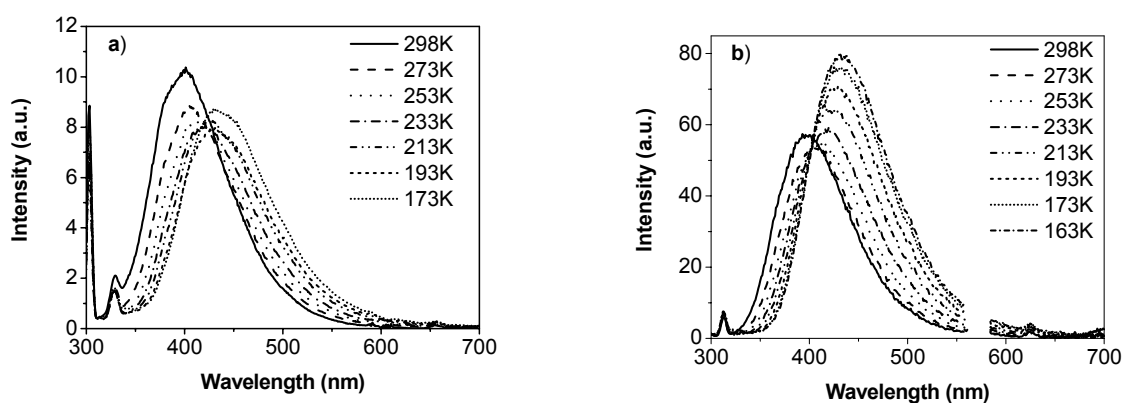

Figure 6.5: Low temperature fluorescence spectra of a) m-PBN and b) p-PBN in diethyl ether (EOE). For Fig. 4b, the second order Rayleigh scattering in the spectral region 560-585 nm has been omitted.
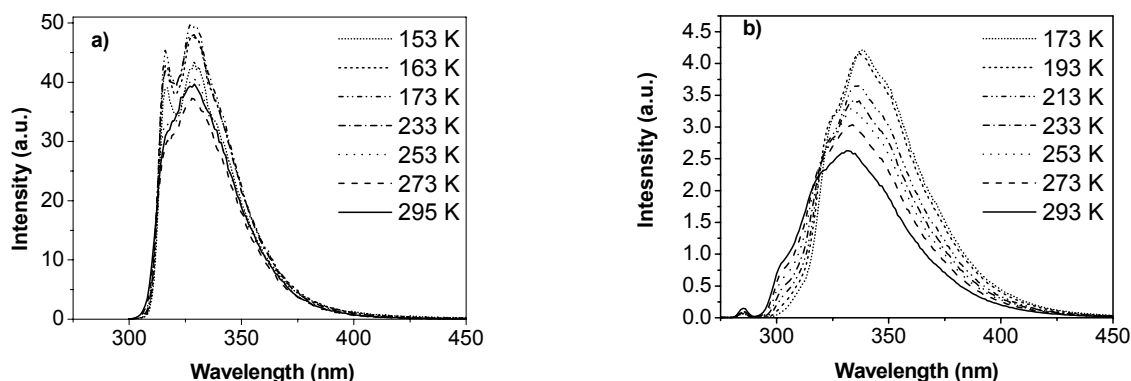

Figure 6.6: Low temperature fluorescence spectra of a) m-PBN and b) p-PBN in the non-polar solvent mixture methylcyclohexane:isopentane, MCH/IP (1:4)

Neither for p-PBN nor for m-PBN, the low temperature spectra in EOE (Fig. 6.5) show an indication of dual fluorescence. But a more complex spectral behavior is exhibited by the development of the vibrational structure for p-PBN and m-PBN in the non polar solvent mixture (MCH-IP), upon cooling (Fig. 6.6).

Upon cooling, the behavior of m-PBN and p-PBN in the alkane solvent is opposite: Whereas the highest energy vibronic band is enhanced in m-PBN upon cooling, this spectral feature diminishes for p-PBN at low temperature. Moreover, the spectra are significantly broader for p-PBN. The behavior of m-PBN can be understood as the normal behavior at low temperature, where the structuring of vibronic bands is enhanced upon cooling. The diminishing of the vibronic feature at around 305 nm for p-PBN at low temperature can then be understood on dual fluorescence, with an LE/CT excited state equilibrium and a thermodynamically more stable CT state [66].

Upon closer inspection, the 0-0 vibronic band is seen to be situated at lower energy in m-PBN (~316 nm) than in p-PBN (~305 nm) reflecting the decreased energy of the emitting LE state for m-PBN (meta-effect), as is already visible in the absorption spectrum (see section 6.3.1 above).

6.4   Computational Results

6.4.1   AM1 Calculations

The ground state optimized geometries of the benzonitrile radical anion, p-PBN and m-PBN as calculated by using the AM1 method are shown in Fig. 6.7. Table 6.3 shows the equilibrium twist angles, rotational barriers to planarity and perpendicularity as well as dipole moments, which were calculated for the ground state. These values are compared with the parent compound, N-phenyl pyrrole (PP). The twist angle and rotational barrier for m-PBN are slightly higher than for p-PBN, but comparable with PP. The rotational barrier for m-PBN and PP to reach the perpendicular geometry is less than for p-PBN due to their more twisted nature in the equilibrium geometry and smaller intermoiety mesomeric contribution.

TABLE 6.3: Equilibrium Twist angles, Rotational barriers to each the Planar and the Perpendicular Geometry and Dipole moments in the S_0 state as Calculated by AM1.

Molecules	Eq. twist angle (degrees)	ΔE_{planar} (kcal/mol)	$\Delta E_{perpendicular}$ (kcal/mol)	μ_0(D)
p-PBN	23.3	0.27	2.59	2.09
m-PBN	26.4	0.40	2.05	2.78
PP	26.5	0.39	2.01	1.77
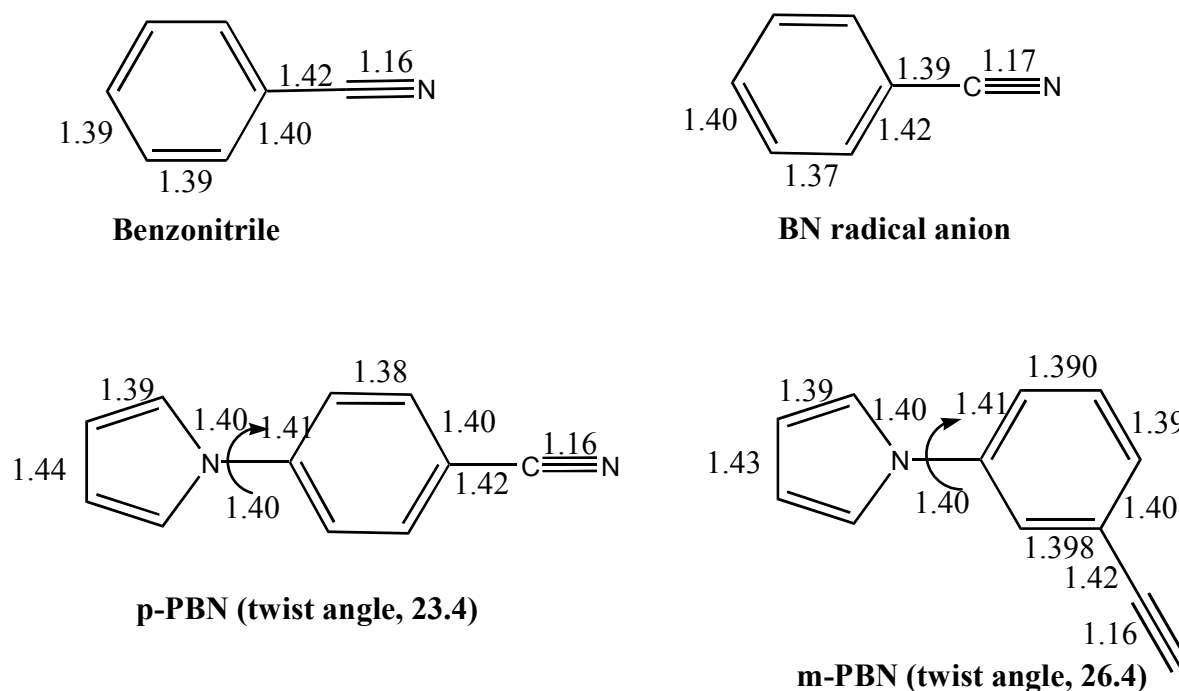
Figure 6.7: Equilibrium structures of benzonitrile (BN), BN radical anion, p-PBN and m-PBN in the S_0 state.

The three ground state optimized conformations (equilibrium twist angle, as well as planar and perpendicular one) were also analysed regarding excited-state energies and properties. Configuration interaction (CI) for the excited states was used. The calculated values of transition energy, relative energy, dipole moments and oscillator strengths of the low lying excited states are collected in Table 6.4 and are discussed below.

6.4.2 CASSCF Calculations

The results on para-PBN have been given in detail previously [73]. The most important observation was that the charge transfer excited state of A symmetry has two minima on the hypersurface which involve both changes in the twist angle α between the pyrrole and the benzene ring as well as characteristic bond length changes in the benzene ring. The so-called quinoid minimum is situated at $\alpha=0°$ (planarity), and the central bonds in the benzene ring are shortened, characteristic for a quinoid distortion. On the other hand, the so-called antiquinoid minimum AQ is characterized by a perpendicular structure ($\alpha=90°$) and by

long central benzene bonds, which are longer than the adjacent ones. It is called an antiquinoid structure [73].
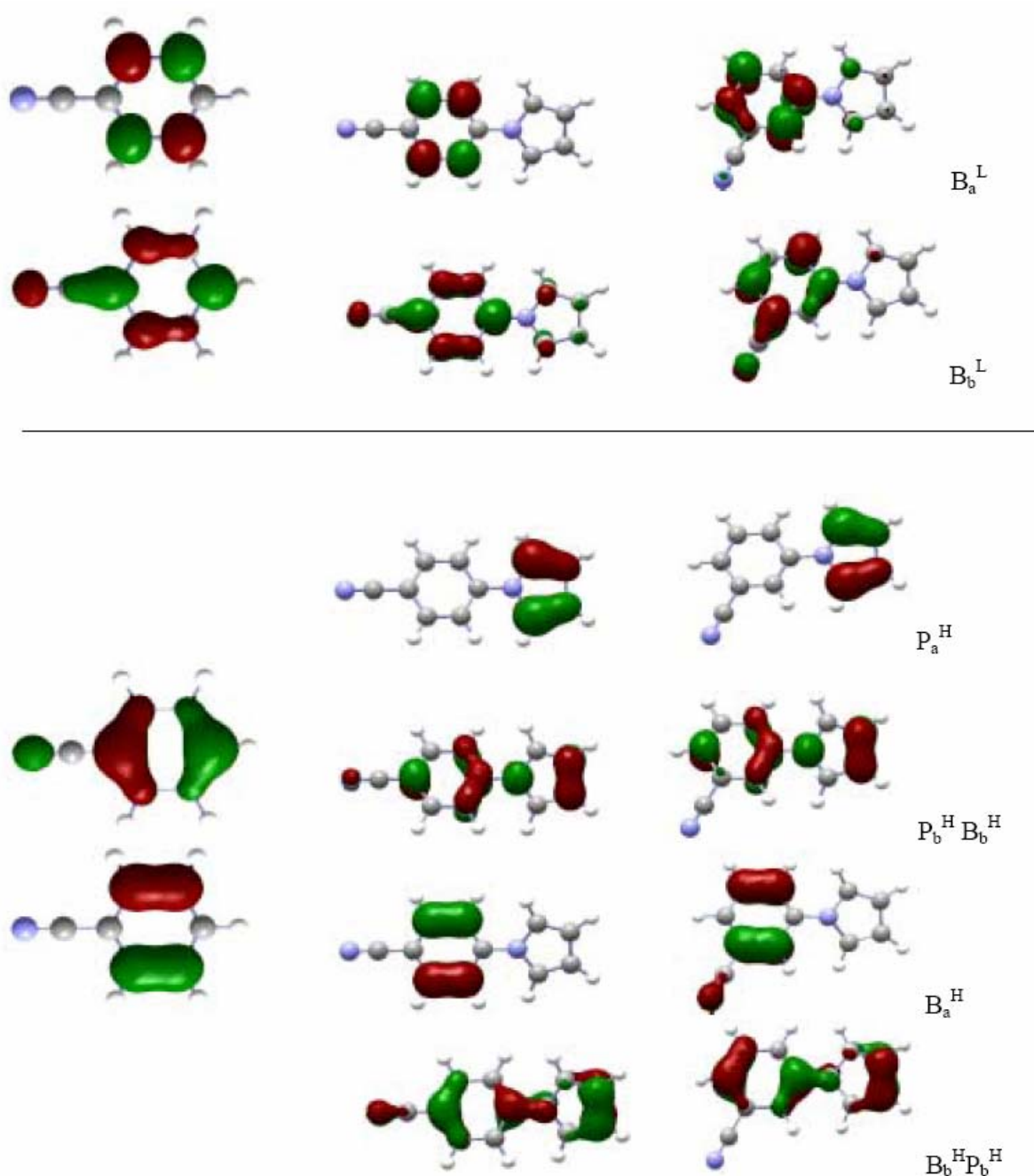
Figure 6.8: The highest four occupied and lowest two unoccupied molecular orbitals for p-PBN and m-PBN in the equilibrium S_0 geometry as calculated by AM1. The corresponding molecular orbitals for benzonitrile are also shown and arranged such that the coupling pattern with the orbitals of the pyrrole group becomes visible. The lower indices a and b denote subgroup orbitals transforming as symmetry species a and b in the symmetry point group C_2. As can be seen, only the subgroup orbitals of b-symmetry can couple leading to the a^+ (bonding) and a^- (antibonding) combination. The position of the cyano group is not important here: Even for m-PBN, the orbitals correspond approximately to the a and b symmetry species.

In the AQ minimum, the orbitals involved in the charge transfer state of symmetry A (HOMO-1 P_b to LUMO B_b, see Table 6.4 and Fig. 6.8), are localized on the subunits (Fig. 6.8 shows the near-planar equilibrium conformation where HOMO-1 is somewhat delocalized), so that the dipole moment is very high (16 D from the AM1 calculations reported in Tab. 6.4; the dipole moment value from the CASSCF calculations is 16.2 whereas for the quinoid minimum Q, the HOMO-1 is strongly delocalized over both rings (see Fig. 6.8: P_bB_b), and the calculated dipole moment is smaller (4.9 D from AM1 and 11.0 D from CASSCF). Note that according to the AM1 calculations (without geometry optimization in the excited state, the energy of the AQ state is very high (S_7), but the Q state is the lowest CT state (S_2). The CASSCF calculations with geometry optimization lower especially the AQ state, so that its minimum becomes lower lying than the minimum of the quinoid state Q, and the energy difference between Q and AQ states has been found to be -0.55 eV in the gas phase.

TABLE 6.4 Results of Semiempirical AM1-CI Calculations for the BN radical anion, and for p-PBN and m-PBN in the Planar and Perpendicular Geometry.

Compounds	Geometry	State	Exc. energy (eV)	Dipole moment (D)	f	C.I. analysis	Orbital notation with symmetry
p-PBN	Planar (0°)	S_0		2.18			
		S_1	3.89	4.03	0.0002	31--33(48%)	
						29--32(36%)	
		S_2	3.94	5.23	0.4222	31--32(76%)	
		S_3	4.45	10.76	0.0237	30--32(74%)	
		S_4	4.64	6.88	0.0000	30--32(90%)	
		S_5	4.83	2.79	0.0195	30--37(32%)	
						31--34(30%)	
p-PBN	eq.(23.3°)	S_0		2.08			
		S_1	3.99	3.92	0.0000	29--32(38%)	
						30--33(46%)	
		S_2	4.02	4.78	0.3525	30--32(68%)	
		S_3	4.47	11.65	0.0239	31--32(76%)	
		S_4	4.73	7.13	0.0053	31--35(80%)	
		S_5	4.74	3.78	0.0561	31--38(28%)	
						31--35(12%)	
p-PBN	(90°)	S_0		1.11			

		S_1	4.17	1.21	0.0030	28--32(48%)
						29--33(44%)
		S_2	4.47	0.83	0.0108	30--34(36%)
						31--38(44%)
		S_3	4.79	17.97	0.0009	31--32(88%)	P_b->B_b
		S_4	4.81	7.04	0.0000	31--37(92%)
		S_5	4.91	1.39	0.1565	29--32(66%)
						28--33(30%)
		S_6	5.12	0.72	0.0705	31--34(78%)
		S_7	5.14	16.02	0.0000	30--32(86%)	P_b->B_b
		S_8	5.26	6.32	0.0223	30--32(86%)
		S_9	5.46	17.21	0.0025	31--33(90%)	P_a->B_a
		S_{10}	5.93	15.02	0.0011	30--33(84%)	P_b->B_a
m-PBN	Planar (0°)	S_0		2.85		
		S_1	3.72	4.03	0.0123	31--32(30%)
						31--33(22%)
		S_2	4.08	3.70	0.2562	31--32(32%)
						31--33(38%)
		S_3	4.53	7.21	0.0269	30--33(34%)
						30--32(38%)
		S_4	4.79	3.15	0.0230	30--38(22%)
						31--34(26%)
		S_5	4.98	7.38	0.0000	30--35(54%)
						30--36(40%)
m-PBN	eq.(26.4°)	S_0		2.75		
		S_1	3.80	3.67	0.0073	30--32(28%)
						29--32(14%)
		S_2	4.15	3.64	0.2233	30--33(38%)
						30--32(28%)
		S_3	4.59	7.47	0.0306	31--33(32%)
						31--32(38%)
		S_4	4.77	3.01	0.0159	31--38(24%)
						30--34(24%)
		S_5	4.95	7.22	0.0003	31--36(52%)
						31--35(42%)
m-PBN	(90°)	S_0		2.73		
		S_1	4.18	2.74	0.0013	28--32(44%)
						29--33(40%)
		S_2	4.45	2.87	0.0063	31--38(46%)
						30--34(36%)
		S_3	4.91	2.63	0.0187	29--32(50%)

				28--33(36%)
S$_4$	4.93	5.56	0.0005	31--37(70%)
S$_5$	4.94	14.79	0.0004	31--32(52%)
				31--33(34%)
S$_6$	5.09	2.87	0.0722	31--34(78%)
S$_7$	5.29	16.55	0.0010	31--32(36%)
				31--33(54%)

The calculations in Tab. 6.4, and also the results of Parusel [78] indicate that for the (rigid) perpendicular geometry (as optimized in the ground state), AQ is not the lowest CT state but a state B(90°) of B symmetry (S$_3$, involving HOMO and LUMO orbitals P$_a$ and B$_b$. The dipole moments are very large in both perpendicular (18 D) and planar conformation (^{1}B(0°) state with 11.7 D) because the orbitals are rather localized even for the planar geometry. Of course, geometry relaxation is again expected to lead to changes in the relative ordering of ^{1}B(0°) and ^{1}B(90°). The energetics of this B-CT state have not yet been calculated with CASSCF geometry optimization. But the arguments and results given below indicate, that the same Q and AQ isomers should be expected for this state.

Because of the decoupled orbitals in the perpendicular conformation, the CT state can be regarded as the combination of an anion radical of benzonitrile and a cation radical of pyrrole. We can therefore expect to get a deeper insight by having a closer look on the benzonitrile anion radical alone, which is of doublet electronic structure but can be calculated as open-shell ground state molecule with somewhat simpler geometry optimization than for the excited state of PBN, and it can readily be treated with the CASSCF calculations. The electronic structure of the benzonitrile anion radical is determined by the occupancy of the doubly occupied and one singly occupied orbital:

Benzonitrile has three low-lying LUMO's, which provide its acceptor ability:

b$_1$(π_x*) a$_2$(π_x*) b$_2$(π_y*)
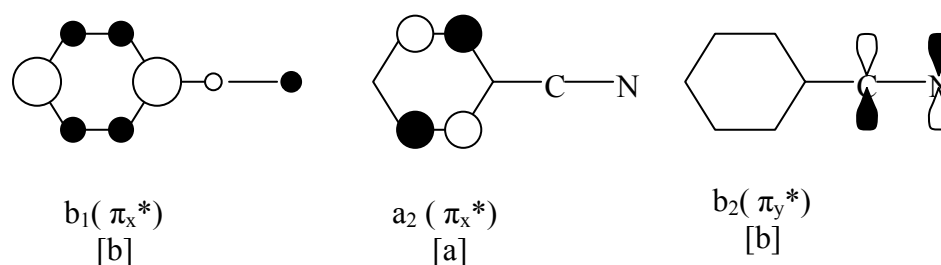[b] [a] [b]

Figure 6.9: The lowest unoccupied MOs of benzonitrile, labelled according to C$_{2v}$ symmetry. The corresponding symmetry species in the C$_2$ point group is given in square brackets (see also the lower indices of the orbitals shown in Fig. 7).

The first two MOs in Fig. 6.9 are normal π orbitals perpendicular to the benzene plane, corresponding to B_b^L and B_a^L in Fig. 7. If the lone electron occupies the b_1 MO, this leads to a
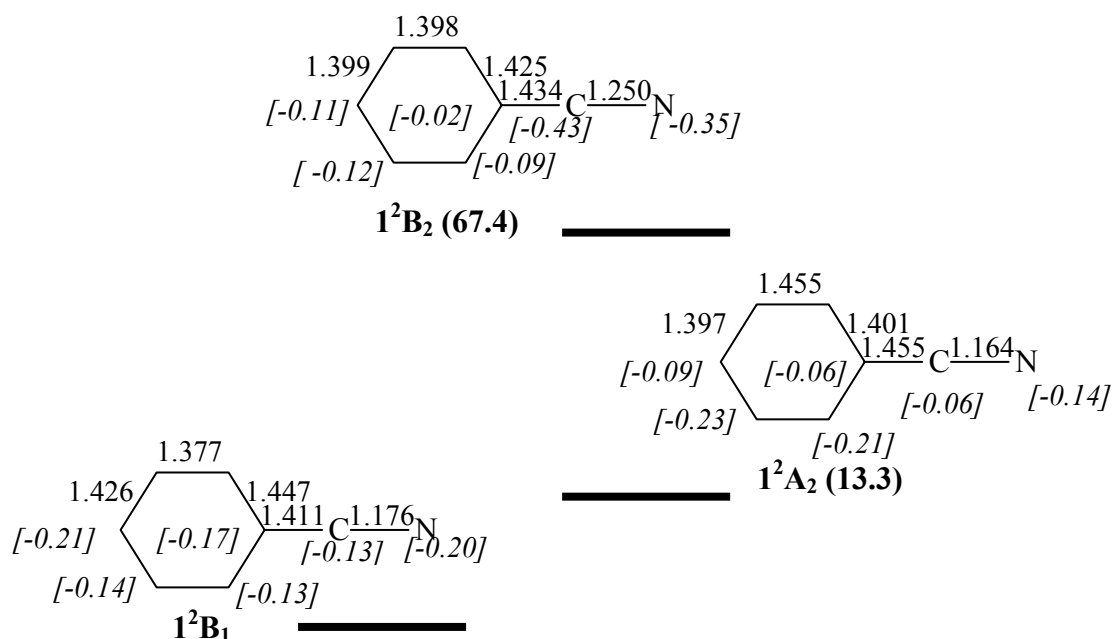

Figure 6.10: Optimized structure with bond lengths given, and Mulliken charges (italic numbers in square brackets) of three states of the benzonitrile radical anion with different orbital occupation patterns. The 1^2B_1 state is the global minimum on the PES of the anion radical. The relative energies in kcal/mol are given in round brackets.

1^2B_1 electronic state of the anion-radical, which has some delocalization of the additional electron on the benzene ring and on the cyano group leads to a 1^2A_2 electronic state of the anion radical and shows the acceptor activity of the benzene ring, without participation of the substituent. Occupation of MO b_2 with one electron leads to a 1^2B_2 electronic state of the anion radical and shows the pure acceptor activity of the cyano substituent.

The choice of the active space for CASSCF calculations was dictated by the needs to take into account all three possible situations. The active space includes four occupied π_x and four unoccupied π_x^* orbitals, and also the orthogonal π_y-system of the CN group: one occupied π_y and one unoccupied π_y^*. The results of the CAS(11/10)/cc-pVDZ calculations (11electrons on 10 orbitals) show the expected changes:

a) the optimized 1^2B_1 state has a quinodal structure (see Fig 6.10 for the bond lengths, with the atomic charges given in square brackets (Lowdin atomic populations) distributed between the benzene ring and the CN group,

b) The 1^2A_2 state has an anti-quinodal structure with the additional electron delocalized on the benzene ring,

c) the 1^2B_2 state has a lengthened CN bond with charge localized on the CN group.

The 1^2A_2 electronic state crosses the 1^2B_1 state along the relaxation coordinate connecting these two states, but it is situated 13.3 kcal/mol above the global minimum. The 1^2B_2 state is an excited state of the anion radical and 67.4 kcal/mol above the global minimum.

6.5   Discussion

6.5.1   Absorption

Excited states of para donor-acceptor substituted benzenes possess two close lying π,π^* excited states: the long axis polarized ^1L_a-type constituting the main long wavelength absorption band and a perpendicularly polarized ^1L_b-type state with much weaker absorption intensity which can cause some structural features in the long wavelength tail of the absorption spectra or which may be completely hidden underneath the much stronger ^1L_a-type band. Depending on the substituents, the role of ^1L_b- and ^1L_a- states as S_1 and S_2 can interchange [79, 80, 81]. For both m-PBN and p-PBN, the main absorption band can be assigned to the ^1L_a-state. The latter is blue shifted in the meta compound because resonance contributions are disfavoured. The ^1L_b band, on the other hand, is slightly red shifted for m-PBN due to the meta-effect [76]. The weak shoulder around 300 nm in the absorption spectrum for m-PBN can therefore be attributed to the well-separated ^1L_b absorption band.

6.5.2   Dual Fluorescence at Room Temperature

The fluorescence maxima of p-PBN and m-PBN show a continuous red shift from non-polar solvents to highly polar solvents indicating that a highly polar CT state is emitting in both compounds. The fluorescence spectrum of m-PBN in n-hexane appears structured fluorescence, and is assigned to an LE emission band ($\Delta\nu_{1/2} = 4064$ cm^{-1}). In the case of p-PBN, however there is a significant broadening ($\Delta\nu_{1/2} = 6233$ cm^{-1}) of the emission spectrum,

which arises due to the overlapping of two emission bands. The corresponding emitting states can be assigned as LE and CT, the former one with a structured spectrum, the latter one with completely structureless emission. The low-temperature experiment (Fig. 6.6) shows that the CT band is enhanced upon cooling. This corresponds to a situation, where CT is situated energetically below LE [66]. In the more polar solvents, this energetic preference is enhanced such that no trace of structured LE emission remains visible.
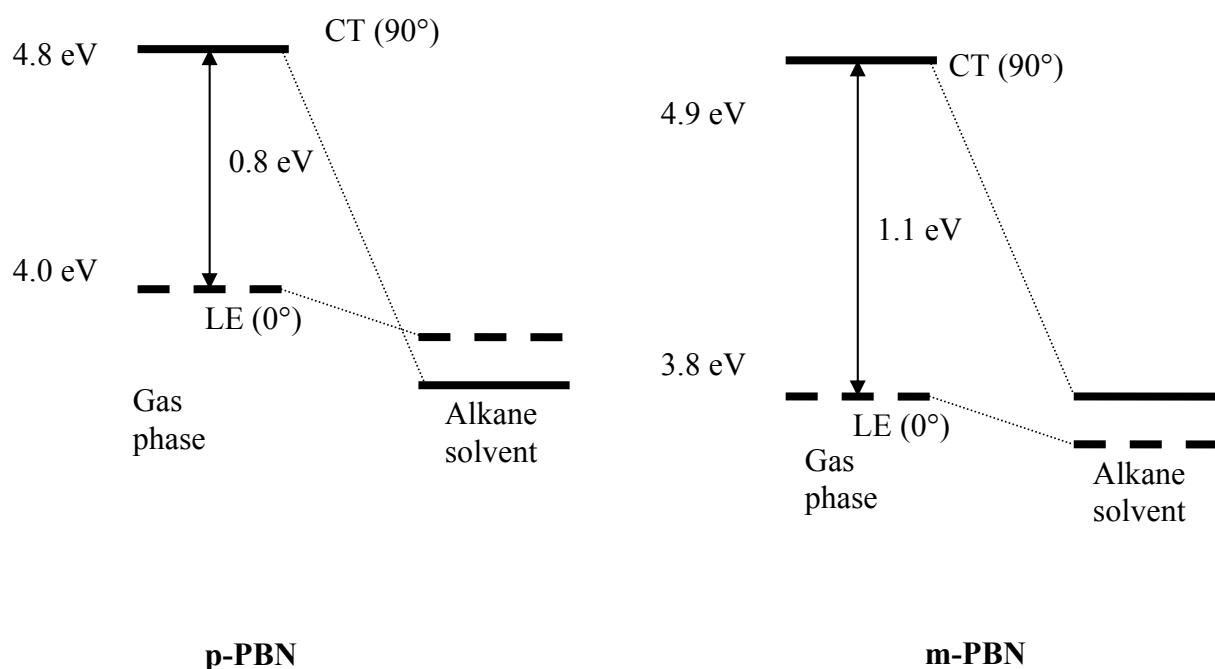
Figure 6.11: Energy differences between the LE State (broken line) and the CT State (full line) of p-PBN and m-PBN in the Gas Phase as calculated by AM1 and Schematic Energy Ordering of these States in Alkane Solvents.

In m-PBN, the LE state is energetically lowered, but the CT state remains approximately at the same energy such that the energetic order is reversed in non-polar solvents, and CT emission only appears in the more polar solvents due to the preferential lowering of the CT state. Moreover, the energy difference between the LE and CT state of m-PBN is only 1.1 eV which is slightly higher than that of p-PBN (0.8 eV) in the gas phase. The latter observations support the evidence for the appearance of a single fluorescence band of m-PBN in n-hexane (fig. 6.11).

6.5.3 Radiative rates and Dipole Moments

The fluorescence rate constant, k_f is significantly larger in alkane solvents as compared to polar solvents indicating a more allowed character of the emission for m-PBN and p-PBN in alkanes, and the values were found to be similar (Table 6.1). With increasing solvent polarity, there is a sudden drop in k_f values corresponding to the change to a forbidden transition. This forbidden character present in medium and highly polar solvents for both compounds is most readily explainable by the population of a CT state with a twisted geometry (TICT state) due to the complete decoupling of the subgroup molecular orbitals [82, 83]. This can also be concluded from sterically hindered model compounds like p-PBN with two ortho methyl groups [66] where the structured LE-features observed for p-PBN are absent. p-PBN and m-PBN behave similar, with k_f values being around 3×10^6 s^{-1} (radiative lifetimes longer than 300ns), quite comparable to the TICT state of DMABN and derivatives [9]. The excited state dipole moment values (Table 6.2) for m-PBN and p-PBN resulting from room temperature and low temperature emission spectra are found to be similar (see ref.4). This gives additional evidence that both m-PBN and p-PBN possess the same highly polar TICT state. Yoshihara *et al.* [67] calculated the excited state dipole moment values for p-PBN and m-PBN by taking the Onsager radii derived from the molecular crystal density. Their values are in good agreement with the values obtained in this work.

Recently, dual fluorescence has been reported also for a rigidized planar derivative of p-PBN [68], however without giving any indication of the associated k_f values. Two models can be discussed for the CT fluorescence in this case:

Model A would associate the CT state with the so-called PICT state [69] with strong mesomeric coupling and preferred planar geometry corresponding to the ^1L_a-type state according to Platt's nomenclature. In this case, the subgroup orbitals (both of symmetry species b in C_2) are strongly coupled, and the resulting k_f values should be larger and the excited state dipole moment should be smaller than for the perpendicular twisted TICT state. The transition moment should be approximately in the long molecular axis (state with symmetry species A in C_2)

Model B would be associated with an electronic configuration with full orbital decoupling available also for the planar geometry. In the case of PP and PBN [29, 55, 79, 80, 81], the donor orbitals on pyrrole should possess a node (this is actually the HOMO in all pyrrole derivatives studied here, see the calculational results), with symmetry species a in C_2, and the acceptor orbital on benzonitrile should also possess a node through the carbon atom

linking the benzene to the pyrrolo group, with symmetry species *a*, resulting again in an emissive state of *A* symmetry, but large dipole moment and very small k_f value. According to CASSCF calculations [73] on p-PBN, this state prefers to be in the perpendicular conformation and has an antiquinoid distortion at 90° (and a quinoid one in the planar minimum, see below). Chemical bridging enforcing planarity could allow this state to be populated provided that the CT state of *B* symmetry or an LE state are not lower in energy. Clearly further studies reporting k_f values and polarization results are necessary to clarify this question.

6.6   Theoretical Investigations

6.6.1 AM1 Calculations

The twist angles of m-PBN (26.4°) and PP (26.5°) are similar in values (Table 6.3), and both compounds have the same rotational barriers towards both planar and perpendicular geometries. In both compounds, the mesomeric interactions stabilizing the planar geometry are similarly weak. In contrast, p-PBN has a smaller twist angle (23.3°), leading to a smaller rotational barrier to planarity: 0.27 kcal/mol as compared to m-PBN (0.40kcal/mol) and PP (0.39 kcal/mol). On the other hand, the rotational barrier (2.59 kcal/mol) of p-PBN towards perpendicularity is considerably higher than for m-PBN (2.05 kcal/mol) and PP (2.01 kcal/mol). This can be directly correlated with the increased importance of the quinoid resonance structure for p-PBN stabilizing the planar geometry. The increased quinoid contribution can also be seen from the S_0 equilibrium structures calculated for both compounds. The benzene bond lengths are very similar for m-PBN, whereas in p-PBN, the middle benzene bonds are clearly shortened with respect to the adjacent ones. The quinoid stabilization becomes even more important in the excited state. Based on valence bond theory, Zilberg *et al.* [73] have proposed two excited state structures on the potential energy surface for donor-acceptor substituted benzene derivatives such as p-PBN. One has the quinoid form, in which the central C-C bond of the benzene ring is shorter than the adjacent bonds and which possesses a planar geometry at the energy minimum. The other excited state conformer possesses central C-C bonds, which are longer than the adjacent ones. This conformer was called the antiquinoid form or AQ state, and it has an energy minimum with the pyrrolo group twisted at 90° with respect to the benzene ring. Attempts to reproduce these results for p-PBN with excited-state optimization in AM1 did not lead to stable AQ geometries and were abandoned. AM1-geometries also did not converge for the AQ-

minimum of ground-state benzonitrile radical anion (see however the next section on ab initio CASSCF calculations), whereas the minimum reached for neutral p-PBN showed a clear quinoid bond length distribution (Fig. 6.7)

Fig. 6.8 and Table 6.4 contain results for single-point calculations of the excited state of p-PBN and m-PBN for three selected optimized ground state geometries which performed in order to understand and assign the various excited states for differently twisted conformations. The calculations include configuration interaction between single and multiple excited configurations and are considered to contain a large part of dynamic correlation, approaching quite closely the experimental absorption energies consistent with the experiment, the main absorption band (S_2) is shifted to the blue when going from p-PBN to m-PBN (testifying for the smaller quinoid stabilization in m-PBN), but the S_1 state shifts to the red, as is typical for meta-substituted donor-acceptor benzenes. In m-PBN, S_1 and S_2 are clearly separated (0.4 eV) and can therefore be seen as separate bands, whereas in p-PBN, both states are calculated to be nearly degenerate, therefore appearing as one of the single absorption band in the experimental spectrum.

According to the calculations (p-PBN, 0°) [84], S_1 is the forbidden ^1L_b-type state (Platt nomenclature) with b-symmetry in C_2, closely followed by S_2 (a-symmetry, ^1L_a-type state) which possess some CT character and is allowed. It is equivalent to the "PICT" state in literature [69]. It is followed by a further state S_3 of b-symmetry with stronger CT (11 D) but forbidden character, which corresponds to the HOMO to LUMO transition (orbital P_a^H to B_b^L in Fig. 6.8). The high dipole moment and forbidden character derives from the localized nature of P_a^H (pure HOMO of pyrrole, Fig. 6.8), whereas the reduced dipole moment (5-6 D) and allowed character of S_2 (PICT) can be traced back to the delocalized nature of the corresponding occupied orbital ($P_a^H B_b^L$) in Fig.7. At 90° twist, S_1 and S_2 develop into pure LE states with a small dipole moment (^1L_b and ^1L_a of benzonitrile) whereas S_3 develops into the TICT state of b-symmetry (18 D dipole moment).

6.6.2 CASSCF Calculations

When comparing the structures of the benzonitrile anion from AM1 (Fig. 6.7) and from CASSCF ab initio (Fig. 6.10), it is seen, that AM1 only converges to the Q form for AM1, although effort was given to find the minimum of the AQ conformer also with AM1. In the neutral benzonitrile, the Q deformation is very small, but significantly larger, if benzene possesses both a donor and an acceptor substituent (p-PBN, Fig. 6.7).

The CASSCF calculations show that the charge distribution in the Q and AQ conformers is quite different. In the former, much charge is localized on the atoms linking the substituent, whereas in the AQ conformer, most negative charge is concentrated on the four central carbon atoms. The Q conformer (1^2B_1) is more stable than the AQ (1^2A_2) one. In terms of orbital involvement, the Q (1^2B_1) state possesses a singly occupied orbital with an antinode through the linking atoms (B_b^L in Fig. 6.8), the AQ (1^2A_2) state a singly occupied orbital with a node through the linking atoms (B_a^L in Fig. 6.8).

When the AQ radical anion conformer of benzonitrile is linked to a π-system at any twist angle such that a CT state is formed, (e.g. linkage to the pyrrolo radical cation in p-PBN), the overall symmetry point group is reduced to C_2, and Q and AQ states of benzonitrile radical anion are of A and B symmetry, respectively, and the singly occupied orbitals similarly. The CT transition from pyrrole to benzonitrile can involve orbitals of the same or of different symmetry on the pyrrolo unit. In the Q state of A symmetry (as calculated in ref. 11), the singly occupied orbital on pyrrole must have an antinode through the linking atom (P_b^H in Fig. 6.8) in order to yield an overall symmetry species A. In the AQ state of A symmetry, both singly occupied orbitals on the two units must have B symmetry in order to yield the overall symmetry A. This means that the planar Q-CT state of A symmetry in PBN involves the transition between orbitals $P_b^H B_b^H$ and B_b^L in Fig. 6.8, but the AQ-CT state of A symmetry involves the orbitals P_a^H and B_a^L. This can be nicely followed by the CASSCF calculation, which shows that for intermediate twist angles, these two conformation mix through configuration interaction. The single occupancy of B_a^L in the AQ state explains both the long central bonds in benzene (orbital node between the central atoms) and the accumulation of negative charge on the adjacent atoms (orbital coefficients only on these atoms in B_a^L).

There are, of course, further CT states present which can most readily be identified at 90° twist. There is a further A state with CT between P_b^H and B_b^L which corresponds in nature to the TICT state in DMABN. And there are two further CT states of B symmetry, combining the orbital pairs P_b^H with B_a^L and P_a^H with B_b^L (see Fig. 6.8). All these states have been calculated for the rigid ground state geometry with AM1 and are contained in Table 6.4 (last column).

The main discrepancy between the CASSCF optimized excited state energies (ref [73]) and the semiempirical (this work) or DFT/MRC results for the rigid geometries [78] is that the A-CT of AQ character is the lowest CT state at 90° after geometrical relaxation [73] whereas for the Franck Condon situation, the CT state of B symmetry (and Q character

involving B_b^L and P_a^H) is the lowest one. We conclude that the excited-state geometrical relaxation must switch these two CT states.

We can also conclude on the two CT states present in DMABN for 90° twist: Because the amino group possesses a donor orbital of B symmetry, two of the CT states in PBN (involving P_a^H) must be absent in DMABN. The lowest TICT state is of A symmetry involving the B_b^L orbital on benzonitrile. We therefore expect that this state has the Q bond length pattern in benzonitrile, as found by all calculations until now [9]. But the second TICT state, somewhat higher lying in energy, will be of B symmetry and involve B_a^L as accepting orbital and is therefore expected to possess the AQ bond length pattern.

Finally, due to the localized LUMO for meta-PBN (Fig. 6.8) we can likewise expect that the geometry-relaxed lowest CT state at 90° will be an AQ state of A symmetry, similarly as in para-PBN.

6.7   Conclusion

The photophysical properties of meta- and para-cyano-N-phenylpyrrole (m- and p-PBN) have shown that both compounds show highly red shifted and strongly forbidden emission in polar solvents, assigned to a TICT state. It is concluded that m-PBN differs from p-PBN by a less exergonic formation of the TICT state from the LE/ICT quinoid state, and it therefore shows only single LE/ICT fluorescence in nonpolar alkane solvents, whereas p-PBN shows dual fluorescence (LE/ICT and TICT).

7 Meta- positioning effect in DPBN: a photophysical study

Abstract

The photophysical properties of the dimethyl derivative of N-Pyrrolo-4-benzonitrile (DPBN), with a change in the position of the acceptor moiety (m-DPBN), have been investigated and compared with the parent compound (p-DPBN). The values of the Stokes shift and of the excited-state dipole moment indicate that both meta- and para-DPBN possess similar excited-state properties regardless of the meta-positioning of the cyano group. The low values for the radiative rate constant suggest the presence of a strongly forbidden transition supporting the model of twisted intramolecular charge transfer (TICT) states.

7.1 Introduction

The charge transfer (CT) states occurring in donor-acceptor systems essentially are driven by two forces: (1) mesomeric forces which involve the resonance interaction between the donor-acceptor moieties. The corresponding states are usually called mesomeric intramolecular charge transfer (MICT) states [40]. (2) A second factor is dipolar solvation, which preferentially stabilizes the largest dipole, hence twisted conformations in CT systems. The CT is therefore often connected with twisting between donor and acceptor leading to so-called twisted intramolecular charge transfer (TICT) states [1, 9, 16, 85]. In this latter process, donor and acceptor moieties are completely decoupled in the CT excited state due to their perpendicular arrangement. The mesomerically stabilized CT state (MICT) always tends to be planar due to this mesomeric interaction, and it is also associated with a smaller dipole moment as compared to the TICT state [40]. This gives the possibility for observing two stable CT minima on the excited state hypersurface, and this can lead to dual fluorescence. The most well known compounds showing dual fluorescence are 4-N,N-dimethylaminobenzonitrile (DMABN) and its derivatives. It is also observed in other donor-acceptor molecules such as phenyl pyrroles with different substituents on the donor-acceptor part [29, 66, 82, 83]. According to the TICT model, the short wavelength fluorescence originates from the primarily excited "Locally Excited" (LE) state, from where the charge transfer (CT) state is accessible by an adiabatic photoreaction including a rotational motion around the bond linking the donor and acceptor moieties and leading to the long wavelength fluorescence band.

In previous work [67, 86] the excited state properties of N-Pyrrolo-4-benzonitrile (p-PBN) have been compared with those of its meta derivative, namely m-PBN. It was found that both compounds possess similar and very large excited state dipole moments. This emission from the excited CT state is of forbidden nature, consistent with the complete decoupling of the donor and acceptor orbitals.
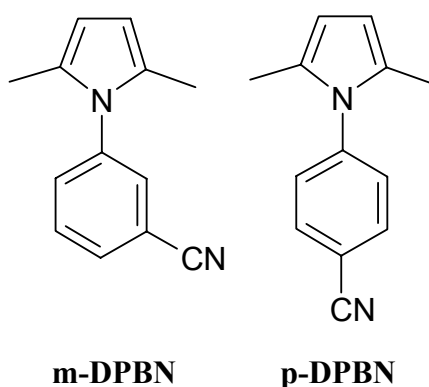

m-DPBN   **p-DPBN**

Figure 7.1: Structures of the molecules investigated

Theoretical calculations by Zilberg *et al* [73] on N-Phenyl pyrroles also helped to interpret the experimental findings. These calculations support two distinct geometrical structures for two different states of CT nature. One has a quinoid (Q) structure and a planar geometry for the energy minimum consistent with the PICT model [69]. The other CT state is of anti-quinoid (AQ) nature, i.e., has lengthened central bonds and its dipole moment is larger than that of the quinoid state. The AQ state has an energy minimum with the pyrrolo group twisted by 90° with respect to the benzene ring.

In the present work, we can ask the question, how the two different CT states will be affected by a) increasing the donor strength b) introducing sterical hindrance to planarity in the ground state. This is achieved by comparing the dimethyl analogues of m- and p-PBN, namely m- and p-DPBN (see Fig. 7.1). The results show that the emissive ICT states of the PBN and DPBN are very similar (forbidden, with large dipole moment) indicating a decoupled ICT nature. Moreover, these properties are similar for meta and para substitution.

7.2   Experimental Section

Technical details about the measurement of absorption and fluorescence spectra and quantum yields are reported in chapter 3.

7.3 Results and Discussion
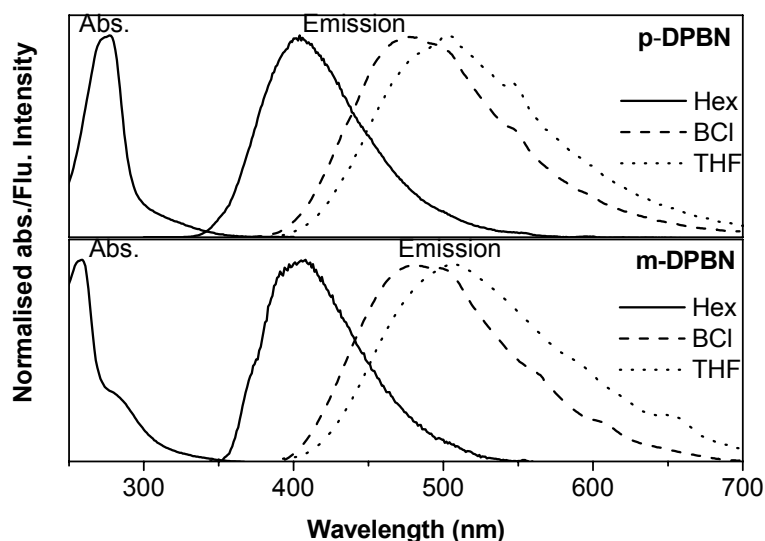
7.3.1 Absorption and Emission Spectra

Figure 7.2: Normalised Absorption and fluorescence spectra of p- DPBN and m-DPBN at room temperature in various solvents of different polarity (HEX = n-hexane; BCl = n-butyl chloride; THF = tetrahydrofuran).

Table 7.1: Spectral and photophysical data of p-DPBN and m-DPBN in various solvents at room temperature.

Sol	λ_{max}^{em} (nm)	Δv_{st} (10^3cm^{-1})	ϕ_f	τ_f (ns)	k_f (10^6s^{-1})	k_f (10^6s^{-1})	k_{nr} (10^8s^{-1})
p-DPBN[a]							
Hex	406	11.7	0.026	2.92	8.90	31.8[c]	3.33
EOE	479	15.7	0.019	8.79	2.16	6.1[c]	1.12
BCl	480	15.8	0.035	8.76	3.99		1.10
THF	501	16.7	0.025	7.00	3.57		1.39
DCM	517	17.3	0.033	9.55	3.45	7.1[c]	1.01
ACN	--	-	<10^{-4}				
m-DPBN[b]							
Hex	403	10.9	0.004	3.56	1.21	46.8[d]	2.80
BOB	444	13.2	0.006				
EOE	477	14.7	0.004	8.46	0.53	4.7[d]	1.17
BCl	481	14.9	0.006	6.67	0.91		1.48
THF	504	15.8	0.003	9.51	0.36	3.2[d]	1.05
ACN	--	-	<10^{-4}				

[a]λ_{max}^{abs} = 275nm, solvent independent (used for excitation); [b]λ_{max}^{abs} = 259nm, solvent independent (280nm is used for excitation); Percentage of error in the measurement: 10% in ϕ_f and 5% in τ_f. [c] for p-PBN; [d] for m-PBN

The absorption and emission spectra of p-DPBN and m-DPBN are almost identical regarding the Stokes shift but the absorption maximum is slightly blue shifted in the case of m-DPBN. The spectra of the two compounds in solvents of varying polarity are shown in Fig.7.2. The corresponding photophysical parameters are collected in Table 7.1. The fluorescence spectra of both compounds show a significant solvatochromic effect, indicating a high charge transfer (CT) character of the emitting state. However, the absorption bands do not show any shift in their maximum in solvents of increasing polarity. The molar absorption coefficients were determined for both p-DPBN and m-DPBN in n-hexane as $\varepsilon\,(\lambda_{275}^{max}) =$ 10350 $M^{-1}cm^{-1}$ and $\varepsilon\,(\lambda_{259}^{max}) = 6369$ $M^{-1}cm^{-1}$ respectively. Donor-acceptor substituted benzenes in para position possess two close lying excited states. One is the long axis polarized, $^{1}L_{a}$- type state, and the other one is the perpendicularly polarized, $^{1}L_{b}$- type state with much weaker intensity which may be completely hidden under the main $^{1}L_{a}$ band although the $^{1}L_{b}$- type state is often the lower one. The main absorption bands for p-DPBN and m-DPBN are 275 nm and 259 nm respectively. For p-PBN, the main absorption band at 287 nm can be assigned to the $^{1}L_{a}$-type excited state (S$_2$) [66]. In the case of m-PBN [86], the main absorption band was observed at 258 nm, which was the similar case in m-DPBN. In going from the para-substituted to the meta-substituted compound, m-DPBN, the weak shoulder around 310 nm is blue shifted to around 285 nm.

The blue shift of the absorption maximum of p-DPBN as compared to p-PBN can be rationalized in terms of the partial CT character of this band connected with a quinoidal resonance structure, which is lowered in energy for the compound with the better donor (p-DPBN). In contrast, the red shifted CT band for p-PBN signifies that that the quinoidal contribution is higher in p-PBN than in p-DPBN. This is probably due to the twisted ground state structure in p-DBPN which disfavours the quinoid contribution. In contrast, for both m-DPBN and m-PBN, the quinoid contribution is less predominant or completely absent. Therefore, the main absorption band is observed at nearly the same energy.

The Stokes shift is also very large in nonpolar solvents indicating that it is not emission from the S$_1$ state, which is visible in absorption but necessitates a photochemical reaction.

7.3.2 Fluorescence Quantum Yields and Rate Constants

The measurements of fluorescence quantum yields and lifetimes for the investigated compounds were done in various solvents of different polarity. The fluorescence

decay curves are monoexponential, which allows the evaluation of radiative and nonradiative rate constants according to equations 7.1 and 7.2. In eqn. 3, $k_{nr.}^{tot}$ corresponds to the sum of all nonradiative processes including triplet formation. The measured data and calculated photophysical values of p-DPBN and m-DPBN are collected in Table 7.1.

$$k_f = \phi_f / \tau_f \qquad (7.1)$$

$$k_{nr.}^{tot} = k_f(\phi_f^{-1} - 1) \qquad (7.2)$$

As one can see from this Table 7.1, the fluorescence quantum yield values show only a small variation in the range of solvents from low to high polarity for both compounds investigated. However, for p-DPBN, the quantum yield values in alkane solvents are significantly larger. For m-DPBN, the value in most other solvents does not differ from n-hexane. For p-PBN [66] and p-DPBN in n-hexane, the quantum yield values are comparable in contrast to m-DPBN as compared to m-PBN with a much larger quantum yield of 0.155 [86]. This latter observation suggests that all compounds except for m-PBN possess a similar electronic structure in this non-polar solvent, namely CT character, whereas the emission of m-PBN is of LE type n-hexane [86]. In highly polar solvents like acetonitrile, m-DPBN becomes non-fluorescent.

The k_f values for both compounds decrease from alkanes to polar solvents by a factor of around 3, indicating a less allowed emission in solvent of high polarity. For both p-DPBN and m-DPBN, the significant decrease of k_f values as compared to p-PBN and m-PBN (see Table 7.1) in going from low- to high-polarity solvents points to a change of the average emitting conformation of the CT state from a less twisted to or more twisted one in the excited state. For TICT systems this can occur with broad (hexane) and narrower angular distribution around the perpendicular minimum of the CT state [9].

7.3.3 Low Temperature Studies

Fluorescence measurements of m-DPBN at lower temperatures were done in the alkane mixture methylcyclohexane/isopentane (1:4), and in the medium polar solvent diethylether in order to study the temperature dependence of the emission maxima and the possibility of dual fluorescence. For the medium polar solvent EOE, with a lowering of temperature, a red shift of the emission maxima is observed (Fig. 7.3a). This thermochromic redshift can be explained by the enhancement of the dielectric constant with a lowering of

temperature and can be ascribed to the solvent stabilization of the CT state. The emission maxima and the associated quantum yields are collected in Table 7.2.

Table 7.2: Temperature dependence of the photophysical data of m-DPBN in the solvent mixture Methylcyclohexane:Isopentane (1:4) and in diethylether.

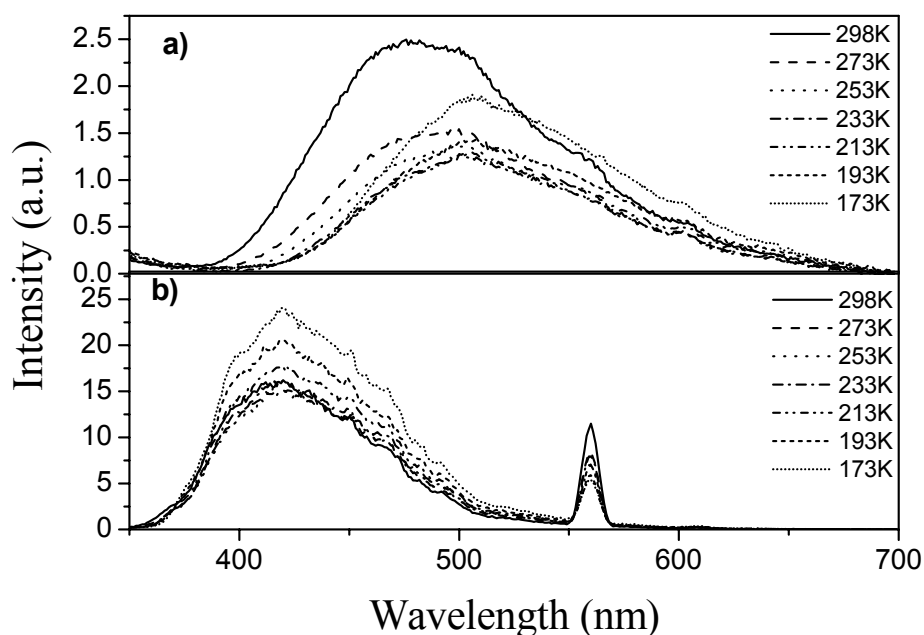| Solvent		298 K	273 K	253 K	233 K	213 K	193 K	173 K
MCH/IP	λ^{em}_{max} (nm)	418	422	423	422	422	422	423
	ϕ_f	0.0350	0.0336	0.0329	0.0345	0.0375	0.0418	0.0487
EOE	λ^{em}_{max} (nm)	477	491	498	504	508	511	515
	ϕ_f	0.0045	0.0028	0.0026	0.0024	0.0025	0.0029	0.0036

Figure 7.3: Temperature effects on the fluorescence spectra of m-DPBN in a) diethyl ether and in b) methylcyclohexane and isopentane mixture (1:4)

In the case of m-DPBN in the non-polar solvent mixture (MCH:IP), the emission maxima observed do not show a noticeable shift (Fig. 7.3b). A similar behaviour has been observed in the case of p-DPBN [66]. For p-PBN, a dual fluorescence was observed in the non-polar solvent mixture [66, 67, 86]. In this case, there is a continuous red shift of the

maximum in going down from higher to lower temperature with the disappearance of the short-wavelength shoulder [86]. Neither for m-DPBN in the alkane solvent mixture or in EOE nor for p-DPBN [66] in the alkane mixture and in the highly polar solvent ethanol in the fluid range, there is any dual fluorescence detected upon cooling. The latter observation can be rationalized by the strong donor nature of the ortho-dimethyl pyrrolo part as compared to pyrrole, which leads to a corresponding stabilization of the CT band even in alkanes such that the LE state is considerably higher in energy than the CT state. The temperature dependent quantum yield values do not show any significant trend in both measurements for different polarity. There does not seem to be a strong temperature dependent fluorescence quenching channel in m-DPBN.

7.3.4 Excited State Dipole Moments

The excited state dipole moments μ_e are calculated from a plot of the solvatochromic shift of the emission maxima versus solvent polarity (see Fig. 7.4), and are calculated using the Mataga equation (eq. 7.3), where μ_g and μ_e are the ground and excited state dipole moments, respectively.
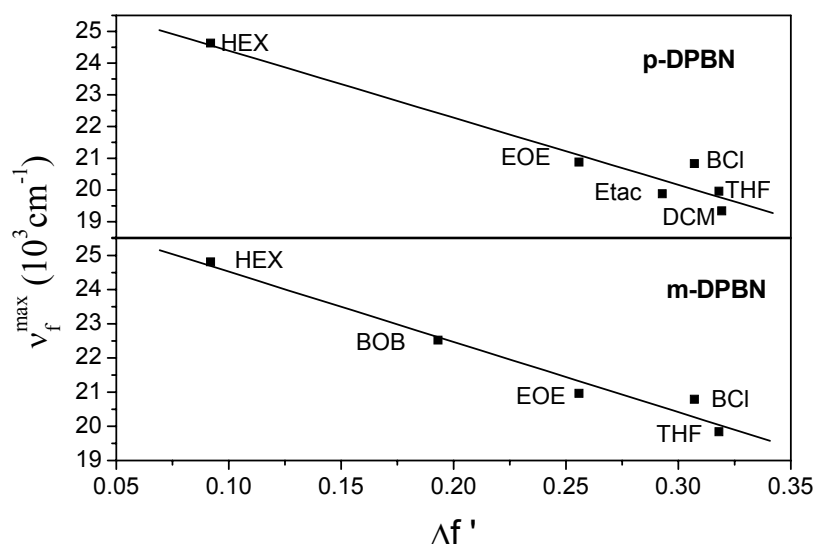

Figure 7.4: Mataga plot of p-DPBN and m-DPBN in various solvents of different polarity.

86

Table 7.3: Dipole moments for the ground and excited states derived for p-DPBN and m-DPBN from the Mataga plot (see fig. 7.4).

	a (Å)[a]	Slope ($10^3\,cm^{-1}$)	μ_g (D)[b]	μ_e (D)
p-DPBN	4.3	-21.1	1.68	13.8
m-DPBN	4.3	-20.6	2.72	14.3

a) from eq. (7.4) by assuming equal densities; b) calculated from AM1 calculation

$$v_f = -\frac{2\Delta f'}{4\pi \in_0 hca^3} \mu_e\,(\mu_e - \mu_g) + \text{const} \qquad (7.3)$$

with $\Delta f' = (\varepsilon\text{-}1)/(2\varepsilon+1) - 1/2(n^2\text{-}1)/(2n^2+1)$

$$a = \sqrt[3]{3M/4\pi N_A \rho} \qquad (7.4)$$

where h is the Planck's constant, $\in_0$ is permittivity constant of vacuum and c is the velocity of light. $\Delta f'$ is the solvent polarity parameter, consisting of dielectric constant ε and refractive index n. The Onsager radii 'a' for p-DPBN and m-DPBN were calculated from the mass-density formula eq. (7.4) by assuming equal densities for both compounds, and the ground state dipole moments, μ_g, are calculated by using the AM1 semiempirical method embedded in the Ampac software package [44]. The resulting μ_e values of p-DPBN and m-DPBN are shown in Table 7.3. By taking similar Onsager radii for both compounds, the calculated excited state dipole moments values are close to 14 D. The high dipole moment values in the excited state indicate that CT state exist in these compounds. This value is comparable to the parent compound PBN (14.8 D) [86]. These observations suggest that the o-dimethyl pyrrole derivatives of PBN possess similar CT excited state properties.

7.4   Discussion

The lower fluorescence quantum yield values of m-DPBN as compared to p-DPBN are linked to significantly lower k_f values (Table 7.1) whereas the non-radiative rates are similar. This strong difference between meta and para substitution is not present for the

corresponding PBN pair of compounds [86]. At present, the reason for this different behaviour is unclear.

In principle, another type of CT state can also be discussed, namely the highly coupled and mesomerically stabilized CT state with a preference for the planar conformation (mesomeric intramolecular charge transfer (MICT) state [40]). In this case, high k_f values would be expected, and the population of a MICT state can therefore be ruled out. A further possibility is the so-called planar intramolecular charge transfer (PICT) state [69]. This model has been formulated in conjunction with a crossing of both S_1 (^1L_b-type) and S_2 (^1L_a-type) states, and is thought to possess a planar quinoid structure with high coupling and allowed emissive character. These expectations are not supported by our observations on k_f. Zilberg *et al* [73] proposed a model where the most stable CT state is twisted and is of antiquinoid nature and decoupled. This latter model is consistent with the findings in this work.

7.5   Conclusion

Both p-DPBN and m-DPBN have similar values in the amount of Stokes shift and polarity induced red shifts evidencing their large excited-state dipole moments. The lower k_f values of m-DPBN and p-DPBN as compared to the PBN pair give evidence that the transition is more forbidden in the DPBN pair. Since the introduction of the two methyl groups in ortho position considerably increases the average twist angle of the donor moiety both in the ground and the excited state, this sterical influence will also narrow the rotational distribution function around the perpendicular TICT minimum and therefore lead to the reduced transition moment values [1, 9]. In summary, it is concluded that the DPBN compounds possess similar excited state properties irrespective of the position of the cyano group in the acceptor moiety and similarly as the PBN pair form a TICT state of forbidden emissive properties and very large dipole moment.

8 Photophysical Properties of Pyrrolobenzenes with Different Linking Pattern: The Transition Between Large (MICT) and Small (TICT) Charge Transfer Interaction behaviour

Abstract

Pyrrolobenzenes with different substitution patterns, MP2BN and MP2-B25CN, are investigated by using steady-state and time-resolved optical spectroscopy. The absorption and fluorescence spectra of these compounds are red shifted with respect to the parent compound p-PBN, indicating a stabilisation of the Franck-Condon (FC) excited state by mesomeric interaction. Both the position and strength of the electron acceptor moiety influence the emission characteristics of these molecules. The large radiative rate constant of MP2BN indicates an allowed emission due to mesomeric interaction between the donor and acceptor moieties, (MICT), whereas in the case of p-PBN and MP2-B25CN, the reduced radiative rate constant indicates a forbidden emission from a twisted intramolecular charge transfer (TICT) state.

8.1 Introduction

The photophysics of donor-acceptor substituted benzenes are of great interest in the study of intramolecular charge transfer (ICT) states. ICT states are commonly observed in N-phenylpyrrole (see Fig. 8.1) and several sterically hindered derivatives [29, 66, 82] and are identified by their large fluorescence red shift in medium and strongly polar solvents. ICT compounds either have an allowed emission (high transition dipole moment, M_f) or a forbidden emission (small M_f). The difference between the two types of CT states is the mesomeric interaction between the molecular subsystems [40]. ICT states with allowed emission are generally found in nearly coplanar compounds with high mesomeric interaction (mesomeric ICT state, MICT). For planar systems, this corresponds to the so-called PICT (Planar Intramolecular Charge Transfer) state as introduced by Zachariasse et al [69], but is more general and can also be used for compounds which cannot become planar but nevertheless show dual fluorescence [87]. ICT states with forbidden emission in nearly perpendicular compounds with small mesomeric interaction are commonly called TICT (Twisted Intramolecular Charge Transfer) states [1, 9].
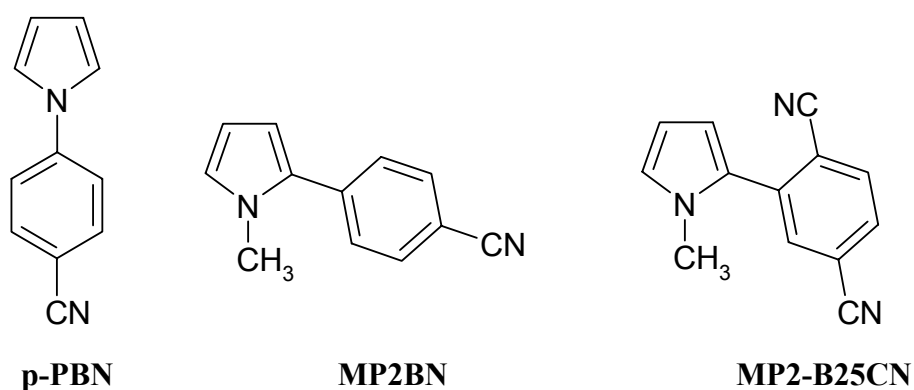
Fig. 8.1 Molecular structures of the investigated compounds and their abbreviated formulas.

Phenyl pyrroles contain an sp^2 hybridized nitrogen, thus the inter-moiety twist angle α is better defined than in dimethylanilino derivatives with a pyramidal nitrogen, and these compounds can in principle populate an ICT state in the twisted geometry [29, 66, 82]. In other cases, the population of nonfluorescent TICT-like states has been identified as the cause for intramolecular fluorescence quenching in many commonly used dyes [88, 89] and even laser dyes [90, 91, 92]. According to the TICT model, the fluorescence can originate from the primarily excited 'locally excited' (LE) state as well as from the charge transfer (CT) state accessible only by an adiabatic photoreaction from the LE state, which includes a torsional motion around the bond linking the donor and acceptor moieties. The relative amount of TICT fluorescence depends on the height of the barrier separating the LE and CT states and on their energy difference. If there is no barrier between these two excited states and their energy difference is large enough, the LE state population is rapidly converted into the TICT state and only the long wavelength emission from the charge transfer state is observable. This TICT emission probability is usually small, i.e. with a reduced value of the transition moment, due to the small π overlap in the strongly twisted arrangement of chromophores [16, 19, 93].

Recently, theoretical studies on N-pyrrolobenzene (PB), N-pyrrolobenzonitrile (PBN) and 4-N,N-dimethylaminobenzonitrile (DMABN) for the ground and excited states were done by Parusel [78] using a DFT/MRCI approach. It was found that the TICT state of PB is stabilized only in polar solvents whereas in the case of p-PBN, the TICT state is more stable than the LE state even in non polar solvents.

Zilberg et al. [73] calculated the energies, dipole moments and molecular structures of the locally excited (LE) and charge transfer (CT) states of DMABN, PP and p-PBN by DFT (used only for optimization), CASSCF and CASPT2 methods (for calculating energies). Their calculations support the existence of two distinct structures for the CT states. One possesses a quinoid structure that has a coplanar arrangement of the chromophores at the energy minimum, corresponding to the MICT [40] or PICT model [69, 71] (in both cases a planar intramolecular charge-transfer state with large interchromophoric coupling). The other one has an antiquinoid bond length distribution in the benzene ring and an energy minimum for the twisted structure connected with a larger dipole moment consistent with the TICT model [9].

Recently, Yoshihara et al. [67] experimentally determined the excited state dipole moments of both ICT and LE states for dual fluorescent molecules such as N-phenylpyrrole, N-(4-methylphenyl)pyrrole, N-(4-cyanophenyl)pyrrole and N-(3-cyanophenyl)pyrrole from solvatochromic and thermochromic measurements. They also compared the experimental ICT state dipole moments with theoretical values from the literature calculated for both coplanar (PICT) and twisted (TICT) conformations of the phenyl pyrrole and cyanophenyl pyrroles. It was found that for N-phenylpyrrole and N-(4-methylphenyl)pyrrole the main fluorescence is of LE character, while N-(4-cyanophenyl)pyrrole and N-(3-cyanophenyl)pyrrole exhibit major emission from the ICT state.

In the PICT and TICT states of pyrrolobenzenes, the pyrrole unit acts as the donor moiety and benzonitrile as the acceptor, and electron transfer (ET) takes place from the pyrrolo group to the center of the phenyl ring, or still farther toward the acceptor substituent. The aim of the present study is to investigate whether the CT nature (either allowed (MICT/PICT or forbidden (TICT)) can be influenced by changing the position of the acceptor moiety on the pyrrole unit, and also how it depends on the acceptor strength. For this purpose, the pyrrolo benzonitrile derivatives 2-(4-cyanophenyl)pyrrole (MP2BN) and 2-(2,5-cyanophenyl)pyrrole (MP2-B25CN) have been synthesized with a linkage in 2-position of pyrrole, and their photophysical characteristics have been compared with those of p-PBN.

8.2   Experimental Section

The experimental details about the absorption, fluorescence, lifetime and quantum yield measurements are described in chapter 3.

8.3 Results and Discussion

8.3.1 Absorption and Fluorescence Spectra

The absorption and fluorescence spectra of p-PBN, MP2BN and MP2-B25CN in solvents of varying polarity are shown in Fig. 8.2. The corresponding photophysical parameters are collected in Table 8.1. The absorption spectrum of p-PBN is a single and broad band whereas in the case of MP2BN and MP2-B25CN, a slightly structured band can be observed. For all three compounds, the absorption maximum changes very little with the polarity of the solvent. In nonpolar hexane, the absorption and fluorescence maxima of MP2BN and MP2-B25CN are significantly red-shifted with respect to the parent compound (p-PBN), indicating the stabilization of both their excited and ground states by the larger mesomeric interaction.
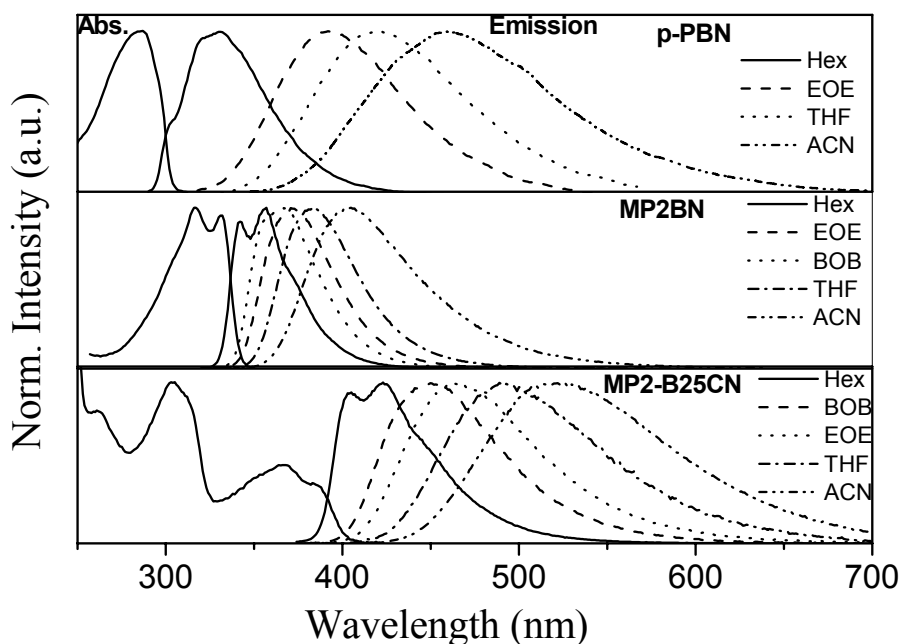

Figure 8.2: Normalised Absorption and fluorescence spectra of p-PBN, MP2BN and MP2-B25CN in solvents of different polarity (Hex – n-hexane, BOB – dibutylether, EOE – diethylether, THF – tetrahydrofuran, ACN – acetonitrile.

Table 8.1: Spectral and photophysical data of p-PBN, MP2BN and MP2-B25CN in various solvents at room temperature.

Sol	λ_{abs} (nm)	λ_{flu} (nm)[a]	$\Delta\nu_{st}$ (10^3cm^{-1})	$\phi_f^{b,a}$	ϕ_f^c	τ_f (ns)[d,a]	k_{rad} (10^7s^{-1})	k_{nr}^{tot} (10^7s^{-1})
p-PBN								
Hex	287	332	4.72	0.077	0.028	2.42	1.16	40
EOE	287	393	9.39	0.023	0.022	3.80	0.57	26
THF	287	422	11.15	0.024	-		-	-
DCM	287	412	10.57	0.022	0.022	3.10	0.72	32
ACN	287	460	13.10	0.024	0.036	8.20	0.43	12
MP2BN								
Hex	317	357	3.53	0.92		1.8	51.1	4.44
BOB	321	367	3.90	1.03		-	-	-
EOE	321	371	4.35	0.98		5.21	18.8	0.38
THF	326	383	4.70	0.94				
ACN	322	407	6.49	0.51		5.4	9.4	9.03
MP2-B25CN								
Hex	366	423	3.68	0.378		7.47	5.06	8.33
BOB	370	455	5.05	0.281		11.43	2.45	6.26
EOE	364	463	6.15	0.206		12.60	1.63	6.28
THF	370	489	6.91	0.139		13.12	1.05	6.50
ACN	359	524	9.27	0.024		2.78	0.86	34.9

[a] Excitation wavelength was fixed at the absorption maximum. [b] error in the measurement: 10%. [c,d] from ref.66.

On the other hand, the solvatochromic shift of the fluorescence of these compounds is much smaller (3400 and 4700cm^{-1}) than for p-PBN (8500 cm^{-1}) indicating smaller changes in their dipole moment from ground to excited state. The fluorescence quantum yield decreases from solvents of low to high-polarity for all three compounds investigated in this work. However one notes that p-PBN is weakly fluorescent with a yield smaller than 8%, MP2-B25CN exhibits a yield smaller than 40%, whereas MP2BN, has a yield close to 1 in all solvents except in acetonitrile where it drops to 50%. As pointed out below, these differences can mainly be traced back to changes in the radiative rate constant k_{rad}.

8.3.2 Potential Energy Surfaces

The schematic excited-state hypersurfaces for p-PBN, MP2BN and MP2-B25CN as a function of the twist angle are shown in Fig. 8.3. It explains the relative energetic position of the excited states both in the planar (0°) and perpendicular (90°) geometries. In going from 0° to 90° there is a stabilization of the TICT state (twisted geometry) for p-PBN and MP2-B25CN.
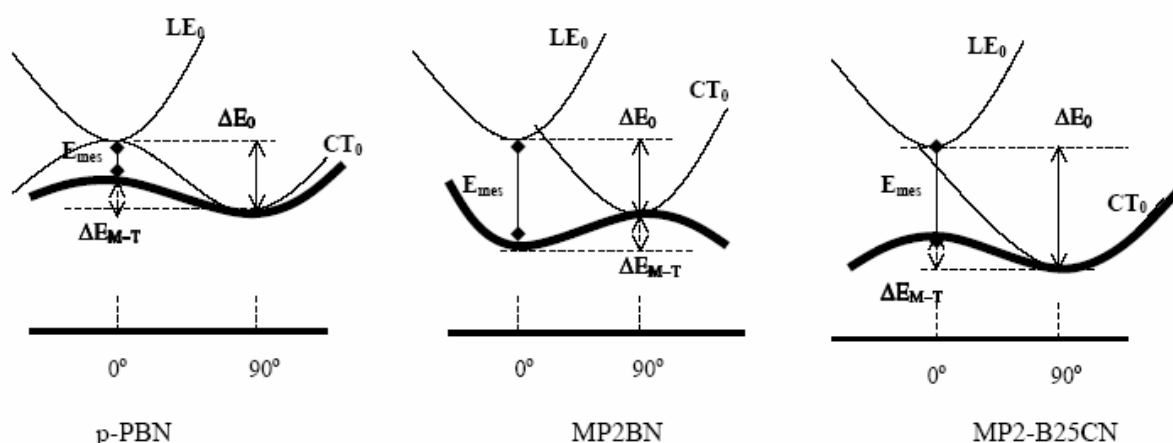

Figure 8.3:. Schematic representation of the excited state hypersurfaces for p-PBN, MP2BN and MP2-B25CN in the planar and perpendicular geometry. *(LE$_0$- locally excited state; CT$_0$- charge transfer state, both without mesomeric interaction; E$_{mes}$- Mesomeric energy – zero for the perpendicular, of varying size for the planar geometry resulting in the TICT (perpendicular) and the MICT states (planar geometry; ΔE_{M-T}- energy difference between MICT and TICT states; ΔE_0- energy difference LE$_0$ and CT$_0$ states)*

On the other hand, for MP2BN as compared to p-PBN, the MICT state (planar form) is more stable than the TICT state due to the increased mesomeric interaction between the two submoieties. This is a consequence of the different size of the coefficients of the donor orbital on the pyrrole, with a large value on carbon atom 2 (MP2BN) and a node on the nitrogen (p-PBN). In MP2-B25CN, the TICT state is lower than the MICT state in spite of the larger mesomeric interaction, due to the increased energy gap ΔE_0 between the zero order LE and TICT states.

8.3.3 Dipole Moments and Radiative and Nonradiative Rate Constants

In Table 8.2, the ground and excited state dipole moments of all three compounds are collected. The excited state dipole moments, μ_e are calculated from the plot of the solvatochromic shift of the emission maxima (ν_f) versus the solvent polarity function $\Delta f'$ (see fig. 8.4a and fig. 8.4b), and are calculated from the following equation [53, 54]:

$$\nu_f = -\frac{2\Delta f'}{4\pi \in_0 \, hca^3} \mu_e \, (\mu_e - \mu_g) + \text{const} \qquad (8.1)$$

with $\Delta f' = (\varepsilon\text{-}1)/(2\varepsilon+1) - 1/2[(n^2\text{-}1)/(2n^2+1)]$

where ε is the dielectric constant and n the refractive index of the solvent
and a is the Onsager radius, $a = \sqrt[3]{3M/4\pi N_A \rho} \qquad (8.2)$

with ρ the density of the compound, M its molecular weight and N_A Avogadro's number.
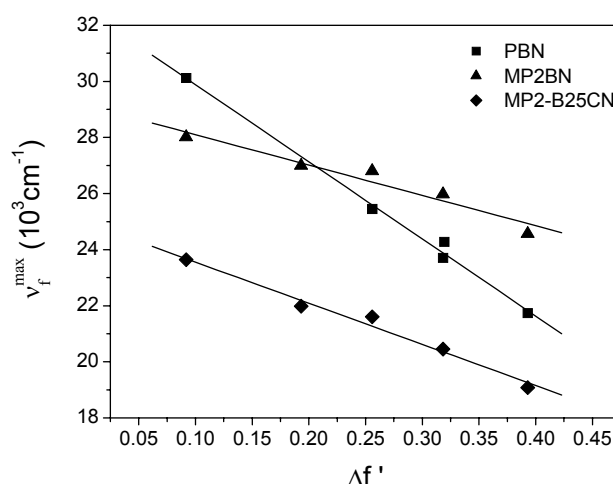

Figure 8.4a: Fluorescence maxima of p-PBN, MP2BN and MP2-B25CN at room temperature versus the solvent polarity parameter Δf' (see text).

Table 8.2: Onsager radius (a), ground state equilibrium twist angles (α) , solvatochromic slopes, ground (μ_g) and excited-state (μ_e) dipole moments derived for p-PBN, MP2BN and MP2-B25N from the Mataga plot [ref.21,22] (Fig 4a and Fig 4b).

	a (Å)	α	Slope (cm^{-1})	μ_g (D)[c]	μ_e (D)
p-PBN	4.1[a]	23.3	-27.501	2.09	14.8
	4.1[a]		-35.489	2.09	16.6[d]
MP2BN	4.2[b]	37.5	-10.823	3.87	11.0
MP2-B25CN	4.3[b]	46.1	-15.441	1.96	12.3

[a] from ref. 8.2. [b] Calculated from eq. (1) relative to p-PBN. [c] Calculated from AM1 calculation. [d] From the Mataga plot [ref.53,54] in diethyl ether at low temperatures
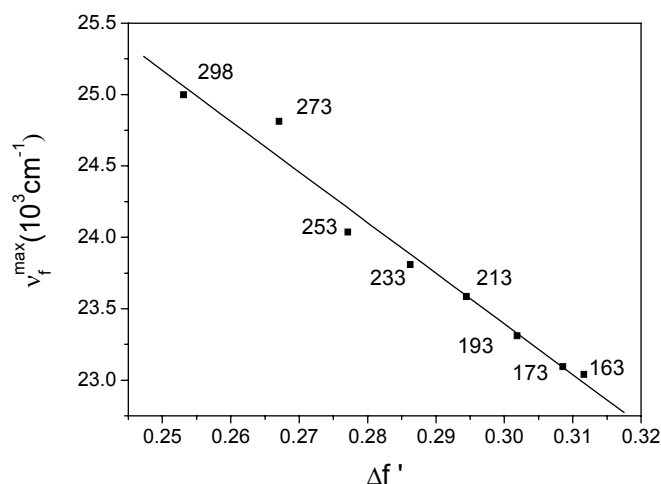
Figure 8.4b: Fluorescence maxima of p-PBN in diethylether versus $\Delta f'$ at different temperatures, indicated in Kelvin on the curve.

The Onsager radii *a* given in Table 8.2 for MP2BN and MP2-B25CN were calculated relative to p-PBN from the mass-density formula (eq. 8.2) by assuming equal densities ρ. The ground-state dipole moments, μ_g, are calculated by using the AM1 (Austin model 1) semiempirical method [42] of the AMPAC software package [44]. As can be seen from Table 8.2, the μ_g values for p-PBN and MP2-B25CN are found to be similar and about half that of MP2BN. The equilibrium twist angle is found to increase from p-PBN (α = 23.3°), to MP2BN (α = 37.5°) and to MP2-B25CN (α = 46.1°), which normally leads to a decrease of the dipole moment. The increased ground-state dipole moment for MP2BN is therefore due to a better electronic coupling between the two moieties, because the pyrrole group is linked in 2-position where the orbital coefficient is large. In MP2-B25CN, the dipole moment is decreased with respect to MP2BN by two sources: the increased twist angle and the CN substituents in positions where they will keep any transferred charge near the center of the benzene ring whereas in MP2BN this charge is pulled towards the CN substituent and hence moved further away from the donor pyrrole group.

Similar arguments hold for the excited state. In contrast to the ground state dipole moments, however, the μ_e values of MP2BN and MP2-B25CN are smaller than for the reference compound p-PBN. This can be rationalized by the assumption, supported by the experimental k_{rad} values, that two different CT states are populated. As detailed above, MP2BN can be assumed to populate a state with maximal mesomeric interaction, close to

96

planarity. In this MICT state, the dipole moment must be lower than for the extreme situation of the 90° twisted TICT state [9, 19], because mixing between the pure CT and nonpolar states occurs. As supported by the very low k_{rad} values (see below), p-PBN and MP2-B25CN both populate a TICT state, which differs however by the center of charge distribution in the LUMO of the acceptor moiety. For p-PBN, the center of negative charge of the acceptor orbital is located further away from the donor pyrrole group, whereas for MP2-B25CN, since the cyano groups are located in the ortho and meta positions with respect to the donor group, the center of negative charge is positioned in the middle of the acceptor orbital. This must lead to a smaller value of μ_e for the TICT state in MP2-B25CN. Thus, the MICT character of MP2BN is characterized by two observables: the somewhat reduced value of the dipole moment when compared to the other two compounds in the excited state, and the increased radiative rate constant.

The fluorescence decay curves are monoexponential, which allows the evaluation of radiative and nonradiative rate constants, k_{rad} and k_{nr} respectively, according to equations 8.3 and 8.4. In eqn. 8.4, k_{nr} corresponds to the sum of all nonradiative processes including triplet formation. The measured data and calculated photophysical values for p-PBN, MP2BN and MP2-B25CN are collected in Tables 8.1.

$$k_{rad} = \phi_f / \tau_f \qquad\qquad (8.3)$$

$$k_{nr.}^{tot} = k_{rad} \ (\phi_f^{-1} - 1) \qquad\qquad (8.4)$$

The k_{rad} values for all three compounds decrease from non-polar to polar solvents, indicating a less allowed emission in solvents of higher polarity. For both p-PBN and MP2-B25CN, k_{rad} values in highly polar solvents are about one order of magnitude smaller as compared to MP2BN. Particularly, the k_{rad} values (see Table 8.1) in acetonitrile are below 10^7 s^{-1} in p-PBN and MP2-B25CN indicating a forbidden emission from a TICT state whereas in the case of MP2BN the CT emission is tenfold more allowed. We assign this emission to a CT state with near planar geometry, i.e. partial twisting and mesomeric stabilization (MICT state).

8.4   Strength and Position of the Acceptor Part

By changing the position of the acceptor part, and also by increasing its acceptor strength by introducing two cyano substituents from MP2BN to MP2-B25CN, interesting changes in the photophysical properties are observed. As discussed above, the nature of the emissive state can be judged from the magnitude of the radiative rate constant (Tables 8.1). The spectra are also affected: as can be seen from fig. 8.2, for MP2BN, where the acceptor has been substituted in 4-position with respect to the donor part of methyl-pyrrole, a blue shift of the emission in both hexane and acetonitrile is observed with respect to the emission of MP2-B25CN. On the other hand, the absorption and emission maxima of MP2-B25CN are both red-shifted with respect to those of p-PBN and MP2BN. This can be attributed to the increased acceptor strength in MP2-B25CN because CT transitions vary with the donor acceptor properties of the constituents.

8.5   Transient Absorption Studies

The transient absorption spectra measured for MP2BN in medium (THF) and strongly polar (ACN) solvents by subpicosecond transient absorption spectroscopy show a dominant absorption band below 400 nm and a residual gain band in the red-wing of the fluorescence spectrum (see fig.8.5). The absorption band is similar to that of the benzonitrile radical anion [94] but is somewhat blue shifted due to the overlap with the gain band. The observation of a gain band indicates that the stimulated-emission cross section is large enough, which is consistent with the allowed MICT-nature of the excited-state. Such a gain band is indeed not observed for DMABN [94] although one cannot exclude that for this latter compound the excited state absorption is only slightly dominant so that the sum of gain and absorption yields a relatively weak transient absorption signal.
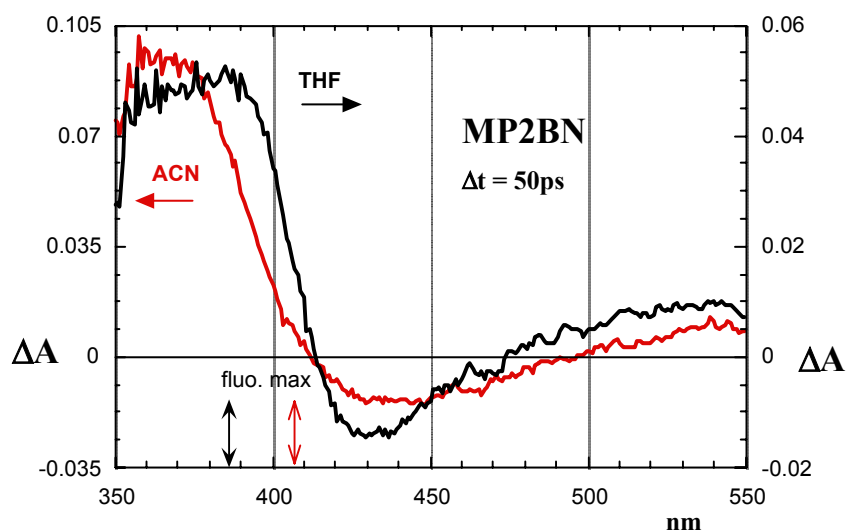
Figure 8.5 : Transient absorption spectra of MP2BN in acetonitrile (red) and in THF (black) measured 50 ps after excitation with a subpicosecond laser pulse. The stimulated emission of the MICT state is observed in the red-wing of the fluorescence spectra, (the maxima of which are indicated by the vertical arrows) due to the overlap with the transient absorption band.

8.6   Conclusion

Steady-state and time-resolved spectroscopy yielded evidence that the excited state CT character in the phenyl pyrrole derivatives p-PBN, MP2BN and MP2-B25CN is different. The MICT character (large mesomeric interaction for near-planar geometries) of MP2BN as compared to the TICT character of p-PBN and MP2-B25CN is supported by its reduced excited-state dipole moment, the enhanced radiative rate constant k_{rad} values and by the observation of stimulated emission in pump-probe experiments. The reason for the increased mesomeric interaction in MP2BN can be traced back to a more efficient orbital interaction for the phenylpyrroles linked in the 2-position. Because the HOMO of the pyrrole has a node on the nitrogen, the HOMO of planar p-PBN is localised on the pyrrole, but delocalised for near-planar MP2BN where the linkage of the molecular moieties involves two carbon atoms with large orbital coefficients. In MP2-B25CN we also expect a MICT state, but the TICT state is energetically lowered much more strongly due to the increased acceptor strength (lower reduction potential) of dicyano-benzene in comparison with mono-cyano benzene, so that it may be the only minimum in polar solvents.

9   Final Conclusion

The investigations of the donor-acceptor DMABN derivatives have been characterized by absorption and fluorescence at both room- and low-temperature, as well as time-resolved absorption and fluorescence spectroscopic methods. Besides, additional supporting evidence has been gained by performing quantum chemical calculations mainly using the semiempirical method with AM1 method. In most of the compounds investigated in this work, intramolecular charge transfer (ICT) formation could well be explained by twisted intramolecular charge transfer (TICT) state through the decoupling of the donor-acceptor moieties in the excited state.

Although, the tetrafluoro analogue of DMABN, DMABN-F4, is closely related to the parent compound spectroscopically, the short wavelength B-band is not observed in the fluorescence spectrum even at 77 K in this compound. This has been explained by the fact that there is an ultrafast access to the CT conformation in the excited state. This could possibly be linked to the pretwisted ground state geometry and the increased acceptor strength. The analysis of the time-resolved measurements indicates that the emission of DMABN-F4 is strongly forbidden and is consistent with the formation of a TICT state with high dipole moment.

New insight was gained by the investigation of other fluorinated derivatives of aniline and phenyl pyrrole. The low fluorescence quantum yield values and the absence of phosphorescence in all of these fluorinated derivatives suggest that the high rate of non-radiative decay takes place through internal conversion rather than intersystem crossing. A possible internal conversion photochemical reaction path could be the folding (butterfly motion) of the benzene ring either towards a Dewar or a prefulvene deformation. It is tentatively concluded that the F-atoms increase this photoreaction tendency already present in the parent benzene (channel III).

From the studies on the photophysical properties of meta- and para-cyano-N-phenylpyrrole (m- and p-PBN), it has been found that both compounds show highly red shifted and strongly forbidden emission in polar solvents, assigned to a TICT state. Comparison to quantum chemical calculations indicates that the twisted structure is connected with an antiquinoid distortion of the benzonitrile group. It has been concluded that m-PBN differs from p-PBN by a less exergonic formation of the TICT state from the LE/ICT quinoid state, and it therefore shows only single LE/ICT fluorescence in nonpolar alkane solvents,

whereas p-PBN shows dual fluorescence (LE/ICT and TICT).

Furthermore, the investigation on dimethyl derivatives of N-phenylpyrrole such as p-DPBN and m-DPBN gave additional insight into the way the photophysical properties would be affected by changing the position of the acceptor group and by increasing the donor-strength and the ground state twist angle. The results led to the conclusion that they emit from a TICT state similarly to the nonmethylated PBN pair, but that this emission is even more strongly forbidden.

Finally, a new perspective regarding the CT state has been gained from compounds with a different linkage position on the donor such as MP2BN and additionally by changing the orientation of the acceptor part and by increasing its strength such as MP2-B25CN. The mesomeric interaction between donor and the different acceptor units has been investigated, and it was found that the behaviour could switch between ICT states with large mesomeric interaction (MICT -Mesomeric Intramolecular Charge Transfer) such as in MP2BN, and with a minimum mesomeric interaction (TICT – Twisted Intramolecular Charge Transfer) states such as in p-PBN and MP2-B25CN. The important factors, such as the relative energies of LE/ICT (MICT) and TICT state and the strength of the mesomeric interaction in the MICT state have been mainly considered.

As a whole, this dissertation mainly deals with the investigation on the photophysical properties of donor-acceptor molecules. All the observations help to understand the ICT processes taking place in the excited state. Throughout this study, the TICT/MICT model could reasonably well explain the CT processes occurring in these molecules. The low fluorescence quantum yields of the fluorinated derivatives of DMABN should be further explored by other techniques such as transient absorption and photo-acoustic spectroscopy as well as preparative photochemistry to get a clear idea on the non-radiative decay pathways involved. A possible clue for this non-radiative decay pathway can also be obtained by performing higher-level quantum chemical calculations such as *ab initio* and time-dependent density functional theory (DFT) calculations with bending, folding or twisting as a reaction coordinate. Concerning the N-phenylpyrrole compounds, fluorescence polarisation spectroscopy can further help to clarify the nature of the CT excited states observed.

References and Notes

[1]   Rettig, W. (1986), Angew. Chem. Int. Ed. (vol. 25), p. 971.

[2]   Rettig, W. (1991), Nachr. Chem. Tech. Lab. (vol. 39), p. 298.

[3]   Al-Hassan, K. A. and Rettig, W. (1986): Free volume sensing fluorescent probes, Chemical Physics Letters (vol. 126), No. 3-4, pp. 273-9.

[4]   Rettig, W.; Fritz, R. and Springer, J. (1991): p. 61, Elsevier, Amsterdam.

[5]   Rettig, W. (1993), Wolfbeis, O.S, Fluorescence spectroscopy- New methods and applications p. 31, Springer, Berlin.

[6]   Plaza, P.; Jung, N. D; Martin, M. M.; Meyer, Y. H.; Vogel, M. and Rettig, W. (1992), Chem. Phys. (vol. 168), p. 365.

[7]   Habib Jiwan, J. L. and Soumillion, J. P. (1992), J. Photochem. Photobio. A (vol. 64), p. 145.

[8]   Lippert, E.; Lüder, W. and Boos, H. (1962), Adv. Mol. Spectrosc. Proc. Int. Meet. 4th (vol. 1959), p. 443.

[9]   Grabowski, Z. R.; Rotkiewicz, K and Rettig, W (2003), Chem. Rev. (vol. 103), No. 10, pp. 3899-4031.

[10]   Turro, N. J.; Mc Vey, J.; Ramamurthy, V. and Lechtken, P. (1979), Ang. Chem (vol. 91), p. 597.

[11]   Marcus, R. A. (1956), J. Chem. Phys. (vol. 24), pp. 979-89.

[12]   Marcus, R. A. (1956), J. Chem. Phys. (vol. 24), pp. 966-78.

[13]   Marcus, R. A. (1959), Canad. J. Chem. (vol. 37), pp. 155-63.

[14]   Marcus, R. A. and Sutin, Norman (1985), Biochim. Biophys. Acta (vol. 811), No. 3, pp. 265-322.

[15]   Kavarnos, G. J (1993): Fundamentals of photoinduced electron transfer, VCH Publishers, Weinheim.

[16]   Grabowski, Z. R.; Rotkiewicz, K.; Siemiarczuk, A.; Cowley, D. J. and Baumann, W. (1979), Nouv. J. Chim. (vol. 3), No. 7, pp. 443-54.

[17]   Rotkiewicz, K.; Grellmann, K. H. and Grabowski, Z. R. (1976), Chem. Phys. Lett. (vol. 19), p. 315.

[18]   Grabowski, Z. R. and Dobkowski, J (1983), Pure App. Chem. (vol. 55), No. 2, pp. 245-52.

[19]   Rettig, W. (1994): Top. Curr. Chem. (vol. 169) p. 253.

[20]   Zachariasse, K. A.; von der Haar, T.; Hebecker, A.; Leinhos, U. and Kuehnle, W. (1993), Pure App. Chem. (vol. 65), No. 8, pp. 1745-50.

[21]   Leinhos, Uwe; Kuehnle, Wolfgang and Zachariasse, Klaas A. (1991), J. Phys. Chem. (vol. 95), No. 5, pp. 2013-21.

[22]   Schuddeboom, W.; Jonker, S. A.; Warman, J. M.; Leinhos, U.; Kuehnle, W. and Zachariasse, K. A. (1992), J. Phys. Chem. (vol. 96), No. 26, pp. 10809-19.

[23]   Sobolewski, A. L. and Domcke, W. (1996), Chem. Phys. Lett. (vol. 250), p. 428.

[24]   Sobolewski, A. L. and Domcke, W. (1996), Chem. Phys. Lett. (vol. 259), p. 119.

[25]   Rotkiewicz, K.; Grabowski, Z. R.; Krowczynski, A and Kuehnle, W. (1976), J. Lumin. (vol. 12-13), pp. 877-85.

[26]   Grabowski, Z. R.; Rotkiewicz, K; Rubaszewska, W and Kirkor-Kaminska, E (1978), Acta Phys. Pol. A (vol. 54), p. 767.

[27]   Grabowski, Z. R.; Rotkiewicz, K and Siemiarczuk, A (1979), J. Lumin. (vol. 18-19), No. Pt. 1, pp. 420-4.

[28]   Rettig, W. and Lippert, E. (1980), J. Mol. Struc. (vol. 80), p. 17.

[29]   Rettig, W. and Marschner, F. (1983), Nouv. J. Chim. (vol. 7), No. 7, pp. 425-31.

[30]   Pinto, D. J. P; Orwat, M. J; Wang, S; Fevig, J. M; Quan, M. L; Amparo, E; Cacciola, J; Rossi, K. A; Alexander, R. S; Smallwood, A. M; Luettgen, J. M; Liang, L; Aungst, B. J; Wright, M. R; Knabb, R. M; Wong, P. C; Wexler, R. R and Lam, P. Y. S (2001), J. Med. Chem. (vol. 44), p. 566.

[31]   Felstead, E.; Fielding, H. C. and Wakefield, B. J. (1966): Reactions of metal cyanides with polyfluorobenzenes, J. Chem. Soc., C. Org., No. 7, pp. 708-11.

[32]   Fischer, H. and Orth, H. (1934): Die chemie des pyrrols, Bd. I., Akademishe Verlagsgessellschaft, Leipzig, 1934.

[33]   Penieres, G.; Soto, V.; Alvarez, C.; Garcia, O. and Garcia, J. G. (1998), Heterocyc. Comm. (vol. 4), No. 1, pp. 31-32.

[34]   Meech, S. R. and Phillips, D. (1983), J. Photochem. (vol. 23), p. 193.

[35]   Heisel, F. and Miehé, J. A. (1985), Chem. Phys. (vol. 98), p. 233.

[36]   Riddick, J. A.; Bunger, W. B. and Sakano, T. K. (1986): Organic Solvents, John Wiley & Sons.

[37]   O' Connor, D. V. and Phillips, D. (1984): Time Correlated Single Photon Counting, Academic Press: London.

[38]   Beechen, J. M.; Gratton, E. and Mantulin, O. M. (1992): Globals Unlimited, Urbana, Laboratory of Fluorescence Dynamics at the University of Illinois

[39]   Vogel, M. and Rettig, W. (1987), Ber. Bunsen-Ges. Phys. Chem. (vol. 91), No. 11, pp. 1241-7.

[40]   Weigel, W.; Rettig, W.; Dekhtyar, M.; Modrakowski, C.; Beinhoff, M. and Schlueter, A. D. (2003), J. Phys. Chem. A (vol. 107), No. 31, pp. 5941-5947.

[41]   Dai Hung, N.; Plaza, P.; Martin, M. M and Meyer, y. H (1992), Appl. Opt (vol. 31), p. 7046.

[42]   Dewar, M. J. S.; Zoebisch, E. G.; Healy, E. F. and Stewart, J. J. P. (1985), J. Am. Chem. Soc. (vol. 107), p. 3902.

[43]   Dewar, M. J. S. and Dieter, K. M. (1986), J. Am. Chem. Soc. (vol. 108), p. 8075.

[44]   (1997): AMPAC 6.0 and AMPAC 6.55, Shawnee, USA, Semichem, Inc.

[45]   Druzhinin, S. I.; Jiang, Yun-B.; Demeter, A. and Zachariasse, K. A. (2001), Phys. Chem. Chem. Phys. (vol. 3), No. 23, pp. 5213-5221.

[46]   Felstead, E.; Fielding, H. C. and Wakefield, B. J. (1966), J. Chem. Soc., C. Org., No. 7, pp. 708-11.

[47]   Frisch, M. J; Trucks, G. W; Schlegel, H. B; Gill, P. M.W; Johnson, B. G; Robb, M. A; Cheeseman, J. R; Keith, T; Petersson, G.A; Montgomery, J. A; Raghavachari, K; Al-Laham, M. A; Zakrzewski, V. G; Ortiz, J. V; Foresman, J. B; Cioslowski, J; Stefanov, B. B; Nanayakkara, A; Challacombe, M; Peng, C. Y; Ayala, P. Y; Chen, W; Wong, M. W; Andres, J. L; Replogle, E. S; Gomperts, R; Martin, R. L; Fox, D. J; Binkley, J. S; Defrees, D. J; Baker, J; Stewart, J. P; Head-Gordon, M; Gonzalez, C and Pople, J. A (1998), Gaussian 98, Pittsburgh, PA, Gaussian,Inc

[48]   Grabowski, Z. R.; Rotkiewicz, K.; Rubaszewska, W. and Kirkor-Kaminska, E. (1978), Acta Phys. Polon (vol. 54A), p. 767.

[49]   Rotkiewicz, K. and Rubaszewska, W. (1982), J. Lumin. (vol. 27), p. 221.

[50]   Murali, S; Changenet-Barret, P; Ley, C; Plaza, P; Rettig, W; Martin, M.M and Tolmachev, A.I (2004): FEMTOCHEMISTRY and FEMTOBIOLOGY: Ultrafast Events in Molecular Science, FEMTOCHEMISTRY and FEMTOBIOLOGY: Ultrafast Events in Molecular Science p. 323, Elsevier.

[51]   Köhler, G. and Rotkiewicz, K. (1986), Spectrochim. Acta (vol. 42 A), p. 1127.

[52]   Lippert, E. (1955), Z. Naturforsch. (vol. 10a), p. 541.

[53]   Mataga, N.; Kaifu, Y. and Kazumi, M. (1955), Bull. Chem. Soc. Jpn. (vol. 690), p. 690.

[54]   Mataga, N.; Kaifu, Y. and Kazumi, M. (1956), Bull. Chem. Soc. Jpn. (vol. 29), p. 465.

[55]   Rösch, N. and Zerner, M. C. (1994), J. Phys. Chem. (vol. 98), p. 5817.

[56]   Köhn, A. and Hättig, C. (2004), J. Am. Chem. Soc. (vol. 126), p. 7399.

[57]   Okuyama, K.; Kakinuma, T.; Fujii, M.; Mikami, N. and Ito, M. (1986), J. Phys. Chem. (vol. 90), p. 3948.

[58]   Tsuda, M.; Oikawa, S. and Kimura, K. (1980), Int. J. Quant. Chem. (vol. 18), p. 157.

[59]   Kato, S (1988), J. Chem. Phys. (vol. 88), p. 3045.

[60]   Sobolewski, A.L.; Woywod, C. and Domcke, W. (1993), J. Chem. Phys. (vol. 98), p. 5627.

[61]   Birks, J. B (1970): Photophysics of Aromatic Molecules, Wiley, New York.

[62]   Lim, E. C (1977), Excited States (vol. 3) p. 305, Academic press, New York.

[63]   Yokoyama, T.; Taft, R. W. and Kamlet, M. J (1983), Aus. J. Chem. (vol. 36), No. 4, pp. 701-709.

[64]   Murali, S.; Kharlanov, V.; Rettig, W.; Tolmachev, A. I. and Kropachev, A. V. (2005), Accepted in J. Phys. Chem. A.

[65]   Rettig, W.; Bliss, B. and Dirnberger, K. (1999), Chem. Phys. Lett. (vol. 305), p. 8.

[66]   Cornelissen-Gude, C. and Rettig, W. (1998), J. Phys. Chem. A (vol. 102), No. 40, pp. 7754-7760.

[67]   Yoshihara, T.; Galievsky, V. A.; Druzhinin, S. I.; Saha, S. and Zachariasse, K. A. (2003), Photochem. Photobiol. Sci. (vol. 2), No. 3, pp. 342-353.

[68]   Yoshihara, T.; Druzhinin, S. I. and Zachariasse, K. A. (2004), J. Am. Chem. Soc. (vol. 126), No. 27, pp. 8535-8539.

[69]   Zachariasse, K. A. (2000), Chem. Phys. Lett. (vol. 320), pp. 8-13.

[70]   Il'Ichev, Y. V.; Kuehnle, W. and Zachariasse, K. A. (1998), J. Phys. Chem. A (vol. 102), No. 28, pp. 5670-5680.

[71]   Zachariasse, K. A.; Grobys, M.; von der Haar, Th.; Hebecker, A.; Il'ichev, Yu V.; Jiang, Y. B.; Morawski, O. and Kuehnle, W. (1996), J. Photochem. Photobiol., A (vol. 102), No. 1, pp. 59-70.

[72]   Zachariasse, K. A.; Grobys, M.; von der Haar, Th; Hebecker, A.; Il'ichev, Yu V.; Jiang, Y. B.; Morawski, O. and Kuehnle, W. (1996), Erratum: J. Photochem. Photobiol., A (vol. 102), No. 1, pp. 59-70.

[73]   Zilberg, S. and Haas, Y. (2002), J. Phys. Chem. A (vol. 106), No. 1, pp. 1-11.

[74]   Schmidt, M. W.; Baldrige, K. K.; Boatz, J. A.; Elbert, S. T.; Gordon, M. S.; Jensen, J. H.; Koseki, S.; Matsunaga, N.; Nguyen, K. A.; Su, S. J.; Windus, T. L.; Dupuis, M. and Montogery, J. A. (1993), J. Comp. Chem. (vol. 14), p. 1347.

[75] Dunning, T.H., Jr. J. Chem. Phys. 1989, 90, 1007; basis sets were obtained from the Extensible Computational Chemistry Environment Basis Set Database, Version 02/25/04, as developed and distributed by the Molecular Science Computing Facility, Environmental and Molecular Sciences Laboratory which is part of the Pacific Northwest Laboratory, P.O. Box 999, Richland, Washington 99352, USA, and funded by the U.S. Department of Energy.

[76] Grinter, R.; Heilbronner, E.; Godfrey, M. and Murrell, J.N. (1961), Tetrahed. Lett. (vol. 21), p. 771.

[77] Maus, M.; Rettig, W.; Bonafoux, D. and Lapouyade, R. (1999), J. Phys. Chem. A (vol. 103), No. 18, pp. 3388-3401.

[78] Parusel, A. B. J. (2000), Phys. Chem. Chem. Phys. (vol. 2), p. 5545.

[79] Rettig, W.; Wermuth, G. and Lippert, E. (1979), Ber. Bunsen-ges. Phys. Chem. (vol. 83), p. 692.

[80] Wermuth, G. (1983), Z. Naturforsch. (vol. 38a), p. 368.

[81] Wermuth, G. and Rettig, W. (1984), J. Phys. Chem. (vol. 88), No. 13, pp. 2729-35.

[82] Rettig, W. and Marschner, F. (1990), New J. Chem. (vol. 14), No. 11, pp. 819-24.

[83] Rettig, W. (1982), J. Mol. Struc. (vol. 84), p. 303.

[84] It is assumed here, that the increased mesomeric interaction in the excited states leads to a planar minimum for the lowest excited states. This is supported by the very low barrier to the planarity.

[85] Sarkar, A. and Chakravorti, S. (1995), Chem. Phys. Lett. (vol. 235), pp. 195-201.

[86] Murali, S.; Rettig, W. and Zilberg, S. Submitted

[87] Maus, M. and Rettig, W. (2002), J. Phys. Chem. A (vol. 106), p. 2104.

[88] Rettig, W.; Vogel, M.; Lippert, E. and Otto, H. (1986), Chem. Phys. (vol. 108), No. 3, pp. 381-90.

[89] Vogel, M. and Rettig, W. (1985), Ber. Bunsenges. Phys. Chem. (vol. 89), No. 9, pp. 962-8.

[90] Jones II, G.; Jackson, W. R; Choi, C. Y and Bergmark, W. R (1985), J. Phys. Chem. (vol. 89), p. 294.

[91] Rettig, W. and Klock, A. (1985), Canad. J. Chem. (vol. 63), No. 7, pp. 1649-53.

[92] Vogel, M.; Rettig, W.; Sens, R. and Drexhage, K. H. (1988), Chem. Phys. Lett. (vol. 147), No. 5, pp. 461-5.

[93] Van der Auweraer, M.; Grabowski, Z. R. and Rettig, W. (1991), J. Phys. Chem. (vol. 95), No. 5, pp. 2083-92.

[94]   Okada, T.; Uesugi, M.; Kohler, G.; Rechthaler, K.; Rotkiewicz, K.; Rettig, W. and Grabner, G. (1999), Chem. Phys. (vol. 241), No. 3, pp. 327-337.

List of Abbreviations and Symbols

ET	Electron Transfer
CT	Charge Transfer
TICT	Twisted Intramolecular Charge Transfer
LE	Locally excited
ICT	Intramolecular Charge Transfer
FC	Franck-Condon
MO	Molecular Orbital
HOMO	Highest Occupied Molecular Orbital
LUMO	Lowest Unoccupied Molecular Orbital
D	Donor
A	Acceptor
IP	Ionisation Potential
EA	Electron Affinity
PJT	Pseudo Jahn-Teller
RICT	Rehybridization Intramolecular Charge Transfer
TLC	Thin Layer Chromatography
UV	Ultra Violet
SPC	Single Photon Counting
OD	Optical density
AM1	Austin Model 1
HF	Hartree-Fock
CASSCF	Complete Active Space Self Consistent Field
C.I.	Configuration Interaction
DFT	Density Functional Theory
SCF	Self Consistent Field
ISC	Inter System Crossing
IC	Internal Conversion
k_{BA}	Rate constant of the reaction from B* to A*
k_{AB}	Rate constant of the reaction from A* to B*
k_{Bf}	Radiative decay constant of B-state
k_{Af}	Radiative decay constant of A-state

k_B^0	Non-radiative decay constant of B-state
k_A^0	Non-radiative decay constant of A-state
ε	Dielectric constant
n	Refractive index
h	Planck's constant
c	Velocity of light
a	Onsager radius
M	Molecular mass
N_A	Avagadro's number
ρ	Molecular density
Δf	Polarity parameter
λ_{abs}	Absorption maximum in nm
λ_{flu}	Fluorescence maximum in nm
ν_f	Fluorescence maximum in cm^{-1}
$\Delta\nu_{st}$	Stoke's shift
ϕ_f	Fluorescence quantum yield
ϕ_{tot}	Total fluorescence quantum yield of both A- and B-band.
k_r	Radiative rate constant
k_{nr}	Non-radiative rate constant
τ_f	Radiative life time
M_f	Radiative transition moment
μ_e	Excited state dipole moment
μ_g	Ground state dipole moment
α_{eq}	Equilibrium twist angle
β_{eq}	Pyramidalisation angle
$\Delta H(00)$	Activation barrier to planar geometry
$\Delta H(90)$	Activation barrier to perpendicular geometry
f	Oscillator's strength
S	Singlet state

Acknowledgement

Eidesstattliche Erklärung

Hiermit versichere ich, die vorliegende Arbeit selbständig und nur unter
Nutzung der angegebenen Hilfsmittel angefertigt zu haben.
Berlin, den 1.4.2005

....
(Murali Sukumaran)

Publications

1. **Murali S**, Sastri C.V and Maiya B.G, "New mixed ligand complexes of ruthenium(II) that incorporate a modified phenanthroline ligand: Synthesis, spectral characterization and DNA binding" *Proc. Ind. Acad. Sci., Chemical Sciences*, 2002 114(4) 403-415.

2. **S. Murali** , P. Changenet-Barret, C. Ley, P. Plaza, W. Rettig, M.M. Martin and A.I.Tolmachev, "Ultrafast photoinduced charge transfer in fluorinated derivatives of DMABN", "FEMTOCHEMISTRY and FEMTOBIOLOGY: Ultrafast Events in Molecular Science"., Elsevier, 2004, 323-326.

3. **Sukumaran Murali** and Wolfgang Rettig, "Photophysics of Pyrrolobenzenes", BESSY Annual Report, 2004.

4. Antje Neubauer, **Sukumaran Murali** and Wolfgang Rettig.; "Charge Transfer Control by Substituents: Donor Pyrroles and Fluoro-Anilines", *Int. J. Photoenergy* (in press)

5. **Sukumaran Murali,** Vladimir Kharlanov, Wolfgang Rettig, Alexei I. Tolmachev, and A.V. Kropachev.; "The Tetrafluoro Analogue of DMABN: Anomalous Fluorescence and Mechanistic Considerations", Accepted in *J. Phys. Chem. A* .

6. **Sukumaran Murali,** Wolfgang Rettig, and Shmuel Zilberg.; "TICT Formation and Antiquinoid Distortion in para- and meta-Derivatives of N-Phenyl Pyrrole", submitted to *J. Phys. Chem. A.*

7. **S. Murali,** P. Changenet-Barret, C. Ley, P. Plaza, W. Rettig, M.M. Martin and R. Lapouyade.; "Photophysical Properties of Pyrrolobenzenes with Different Linking Pattern: The Transition Between Large (MICT) and Small (TICT) Charge Transfer Interaction behaviour", Accepted in *Chem. Phys. Lett.*

Poster Presentations

1. **Murali Sukumaran**, P. Changenet-Barret, C. Ley, P. Plaza,V. Kharlanov, Wolfgang Rettig, Monique M. Martin and Alexei I. Tolmachev, "Redshifted CT Fluorescence in Fluorinated Derivatives of DMABN: Time Resolved Fluorescence and Transient Absorption Results", Femtochemistry VI, Paris, *France*, 6-10 July 2003.

2. **Murali Sukumaran**, V. Kharlanov, Wolfgang Rettig and Alexei I. Tolmachev, "Redshifted CT fluorescence in fluorinated derivatives of DMABN: Mechanistic considerations", 8th Conference on Methods and Applications of Fluorescence, Prague, *Czech Republic*, Aug. 24-27, 2003.

3. **Murali Sukumaran**, P. Changenet-Barret, C. Ley, P. Plaza, Wolfgang Rettig, Monique M. Martin and René Lapouyade, "Photophysics of Pyrrolobenzenes", ESF ULTRA conference, Pécs, *Hungary*, 25-28 March 2004.

4. **Murali Sukumaran**, P. Changenet-Barret, C. Ley, P. Plaza, Wolfgang Rettig, Monique M. Martin and René Lapouyade, "Photophysical study of Pyrrolobenzenes", Workshop on Photoinduced Charge (Proton and electron) Migration, Wdzydze, *Poland*, 30.05-05.06.2004.

5. **Murali Sukumaran**.; Wolfgang Rettig, "Comparative photophysical study of meta- and para-cyano phenylpyrroles." XX IUPAC Symposium on Photochemistry, Granada, *Spain*. July 17-22, 2004.

Co-author Poster Presentation

1. Antje Neubauer, **Sukumaran Murali** and Wolfgang Rettig.; "Charge Transfer Control by Substituents: Donor Pyrroles and Fluoro-Anilines", Proceedings of the 8th International Conference on Solar energy and applied photochemistry [SOLAR'05], Luxor, Egypt. Feb.17-23, 2005.

Lebenslauf

Name: Murali Sukumaran

Geburtsdatum: 5.6.1978

Geburtsort: Cheyyar

Familenstand: Ledig

Schulbildung: 1983-1988   Grundschule "Govt. Middle School" Cheyyar.
                        1988-1993   Gymnasium "Govt. Boys Hr. Sec. School" Cheyyar.
                        1993-1995   Abitur "Govt. Boys Hr. Sec. School" Cheyyar.

Studium: 1995-1998   B.Sc (Chemistry), Arignar Anna Govt. Arts College,
                                             Cheyyar.
                        1998-2000   M.Sc (Chemical Sciences), Pondicherry University,
                                             Pondicherry.
                                             Project title: "Synthesis and characterization of Cu(II)
                                             complexes which act as bio-mimicking models for
                                             hemocyanin enzymes".
                        2000-2001   M.Phil (Chemistry), University of Hyderabad,
                                             Hyderabad.
                                             Dissertation title: "New mixed ligand complexes of
                                             ruthenium(II) that incorporate a modified
                                             phenanthroline ligand: Synthesis, spectral
                                             characterization and DNA binding"

Wissenschaftliche   Seit Ock.2001   Wissenschaftliche Mitarbeiter am Inst. f. Chemie der
Tätigkeit: Humboldt-Universität zu Berlin.